An Experimental Study of Multiphase Behavior for Athabasca-Bitumen/Alkane-Solvent Mixtures

by

Jianyi Gao

A thesis submitted in partial fulfillment of the requirements for the degree of

Master of Science

in

Petroleum Engineering

Department of Civil and Environmental Engineering
University of Alberta

Abstract

Steam-solvent coinjection has been studied and pilot-tested as a potential method to improve steam-assisted gravity drainage for bitumen recovery. Reliable design of coinjection requires reliable PVT data for bitumen/solvent/water mixtures, which are scarce and fragmentary in the literature.

In this study, a new set of pressure-volume-temperature and multiphase data were obtained for Athabasca-bitumen/solvent mixtures at pressures up to 10 MPa and temperatures up to 160°C. The solvents used are n-butane, n-hexane, and n-octane. Also, experiments were conducted for one Athabasca-bitumen/n-butane/water mixture. A single equation-of-state model was developed to correlate all experimental data obtained, and used to interpret complex multiphase behavior observed for the highly size-asymmetric polar mixtures.

An n-butane/bitumen mixture at a high concentration of n-butane (97.24 mol%) exhibited liquid-liquid separation of hydrocarbons, consisting of the bitumen-rich and butane-rich liquid phases, at temperatures from 80°C to 160°C at operating pressures. Addition of water to this complex mixture resulted in four equilibrium phases: the vapor, aqueous, bitumen-rich liquid, and butane-rich liquid phases. This is the first time four coexisting phases were experimentally confirmed for the Athabasca-bitumen/solvent/water system.

The liquid-liquid separation of hydrocarbons indicates that coinjection of steam with highly volatile solvents, such as n-butane, for Athabasca bitumen may result in less effective dilution of bitumen, even when the solvent sufficiently accumulates near the edge of a steam chamber. Unlike n-butane, n-hexane and n-octane did not yield the liquid-liquid immiscibility with Athabasca bitumen in this research. Also, results for the n-hexane/bitumen and n-

octane/bitumen mixtures indicate that n-hexane is a more effective solvent for reducing bitumen viscosity than n-octane at the same solvent-weight fraction in mixtures. However, n-hexane resulted in more asphaltene-precipitation yields than n-octane when mixed with Athabasca bitumen at ambient pressure.

Acknowledgements

I would like to express my sincere gratitude to my supervisors, Dr. Ryosuke Okuno and Dr. Huazhou Andy Li, for their supervision and support during my master program at the University of Alberta. I would like to thank Dr. Okuno for his continuous professional guidance and support. There is no doubt that he is an excellent researcher and keeps inspiring students with his exact attitude to research. Without his supervision, my research work would have not been possible. I would like to thank Dr. Li for his continuous and constructive suggestions on my experimental study, and his encouragement and patience on my work. My experimental work would not have gone well without Dr. Li's kind help. I am definitely a lucky girl under supervision with these two professors. Their hard work and success keeps inspiring me and letting me realize that "the difference between who you are and who you want to be is what you should do". I have learnt a lot from them on critical thinking and self-management during these two years.

I gratefully acknowledge the financial support received from Japan Petroleum Exploration Co., Ltd., Japan Canada Oil Sands Ltd., and the Natural Sciences and Engineering Research Council of Canada (RGPIN 418266 and RGPIN 05394).

I am grateful to our lab technician, Mr. Todd Kinnee. His help on my experiments are highly appreciated. I also want to thank my colleagues, Dr. Ashutosh Kumar, Arun Venkat Venkatramani, and Dr. Francisco Javier Argüelles Vivas for their suggestions and help on my research work.

I would also like to express my gratitude to my best friend, Di Zhu, for her academic suggestions and unconditional help at any time. I sincerely appreciate her encouragement and comfort when I felt desperate. I also want to thank all my friends at Edmonton who brought joy into my daily life. My deepest gratitude goes to my parents, my grandma and all my families for their love, support and companion throughout my life. You mean more to me than you will ever know.

Table of Contents

List of Tables

List of Figures

Nomenclature

Roman symbols

C_{PEN}	Peneloux volume-shift parameter
L_1	bitumen-rich oleic phase
L_2	solvent-rich oleic phase
P	pressure
P_c	critical pressure
S	saturation
S_v	vapor phase saturation
S_L	liquid phase saturation
S_w	water phase saturation
T	temperature
T_c	critical temperature
V	vapor phase
V_c	critical molar volume
W	aqueous phase
x	component mole fraction

Greek symbols

ω	acentric factor

Abbreviations

AARD	average absolute relative deviation
BIP	binary interaction parameter
EOS	equation of state
PR-EOS	Peng-Robinson equation of state
MW	molecular weight
PC	pseudo component
SAGD	steam-assisted gravity drainage
ES-SAGD	expanded-solvent steam-assisted gravity drainage
LV	liquid-vapor equilibrium
LLV	liquid-liquid-vapor equilibrium
WLLV	water-liquid-liquid-vapor equilibrium
PV	pressure-volume
HB	n-hexane/bitumen mixtures
OB	n-octane/bitumen mixtures

Chapter 1 Introduction

1.1 Backgrounds and Problem Statements

Bitumen is one of the main petroleum resources in Canada, and is highly viscous and immobile at reservoir conditions. Improvement on bitumen mobility at in-situ conditions is required for an efficient recovery technology. Several bitumen recovery technologies [e.g., cyclic steam stimulation and steam-assisted gravity drainage (SAGD)] have been applied for bitumen recovery by decreasing bitumen viscosity at reservoir conditions (Butler 1991).

Steam injection has been widely implemented for heavy-oil/bitumen recovery (Prats 1982). Steam-assisted gravity drainage (SAGD) is one of the most important applications of steam injection for bitumen recovery (Butler 1991). Injected steam rises foaming a steam chamber with bitumen flowing along steam-chamber edge. The latent heat of steam would decrease bitumen viscosity, and increase its mobility under reservoirs. Thereafter, the mobilized bitumen can be drained into the production well by gravity. However, SAGD requires a substantial amount of water and energy resources for steam generation. The emission of carbon dioxide associated with steam generation is also a major environmental concern.

Coinjection of a small amount of solvent with steam, such as expanding-solvent SAGD (ES-SAGD), has been proposed and pilot-tested to improve the efficiency of SAGD. Such coinjection processes aim to utilize thermal and compositional mechanisms to increase the mobility of the bitumen-rich phase near the chamber edge (e.g., Nasr and Isaacs 2001; Nasr et al. 2003; Gupta and Gittins 2007). A properly-designed coinjection of solvent with steam can benefit both from the latent heat of the injected vapor and the bitumen dilution by solvent. Successful pilot tests have been reported for enhancement of bitumen drainage rate by use of steam and solvent coinjection, for example, the Imperial Oil's Cold Lake Bitumen Reservoir tried heptane-steam coinjection (Leaute 2002; Leaute and Carey, 2007), and the EnCana's Senlac and Christina Lake Region used butane-steam coinjection (Gupta and Gittins, 2006).

Injection of solvent and steam into bitumen results in highly size-asymmetric polar mixtures, consisting of solvent, bitumen, and water. Solvent selection is the key for the success of coinjection. Design of solvent type and its concentration in coinjection requires a detailed understanding and reliable prediction of multiphase behavior for solvent/bitumen mixtures at a wide range of temperature at operating pressures (Nagarajan et al. 2006). Most of the solvents used in steam-solvent coinjection are asphaltene insoluble solvents (Hascakir 2016), such as the solvents used in this study (n-butane, n-hexane and n-octane). Therefore, the amount of asphaltene precipitation and water-in-oil emulsion due to the asphaltene-water interactions should also be taken into account for the choice of optimum solvent in coinjection. A systematic set of data for solvent/bitumen mixtures, including multiphase boundary data, thermal-dynamic properties and asphaltene precipitation data, are essential for choosing the optimum solvent at in-situ conditions.

Various hydrocarbons were tested as potential additives to steam. Several papers reported that lighter hydrocarbon solvents were suitable for coinjection with steam (e.g., Ardali et al. 2010; Govind et al. 2008). n-Butane was presented as the optimum solvent for providing a lower residual oil saturation and a higher drainage rate at operating pressures from simulation results. However, some of the other researchers indicated that n-hexane or n-heptane may be a better choice due to their similar boiling points with steam for taking advantage of the solvent without losing heat of steam (e.g., Li and Mamora 2010; Yazdani et al. 2011; Nasr et al. 2003; Mohabati et al. 2010). Li et al. (2011) stated that heavy liquid solvents, such as C_{12}, were the optimum solvents to be coinjected with steam for Athabasca bitumen.

Phase-behavior models for bitumen developed on the basis of experimental data were used for prediction of fluid behavior at reservoir conditions. For example, cubic EOS's were used by Díaz et al. (2011), Agrawal et al. (2012), and Kumar and Okuno (2016). Recently, association models were applied for bitumen characterization where molecular association of asphaltene component were considered, for example, the Perturbed-Chain Statistical Association Fluid Theory (PC-SAFT) models (e.g., Ma et al. 2016; Panuganti et al. 2012; Leekumjorn and Krejbjerg 2013) and the Cubic-Plus-Association (CPA) models (e.g., Li and Firoozabadi 2010; Jindrová et al. 2015; Zirrahi et al. 2015a, b). The association models have shown good results on matching asphaltene precipitation data as presented in the literature, and are considered to be an

alternative to cubic EOS for predicting phase behavior of steam and solvent coinjection at in-situ conditions.

Reliable phase-behavior models should be validated by experimental PVT data over a wide range of operating conditions. However, it is not easy to find in the literature a comprehensive set of PVT data for phase behavior (or phase boundaries), density, viscosity, and asphaltene precipitation for the same bitumen sample with different solvents. Therefore, the main objective of this research is to present a new set of PVT data for solvent/bitumen and solvent/bitumen/water mixtures at pressures up to 10 MPa and temperatures up to 160 °C. To our knowledge, this is the first time four co-existing phases were reported for n-butane/bitumen/water mixtures at temperature-pressure conditions relevant to ES-SAGD, and PVT data were presented for n-octane/Athabasca-bitumen mixtures.

1.2 Research Objectives

The objectives of this research are:

- To present a new set of PVT and multiphase boundary data for solvent/Athabasca-bitumen mixtures at pressures up to 10 MPa and temperatures up to 160°C, in order to study on the liquid-liquid separation of hydrocarbons for Athabasca bitumen diluted with different solvents.
- To study the effect of adding water for solvent/bitumen mixtures, in terms of multiphase boundaries and emulsions.
- To present a systematic set of data for Athabasca bitumen diluted with different solvents, including density, viscosity and asphaltene precipitation, in order to study the effect of solvent type on bitumen mobility for coinjection.
- To provide a single equation-of-state model developed to correlate all experimental data obtained and interpret complex multiphase behavior observed for the highly size-asymmetric polar mixtures.

1.3 Thesis Configuration

Chapter 2 presents the multiphase boundary measurement for n-butane/bitumen and n-butane/bitumen/water mixtures. Liquid-liquid separation of hydrocarbons was observed for

binary mixture at the butane concentration of 97 mol%. Also, up to four co-existing phases were observed for the ternary mixture with water in the PVT cell. A single EOS model was developed to correlate all experimental data obtained, and used to interpret complex multiphase behavior observed for highly size-asymmetric polar mixtures.

In Chapter 3, multiphase boundaries and densities were measured for n-hexane/bitumen and n-octane/bitumen mixtures by use of PVT apparatus. In addition, an experimental study on bitumen mobility was conducted, including the viscosity measurement and asphaltene precipitation measurement. Results from the viscosity measurements at atmospheric pressure showed that n-hexane yields more reduction of the bitumen-phase viscosity than n-octane. In asphaltene precipitation experiments at atmospheric pressure, a larger amount of precipitates was observed with n-hexane than n-octane.

In Chapter 4, conclusions of this study were summarized systematically. Suggestions of future work were also presented in this part.

References:

Agrawal, P., Schoeggl, F.F., Satyro, M.A., Taylor, S.D., and Yarranton, H.W. 2012. Measurement and Modeling of the Phase Behavior of Solvent Diluted Bitumens. *Fluid Phase Equilibr.* **334:** 51-64.

Ardali, M., Mamora, D.D., and Barrufet, M. 2010. A Comparative Simulation Study of Addition of Solvents to Steam in SAGD Process. CSUG/SPE paper 138170 presented at Canadian Unconventional Resources and International Petroleum Conference, Calgary, Alberta, Canada, October 19-21.

Bulter, R.M. 1991. Thermal Recovery of Oil and Bitumen. Prentice Hall, New Jersey.

Díaz, O.C., Modaresghazani, J., Satyro, M.A., and Yarranton, H.W. 2011. Modeling the Phase Behavior of Heavy Oil and Solvent Mixtures. *Fluid Phase Equilibr.* **304** (1): 74-85.

Govind, P.A., Das, S.K., Srinivasan, S., and Wheeler, T.J. 2008. Expanding Solvent SAGD in Heavy Oil Reservoirs. Paper SPE/PS/CHOA 117571 presented at the 2008 SPE International Thermal Operations and Heavy Oil Symposium, Calgary, Alberta, Canada, October 20-23.

Gupta, S.C. and Gittins, S.D. 2006. Christina Lake Solvent Aided Process Pilot. *J. Can. Petrol Tech*. **45**(09).

Gupta, S.C., and Gittins, S.D. 2007. Effect of Solvent Sequencing and Other Enhancements on Solvent Aided Process. *J. Can. Petrol. Tech.* **46**(09).

Hascakir, B. 2016. How to Select the Right Solvent for Solvent-Aided Steam Injection Processes. *J. Petrol. Sci. Eng.*

Jindrová, T., Mikyška, J., and Firoozabadi, A. 2015. Phase Behavior Modeling of Bitumen and Light Normal Alkanes and CO2 by PR-EOS and CPA-EOS. *Energy Fuels*. **30**(1): 515-525.

Kumar, A., and Okuno, R. 2016. A New Algorithm for Multiphase Fluid Characterization for Solvent Injection. *SPE Journal.* SPE-175123-PA.

Leaute, R.P. 2002. Liquid Addition to Steam for Enhancing Recovery (LASER) of Bitumen with CSS: Evolution of Technology from Research Concept to a Field Pilot at Cold Lake. Paper

SPE-79011-MS presented at SPE International Thermal Operations and Heavy Oil Symposium and International Horizontal Well Technology Conference, Calgary, Alberta, Canada, November 4-7.

Leaute, R.P. and Carey, B.S. 2007. Liquid Addition to Steam for Enhancing Recovery (LASER) of Bitumen with CSS: Results from the First Pilot Cycle. *J. Can. Petrol Tech.* **46**(09).

Leekumjorn, S., and Krejbjerg, K. 2013. Phase Behavior of Reservoir Fluids: Comparisons of PC-SAFT and Cubic EOS Simulations. *Fluid Phase Equilibr.* **359**: 17-23.

Li, W., and Mamora, D.D. 2010. Phase Behavior of Steam with Solvent Co-injection under Steam Assisted Gravity Drainage (SAGD) Process. Paper SPE 130807 presented at SPE EUROPEC/EAGE Annual Conference and Exhibition, Barcelona, June 14-17.

Li, W., Mamora, D.D., and Li, Y. 2011. Solvent-Type and –Ratio Impacts on Solvent-Aided SAGD Process. *SPE Res. Eval. and Eng.* **14**(3): 320-331.

Li, Z., and Firoozabadi, A. 2010. Modeling Asphaltene Precipitation by n-Alkanes from Heavy Oils and Bitumens Using Cubic-Plus-Association Equation of State. *Energy and Fuels.* **24**(2): 1106-1113.

Ma, M., Chen, S., and Abedi, J. 2016. Predicting the Multiphase Equilibrium and Density of Bitumen with C2H6, C3H8 and CO2 Using the Simplified PC-SAFT Equation of State. *Fuel.* **181**: 652-659.

Mohebati, M.H., Maini, B.B., and Harding, T.G. 2010. Optimization of Hydrocarbon Additives with Steam in SAGD for Three Major Canadian Oil Sands Deposits. CSUG/SPE paper 138151 presented at Canadian Unconventional Resources and International Petroleum Conference, Calgary, Alberta, Canada, October 19-21.

Nagarajan, N.R., Honarpour, M.M., and Sampath, K. 2006. Reservoir Fluid Sampling and Characterization—Key to Efficient Reservoir Management. Paper SPE 101517 presented at the Abu Dhabi International Petroleum Exhibition and Conference, Abu Dhabi, U.A.E., November 5-8.

Nasr, T.N., Beaulieu, G., Golbeck, H., and Heck, G. 2003. Novel Expanding Solvent-SAGD Process "ES-SAGD". *J. Can. Petro. Tech.* **42**(1): 13-16.

Nasr, T.N. and Isaacs, E. 2001. Process for Enhancing Hydrocarbon Mobility Using a Steam Additive. U.S. Patent 6230814.

Panuganti, S.R., Vargas, F.M., Gonzalez, D.L., Kurup, A.S., and Chapman, W.G. 2012. PC-SAFT Characterization of Crude Oils and Modeling of Asphaltene Phase Behavior. *Fuel.* **93**: 658-669.

Prats, M. 1982. *Thermal Recovery.* SPE Monograph Series Volume 7, Henry L. Doherty Series., New York.

Yazdani, A., Alvestad, J., Kjonsvik, D., Gilje, E., and Kowalewski, E. 2011. A Parametric Simulation Study for Solvent Co-injection Process in Bitumen Deposits. Paper SPE 148804 presented at the Canadian Unconventional Resources Conference, Calgary, Alberta, Canada, November 15-17.

Zirrahi, M., Hassanzadeh, H., and Abedi, J. 2015a. Prediction of CO2 Solubility in Bitumen Using the Cubic-Plus-Association Equation of State (CPA-EOS). *J. Supercritical Fluids*. **98**: 44-49.

Zirrahi, M., Hassanzadeh, H., and Abedi, J. 2015b. Prediction of Water Solubility in Petroleum Fractions and Heavy Crudes Using Cubic-Plus-Association Equation of State (CPA-EoS). *Fuel*. **159**: 894-899.

Chapter 2 An Experimental Study of Multiphase Behavior for n-Butane/Bitumen/Water Mixtures

A version of this chapter was presented at the SPE Canada Heavy Oil Technical Conference held in Calgary, Alberta, Canada, 7-9 June 2016, and has been accepted for publication in SPE Journal on September 8, 2016 (SPE 180736-PA).

Abstract:

Steam-solvent coinjection has been studied and pilot-tested as a potential method to improve steam-assisted gravity drainage (SAGD) for bitumen recovery. Reliable design of coinjection requires reliable PVT data for bitumen/solvent/water mixtures, which are scarce and fragmentary in the literature.

The main objective of this research was to present a new set of PVT and multiphase data for n-butane/Athabasca-bitumen/water mixtures at pressures up to 10 MPa and temperatures up to 160°C. Experiments were conducted by use of a conventional PVT apparatus. The data presented include multiphase equilibria up to four coexisting phases and liquid densities for 100% bitumen, two mixtures of n-butane/bitumen, and one mixture of n-butane/bitumen/water.

Liquid-liquid separation of hydrocarbons was experimentally observed at the n-butane concentration of 97 mol% in the n-butane/bitumen system with/without water, for a wide range of temperatures at operating pressures for expanding-solvent-SAGD (ES-SAGD). This may indicate the limited solubility of n-butane in bitumen even when a high level of accumulation of n-butane takes place near a chamber edge in ES-SAGD for Athabasca bitumen. The multiphase transition that involves appearance/disappearance of the vapor phase was observed to occur near the vapor pressure of n-butane or its extension. Such phase transition occurs at a higher pressure in the presence of water, due to its vapor pressure, than in the absence of water at a given temperature. This is the first time four coexisting phases are reported for n-butane/Athabasca-bitumen/water mixtures at temperature-pressure conditions relevant to ES-SAGD.

2.1 Introduction

Steam injection has been widely implemented for heavy-oil/bitumen recovery (Prats 1982). Steam-assisted gravity drainage (SAGD) is one of the most important applications of steam injection for bitumen recovery (Butler 1991). However, SAGD requires a substantial amount of water and energy resources for steam generation. The emission of carbon dioxide associated with steam generation is also a major environmental concern.

Coinjection of a small amount of solvent with steam, such as expanding-solvent SAGD (ES-SAGD), has been studied and pilot-tested as a potential alternative to SAGD for bitumen

recovery. Such coinjection processes aim to utilize thermal and compositional mechanisms to increase the mobility of the bitumen-rich phase near the chamber edge (e.g., Nasr and Isaacs 2001; Nasr et al. 2003). Various researchers showed that steam-solvent coinjection could result in incremental oil recovery compared with steam-only injection in lab-scale physical experiments, pole-scale experiments and numerical simulations (e.g., Redford and McKay 1980; Li and Mamora 2010; Mohammadzadeh et al. 2012; Jha et al. 2012; Keshavarz et al. 2014). Ardali et al. (2012) presented that solvent-assisted SAGD required lower energy and water consumption in comparison with SAGD.

Various hydrocarbons were tested as a potential coinjectant for steam-solvent coinjection. The choice of solvent at operating conditions depends on the composition of bitumen and PVT properties of phases. Redford and McKay (1980) indicated that injection of volatile components, such as propane and n-pentane, with steam into Athabasca bitumen resulted in a substantial in-situ retention of the solvents. Li et al. (2011c) stated that heavy solvents, such as C_{12}, were the optimum solvents to be coinjected with steam for Athabasca bitumen. Yazdani et al. (2011) indicated that n-hexane and n-heptane were preferable for Athabasca bitumen in comparison with propane and n-pentane. Mohabati et al. (2010) found that steam-hexane coinjection could improve SAGD performance for Athabasca bitumen more than for Cold Lake and Lloydminster reservoirs.

Nasr et al. (2003) compared the drainage rates in coinjection of steam and solvents (methane-n-octane), and presented that n-hexane and n-heptane were the optimum solvents for live Cold Lake bitumen. Mohabati et al. (2010) discussed that gaseous butane that accumulated near a chamber edge might limit the heat transfer to bitumen and reduce oil drainage rate. Ardali et al. (2010) simulated the coinjection of steam and normal hydrocarbons (C_3 to C_7), and concluded that n-butane was the optimum solvent for Cold Lake with no initial solution gas at the operating pressure of 3400 kPa. Govind et al. (2008) observed a lower residual oil saturation simulated for n-butane coinjection at a higher operating pressure (4000 kPa).

Injection of solvent and steam into bitumen results in highly size-asymmetric polar mixtures, consisting of solvent, bitumen, and water. Design of solvent type and its concentration in coinjection requires a detailed understanding of multiphase behavior for solvent/bitumen/water mixtures at a wide range of temperature at operating pressures (Nagarajan et al. 2006). There are

many phase-behavior models for bitumen developed on the basis of experimental PVT data in the literature. Liquid-liquid boundaries and vapor-liquid-liquid boundaries for ternary mixtures of Athabasca-bitumen, propane and carbon dioxide were correlated by use of an advanced Peng-Robinson (PR) EOS (Díaz et al. 2011). This EOS was applied to predict phase boundaries and asphaltene precipitation in Agrawal et al. (2012). Kumar and Okuno (2016) developed a new algorithm for bitumen characterization by use of the PR EOS with the van der Waals mixing rules. The perturbed-chain form of the statistical association fluid theory (PC-SAFT) was also applied for bitumen characterization with the consideration of molecular association of asphaltene components (e.g., Ma et al. 2016; Panuganti et al. 2012; Leekumjorn and Krejbjerg 2013). PC-SAFT models have demonstrated good performance for modeling asphaltene precipitation (e.g., Zúñiga-Hinojosa et al. 2014; Tavakkoli et al. 2013). Zirrahi et al. (2015a, b) accurately predicted the solubility of carbon dioxide and water in bitumen by use of a cubic-plus association (CPA) EOS on the basis of the Soave-Redlich-Kwong (SRK) EOS and Wertheim's first–order thermodynamic perturbation theory for the association forces. Self and cross association parameters of bitumen components were adjusted to match experimental solubility data. A CPA EOS was also applied for predicting the solubility of light n-alkanes in bitumen (Jindrová et al. 2015), and asphaltene precipitation (e.g., Li and Firoozabadi 2010; Jindrová et al. 2015). However, experimental phase behavior data for solvent/bitumen/water mixtures are scarce and fragmentary in the literature.

Several papers reported experimental results for multiphase behavior associated with steam-solvent coinjection processes. Badamchi-Zadeh et al. (2009) measured saturation pressures and solubilities of propane in Athabasca bitumen at temperatures up to 50°C. Single liquid phase and liquid-vapor phase equilibria were visually observed with less than 20 wt% propane in bitumen/propane mixtures. A second dense phase was detected by in-line measurement of density and viscosity at propane concentrations above 20 wt% without visual confirmation. Kariznovi et al. (2010) developed a novel experimental design for phase behavior studies, which was shown to be an effective method for phase detection and volume measurement. An in-line densitometer, viscometer, and gas chromatography were connected with an equilibrium cell in order to measure phase properties. They measured solubilities of propane in bitumen at temperatures from 50.9°C to 149.8°C as well as phase densities and viscosities. Vapor-liquid

equilibrium was detected at 100.5°C and 149.8°C. Liquid-liquid equilibrium was detected at 50.9°C. Nourozieh et al. (2014) reported phase transitions for vapor-liquid and liquid-liquid equilibrium for n-butane/bitumen mixtures at temperatures up to 190°C. Agrawal et al. (2012) measured saturation pressures of a Peace River bitumen/n-pentane mixture (11 wt% and 30 wt% n-pentane) from 90°C to 180°C by use of a conventional PVT cell.

Amani et al. (2013) investigated the three-phase equilibrium for Athabasca bitumen/water mixtures, consisting of the vapor, aqueous, and bitumen-rich liquid phase. They measured phase boundaries for a series of mixtures with water concentrations from 9.2 wt% to 89.7 wt% by use of an X-ray view cell. Amani et al. (2014) measured the three-phase behavior (water-rich, bitumen-rich, and vapor phases) for ternary mixtures of Athabasca bitumen, toluene, and water by use of X-ray transmission tomography. Water solubilities in the hydrocarbon-rich phase and density data of the water-saturated hydrocarbon phase were also presented. Volumetric properties for various bitumens and bitumen/solvent mixtures were also presented in the literature (e.g., Svrcek and Mehrotra 1982; Ashrafi et al. 2011; Kariznovi et al. 2014; Nourozieh et al. 2014a, b; 2015).

Glandt and Chapman (1995) stated that water-in-oil emulsion could appear near producing wells in SAGD. Water-in-oil emulsion and oil-in-water emulsion may exist in the well-head effluent, but most of the studies about emulsion in SAGD were based on synthetic emulsion (e.g., Noik et al. 2005; Nguyen et al. 2013). Ezeuko et al. (2013) modeled in-situ formation of emulsification near a steam-chamber edge in SAGD and ES-SAGD (n-hexane, n-heptane and n-octane solvents) via a two-stage pseudo chemical reaction. They explained that a fraction of water might flow as water-in-oil emulsion in the oleic phase, which could improve the effective oil flow at the pore scale.

This chapter presents an experimental study of multiphase behavior for n-butane/Athabasca-bitumen/water mixtures, which is part of a comprehensive study on the phase behavior of different solvents with Athabasca bitumen and water. The main objective in this chapter is to study liquid-liquid separation of hydrocarbons when n-butane is mixed with Athabasca bitumen with/without water. Section 2 presents the experimental setup and procedure adopted in this research. Section 3 shows experimental results and gives an equation-of-state (EOS) model

calibrated with the data. To our knowledge, this is the first time four coexisting phases are reported for n-butane/Athabasca-bitumen/water mixtures at temperature-pressure conditions relevant to ES-SAGD. A limited experimental observation is also reported for water-in-oil and oil-in-water emulsion observed during some of the experiments in this research.

2.2 Experimental Section

2.2.1 Materials

The molecular weight (MW) for the Athabasca bitumen was measured by use of a cryoscope (Cryette^{TM}, GAS 019-90, Precision Systems Inc., Natick, MA, USA) based on freezing-point depression (Exova Lab, Edmonton, Canada). The MW was measured to be 635 gram/mole after preheating the sample to 60°C. The water content was measured to be 0.245 wt% and calculated to be 8.64 mol% in the bitumen sample (Exova Lab, Edmonton, Canada), although the calculation is subject to various uncertainties, such as the bitumen MW. Removal of water from the bitumen sample by heating was not attempted in order to prevent light components from being evaporated. The purity of the solvent used, which is n-butane (Praxair, Mississauga, Ontario, Canada), is 99.5%.

SARA analysis was conducted to obtain weight fractions of saturates, aromatics, resins and asphaltenes in the bitumen sample by use of the liquid-solid chromatography method after preheating the sample to 60°C (Exova Lab, Edmonton, Canada). The analysis indicated that the bitumen contains 28.6 wt% saturates, 30.7 wt% aromatics, 20.8 wt% resins I, 1.8 wt% resins II and 18.0 wt% asphaltenes. Resins I were eluted from the column with methyl ethyl ketone. Resins II were then eluted from the column with tetrahydrofuran.

The compositional analysis was carried out by use of a high-temperature gas-chromatographic method as described in ASTM D7169-05 (Exova Lab, Edmonton, Canada) after preheating the sample to 60°C. The maximum boiling point reported was 720°C. The boiling-point distribution is shown in **Figure 2.1 and Appendix A.** As presented in Díaz et al. (2011), boiling points above 30 wt% distilled for bitumen may be overestimated by simulated distillation.

2.2.2 Experimental Setup

Phase behavior measurements for n-butane/Athabasca-bitumen and n-butane/Athabasca-bitumen/water mixtures were conducted with a conventional PVT apparatus (PVT-ZS-16-2-2-H/AC, DBR, Edmonton, Canada). **Figure 2.2** shows a schematic for the apparatus. The operation limits of the PVT cell equipped in the PVT system are approximately 100 MPa (15,000 psi) and 199°C. The total sample capacity of the cell is 112 cm^3, and the height of the side window slot is 14.100 cm. An isolation piston with a thickness of 4.672 cm isolates the test fluid from hydraulic oil. The pressure of hydraulic oil is controlled by a high-pressure positive displacement pump (PMP-500-1-20-HB, DBR, Edmonton, Canada). The temperature of the PVT cell is controlled by an air bath with a control accuracy of ±0.1°C. The PVT system is equipped with a cathetometer for direct volume measurement by measuring the height of the sample fluid or phases of interest. The uncertainty in volume measurement is ±0.016 cm^3. The accuracy of the Heise pressure gauge (901A-15K-232P-R5, Ashcroft Inc, Stratford, USA) assembled in the system is ±0.07% of full-scale 104 MPa (15,000 psig). In addition, a high-pressure precision test gauge (700RG31, Fluke, Calgary, Canada) with an accuracy of ±0.01% of full-scale 69 MPa (10,000 psig) was also connected to the PVT cell for more accurate pressure measurement. The dead volume of this PVT system is 1.754 cm^3.

A digital densitometer (DDM 2910, Rudolph Research Analytical, Hackettstown, USA) was used to measure liquid densities at atmospheric pressure. The accuracy of temperature control is ±0.05°C. The uncertainty of the density measurement by use of this densitometer is ±0.1 kg/m^3.

2.2.3 Experimental Procedure

Densities of the bitumen were measured with a digital densitometer (DDM 2910, Rudolph Research Analytical, Hackettstown, USA) at atmospheric pressure and temperature between 15.6°C and 80.0°C. Densities of bitumen and n-butane/bitumen mixtures at reservoir conditions were measured with the PVT cell based on mass balance as explained below. The density measurements were conducted at conditions of 15.6°C-160.0°C and 1.0-10.0 MPa.

As the mass injected in the closed PVT cell was conserved, the density at a different temperature-pressure condition was obtained using the reference density that was measured at a known reference condition: i.e.,

$$\rho_2 = \frac{V_1}{V_2}\rho_1 = \frac{H_1}{H_2}\rho_1, \quad (2.1)$$

where ρ_1, V_1 and H_1 are the sample's density (kg/m^3), volume (cm^3), and height in the PVT cell (cm) at the reference condition. ρ_2, V_2 and H_2 are the sample's density (kg/m^3), volume (cm^3), and height in the PVT cell (cm) at a given temperature-pressure condition. The reference density of bitumen was measured at 15.6°C and atmospheric pressure.

In this study, two n-butane/bitumen mixtures (Mixtures A and B) and one n-butane/bitumen/water mixture (Mixture C) were tested in the PVT equipment. The overall compositions of these mixtures are shown in **Table 2.1**. Multiphase equilibrium measurements were conducted with the constant composition expansion test method. Before each measurement, the PVT cell and inlet tubings were cleaned with toluene and evacuated by a vacuum pump. A sufficient amount of bitumen was stored in a transfer cylinder that was placed in the air bath of the PVT system. The high-pressure n-butane cylinder that was equipped with a dip tube allowed for direct withdrawal of liquid n-butane. It was directly connected to the inlet tubing of the PVT cell. After injecting a certain amount of liquid n-butane into the cell at room temperature, the air bath temperature was set to 50.0°C for at least 12 hours, enabling the bitumen sample in the transfer cylinder and n-butane in the PVT cell to reach thermal equilibrium. The injected mass of liquid n-butane was calculated by use of the volume measured by the cathetometer and density values from the NIST database. The bitumen sample was then injected into the PVT cell without turning on the magnetic stirrer. After injection, the volume of bitumen was determined as the difference between the total volume and the liquid n-butane volume as no volume change upon mixing was assumed to occur for the short time period. The composition of this mixture was calculated based on the densities, volumes, and MWs of bitumen and n-butane. After that, the temperature of the PVT cell was increased to the highest operating temperature in this research, 160.0°C. Subsequently, the mixture was vigorously stirred by the magnetic stirrer at 160.0°C for at least 12 hours to ensure that the components were completely mixed.

At each temperature, phase-boundary measurements were initiated from a single-liquid-phase state at a high pressure. Then, the pressure was gradually decreased by step-wise expansion at the rate of 3 cm^3/hr. The mixture was sufficiently stirred for quickly reaching an equilibrium

state prior to measurement at each pressure. Mixing by the stirrer was identified when circular movement for each fluid was observed inside the PVT cell. After reaching each specified pressure, the magnetic stirrer was switched off and the system was kept static for a sufficient duration. An equilibrium state was deemed to be achieved once the cell pressure became steady. Two to three hours were sufficient for a single liquid phase to reach an equilibrium state at each temperature-pressure condition. The time allowed for equilibration was increased to four to five hours for multiphase equilibria. Thereafter, the phase equilibrium state of the mixture was visually identified, and the volume of each phase was measured. For example, the phase interface between an n-butane-rich phase and a bitumen-rich phase was easily identified when the two phases showed distinct colors. It was observed that n-butane-rich liquid was colorless before mixing, but became dark-red after mixing as n-butane extracted a significant amount of light and medium components from the bitumen. A phase-boundary pressure was firstly determined on the basis of visual observation of equilibrium phases, and then calculated by plotting the total volume (V) with respect to pressure (P). The PV relationship often showed a clear change in slope when a new phase appeared as pressure changed. Multiple phase boundaries for Mixtures A and B were sequentially determined with step-wise reduction of pressure at each temperature.

After completion of all measurements for Mixture B, a certain volume of distilled water was injected into the PVT cell to make the composition for Mixture C at around 50.0°C. The procedure described in the previous paragraph was applied to conduct phase behavior tests for Mixture C starting at 160.0°C, the highest temperature in this research.

2.3 Results and Discussions

2.3.1 Bitumen

Table 2.2 gives bitumen densities measured at different temperatures and pressures. As expected, the density of bitumen decreased with increasing temperature at a constant pressure, and increased with increasing pressure at a constant temperature. In **Figure 2.3**, the solid lines show that the effect of pressure on bitumen density is more significant at higher temperatures.

Measured densities were correlated with the Tait equation, taking into account the impact of pressure and temperature, as follows:

$$\rho\,(T,P) = \frac{\rho_0\,(T,P_0)}{1-\beta\ln(\frac{B+0.001P}{B+0.1})}, \tag{2.2}$$

where

$$\rho_0 = 1149.3967 - 0.3822T - 3.5378\times10^{-4}T^2 \tag{2.3}$$

$$\beta = (-16.7695 + 0.0578T) \tag{2.4}$$

$$B = 3.7568\times10^4 - 1.8009\times10^7T^{-1} + 2.0605\times10^9T^{-2}. \tag{2.5}$$

In the above equations, ρ is the density of bitumen in kg/m^3, ρ_0 is the density at atmospheric pressure, T is temperature in K, and P is pressure in kPa. **Figure 2.4** indicates that the correlation yields a good match with experimental data. The coefficient of determination (R^2) for the correlated Tait equation is 0.9971, and the average absolute relative deviation (AARD) is 0.1%.

Saturation pressures of the bitumen sample were measured at 140.2°C and 160.0°C as given in **Table 2.3**. The vapor phase was observed through the PVT-cell window. The total volume and volume of each phase were recorded by use of the cathetometer. For example, **Figure 2.5** shows the measured PV data for bitumen at 140.2°C, in which the saturation point can be clearly determined as the intersection of the two PV curves. **Table 2.4** shows the variation of liquid-phase and vapor-phase volume fractions measured at different pressures for the bitumen sample.

The bitumen was characterized by use of the Peng-Robinson equation of state (PR EOS) with the van der Waals mixing rules (Peng and Robinson 1976, 1978). For consistency, it was aimed to obtain a single set of parameters for the PR EOS to correlate all data obtained in this chapter. The bitumen was split into four pseudo components (PCs) by use of the chi-squared distribution (Quiñones-Cisneros et al. 2004) with the degree of freedom of 4.0. The initial values of critical properties for PCs were calculated through the equations of Krejbjerg and Pedersen (2006). The binary interaction parameters (BIPs) between PCs were set to zero. The initial values of BIPs between water and PCs were calculated through the correlation presented in Venkatramani and Okuno (2016), as follows:

$$BIP = c_1[1 + exp(c_2 - c_3 MW)]^{-1/c_4}, \quad (2.6)$$

where c_1 = 0.24200, c_2 = 65.90912, c_3 = 0.18959, and c_4 = –56.81257. The BIPs between solvent and PCs were firstly calculated from the correlations used in Mehta (1981) and Li (1983) with the constant n = 1.

$$k_{ij} = 1 - [\frac{2\sqrt{V_{C_i}^{1/3} V_{C_j}^{1/3}}}{V_{C_i}^{1/3} + V_{C_j}^{1/3}}]^n, \quad (2.7)$$

where V_{C_i} and V_{C_j} are the critical volumes for components in cm^3/mol.

Then, step-wise adjustment on critical properties and BIPs was applied for matching all experimental data. Critical properties of PCs and BIPs for butane-PCs were adjusted to match L-LV boundaries for n-butane/bitumen (Mixture A), and LL-LLV boundaries for n-butane/bitumen (Mixture B). The water content, 8.64 mol%, in the bitumen sample yielded 2.4 mol% water in Mixture A and 0.2 mol% water in Mixture B. At this point, however, BIPs for water-PCs were not adjusted because of the low water contents in Mixtures A and B. Instead, water-PC BIPs were adjusted to match WLL-WLLV boundaries for Mixture C, in addition to the measured saturation pressures for the bitumen sample. Critical properties and BIPs were finalized primarily for accurate correlation of the phase-boundary data for the presence of the V phase. Then, volume-shift parameters (C_{PEN}) of PCs were used for matching liquid density data. **Tables 2.5 and 2.6** present the components' parameters for use with the PR EOS, along with the overall compositions for all fluids discussed in this chapter. In particular, it was challenging to represent multiphase behavior data for the highly size-asymmetric polar mixtures of n-butane/bitumen/water, as will be shown in this chapter.

The EOS model gives an AARD of 2.6% for the densities listed in Table 2.2. Table 2.3 compares the experimental data with the EOS predictions in terms of saturated-liquid density and saturation pressure. As given in this table, saturation pressure data were accurately represented by the EOS model. The predicted densities at saturation pressures have the AARD of 6.0% compared with the experimental data. The predicted V phase composition from the EOS model is almost pure water, which is consistent with the measured saturation pressures that are close to

water vapor pressures at corresponding temperatures. It is likely that the measured saturation pressures (Table 2.3) are related to emulsified water in the bitumen sample.

2.3.2 Mixture A (72.23 mol% n-butane + 25.37 mol% bitumen + 2.4 mol% water)

With the procedure mentioned in the experimental section, densities of Mixture A were measured at different temperature-pressure conditions, as summarized in **Table 2.7 and Figure 2.6**. The reference density was measured at 51.1°C and 1.115 MPa at AGAT Lab, Calgary, Canada. Figure 2.6 shows that the effect of pressure on density is more pronounced at higher temperatures for Mixture A.

Densities measured for Mixture A were firstly compared with the values calculated with the following equation assuming no volume change on mixing:

$$\frac{1}{\rho_m} = \frac{w_s}{\rho_s} + \frac{1-w_s}{\rho_B}, \tag{2.8}$$

where w_s is the weight fraction of n-butane. ρ_s and ρ_B are the mass densities of n-butane and bitumen, respectively. The values for ρ_s at different conditions were obtained from the NIST database. The ρ_B values were calculated from equation 2.2. The resulting AARD is 6.1%, which indicates that volume change on mixing should be taken into account for Mixture A.

An excess-volume mixing rule is given as

$$\frac{1}{\rho_m} = \frac{w_s}{\rho_s} + \frac{1-w_s}{\rho_B} - w_s(1-w_s)[\frac{1}{\rho_s} + \frac{1}{\rho_B}]\gamma, \tag{2.9}$$

where γ is the binary interaction parameter between solvent (n-butane) and bitumen for this model. The best-fitted γ, 0.1548, was obtained by regression to the measured densities (Table 2.7). It gives the AARD of 1.3%, which is much lower than that from equation 2.8.

Saturation pressures were measured for Mixture A from 51.1°C to 159.0°C. Only one liquid phase and liquid-vapor phase equilibria were visually observed within this temperature range. The total volume and volume of each phase were recorded by use of the cathetometer. **Table 2.8** shows the variation of liquid-phase and vapor-phase volume fractions measured at different pressures for Mixture A. **Table 2.9** summarizes the results and the comparison with predictions from the EOS model (Tables 2.5 and 2.6). The EOS model reasonably correlates the measured

bubble points as shown in **Figure 2.7**. The AARD from the presented data is 46%. The aqueous (W) phase calculated by the EOS model (Figure 2.7) was not observed experimentally likely because of water-in-oil emulsion in the L phase. Also, the calculated W phase is subject to the uncertainty associated with the water content measured for the bitumen sample. Although n-butane BIPs can be adjusted to obtain a higher correlative accuracy for a particular set of data, the EOS model has been developed by considering all experimental data obtained for all mixtures in this research, as mentioned previously. The predicted densities at saturation points by use of the EOS model give an AARD of 2.4% compared with experimental data (Table 2.9). For the data given in Table 2.7, the EOS model gives an AARD of 2.2%. The V phase composition predicted from the EOS model is almost pure butane.

2.3.3 Mixture B (97.24 mol% n-butane + 2.52 mol% bitumen + 0.24 mol% water)

The mole fraction of n-butane in this mixture was specifically chosen for potentially observing three co-existing phases, consisting of the bitumen-rich liquid (L_1), solvent-rich liquid (L_2), and gaseous (V) phases. The phase-boundary pressures measured for Mixture B at different temperatures are listed in **Table 2.10**. These phase-boundary pressures were visually observed, and also confirmed by plotting pressure-volume (PV) data. For example, **Appendix E** shows the measured PV relationship at different temperatures. The slope for PV data exhibits a change when another phase emerges. Therefore, a phase-boundary pressure can be estimated by the intersection of PV segments. The volume of each phase was determined based on visual observation of the interface between phases by use of the cathetometer. The uncertainty in phase-boundary determination is affected by how clear the interface is. It is ± 0.791 MPa (100 psig) for measurement of L_2-L_1L_2 boundary and ± 0.174 MPa (10.5 psig) for L_1L_2-L_1L_2V boundary, except for the measurements at 50.0°C and 79.9°C. At these two temperatures, it was not easy to determine the boundary between L_1 and L_2 due likely to their similarity in composition. Note that, due to the limited cell volume, the lower-pressure boundary for three phases could not be measured, and was not given in Table 2.10. Even when the piston was retracted to the limit of the PVT cell, the mixture still exhibited the three-phase equilibrium as depicted by the asymptotic behavior of pressure depletion in Appendix E.

Figure 2.8 shows the digital images of L_2, L_1L_2, and L_1L_2V phase equilibria captured at 140.1°C for Mixture B. At 140.1°C and 11.105 MPa, a single L_2 phase was detected; at this high

pressure, liquid-liquid immiscibility did not take place. When the pressure was reduced to 8.375 MPa, liquid-liquid immiscibility appeared in the PVT cell; i.e., L_1L_2 equilibrium was observed. Both phases were not transparent. The L_1 phase was denser, black, and rich in bitumen, while the L_2 phase was less dense, red, and rich in n-butane. Because pure liquid n-butane is colorless, the red color of the L_2 phase implied that it selectively extracted a significant amount of intermediate components from the bitumen. The color of the L_2 phase became darker with increasing pressure and decreasing temperature, indicating more extraction of bitumen components. As the pressure was further decreased to 2.921 MPa, the V phase appeared, resulting in L_1L_2V equilibrium. Due to the limited cell volume, the L_1L_2V phases persisted even when the cell volume reached the maximum; therefore, the lower-pressure boundary of L_1L_2V was not detected. Compared to the L_2 phase at 8.375 MPa, the color of the L_2 phase was lighter at 2.921 MPa, implying that n-butane extracted a smaller amount of heavy components from the bitumen at L_1L_2V equilibrium, but still extracted light and medium components from the bitumen.

The L_1 phase in the L_1L_2 and L_1L_2V regions is considered to be richer in asphaltene components than the original bitumen because asphaltene components are insoluble in n-butane, as demonstrated in the research of Zou et al. (2006) for their bitumen/solvent mixtures. It is possible that asphaltene precipitation happened at the temperature-pressure conditions tested (even in the single L_2-phase region), considering the high n-butane concentration in the mixture. Asphaltene components may have resided in an oleic phase as dispersed particles as described in Agrawal et al. (2012). However, it was not possible to observe asphaltene precipitation with the current PVT setup which is not equipped with a solid phase detection unit.

Figure 2.9 shows the comparison of experimental data and predictions for phase boundaries. The phase labeling in this figure is based on the continuity of phase compositions on phase transitions calculated from the EOS model. The three-phase region of L_1L_2V is predicted as a closed loop from the EOS model, near the higher-pressure boundary observed for three phases. However, the three phases observed at 50.0°C, 79.9°C, and 109.8°C are not represented by the EOS model. The lowest temperature for L_1L_2V equilibrium predicted from the EOS model is approximately 122.8°C. The AARD is 4.2% for the boundary for the presence of the V phase (i.e., bubble points), and 71% for the L-LL boundary from 140.1°C to 160.2°C. Figure 2.9 also

shows that higher-pressure boundaries observed for three phases are well correlated with the extension of n-butane's vapor pressure. EOS calculations further indicate that the L_1 and L_2 phases are close to each other near the critical temperature of n-butane in the LV two-phase region. This gives the dashed demarcation line between L_1V on the higher-temperature side and L_2V on the lower-temperature side in Figure 2.9. The W phase calculated by the EOS model was not experimentally observed for the same reasons mentioned in the previous section.

Multiphase flash calculations were performed for Mixture B at 140.1°C as shown in **Figure 2.10**. The water content in each liquid phase is calculated to be smaller than 0.5 mol%, which is not shown in this figure. Figure 2.10a shows that the volumetric predictions for the L_1L_2 region reasonably agree with the measured data, while a larger deviation occurs for the three-phase region.

Phase compositions were calculated as shown in Figures 2.10b-d. Results indicate that, as the pressure is decreased, the L_1 phase is split from the L_2 phase at the L_2-L_1L_2 boundary, and the V phase in the three-phase region is almost pure n-butane. The solubility of butane in bitumen is not sensitive to pressure in the L_1L_2 region as shown in Figures 2.10b and c. The n-butane fraction in the L_1 phase first decreases with decreasing pressure in the L_1L_2 region, but then increases in the three-phase region. In comparison, the n-butane fraction in the L_2 phase increases slightly and gradually with decreasing pressure in the L_1L_2 region. This is consistent with the observation that the color of the L_2 phase became lighter, indicating that the L_2 phase became richer in butane with decreasing pressure in the experiment. After passing the two-phase region and entering the L_1L_2V region, however, the n-butane concentration in the L_2 phase sharply decreases with a further decrease in pressure. Figure 2.10d shows that the V phase contains only n-butane. Figures 2.10e and f show the detailed variations in the fractions of pseudocomponents in the L_1 and L_2 phases, respectively. It can be seen from Figure 2.10f that the concentrations of lighter pseudocomponents in the L_2 phase rapidly increase with decreasing pressure in the three-phase region. The L_2 phase extracts lighter pseudocomponents more than heavier pseudocomponents from the bitumen in the three-phase region. This confirms the experimental observation that the L_2 phase became lighter color as the pressure was decreased (Figure 2.8). As shown in Figures 2.10bcef, the EOS model predicts that the L_1 and L_2

compositions become close to each other at the lower-pressure limit of the three-phase region, indicating near-critical-endpoint behavior of type L_1=L_2-V at 140.1°C.

Figure 2.11 presents volumetric data and volumetric/compositional predictions from the EOS model for Mixture B at 160.2°C. Figure 2.11a the volumetric predictions reasonably agree with the data. The mutual solubility of n-butane and bitumen in the L_1L_2 region is only slightly affected by the pressure change. Figures 2.11bc show the n-butane and bitumen fractions in the L_1 and L_2 phases for Mixture B at 160.2°C. Their trends are similar to those shown for Mixture B at 140.1°C. The L_2 phase contains bitumen components at 160.2°C less than at 140.1°C, which is in line with the experiment observation that the color of the L_2 phase became lighter at higher temperatures at a given pressure. Figure 2.11d shows that the V phase contained only n-butane.

Results in this section indicate that n-butane was able to extract a significant amount of light and medium components from the bitumen in the L_2 phase, while the bitumen was substantially diluted by n-butane in the L_1 phase. The total weight fraction of lighter bitumen pseudocomponents (PC-1 and PC-2) in the L_2 phase is calculated to be approximately 11 wt% (2.0 mol%) in the L_1L_2 equilibrium region at 140.1°C, and around 24 wt% (6.1 mol%) in the three-phase region by use of the PR-EOS model. The L_1 phase is calculated to contain approximately 81 wt% (17 mol%) bitumen components in the L_1L_2 equilibrium region, and 64 wt% (12 mol%) bitumen components in the L_1L_2V region. The L_1 and L_2 phases may contribute to the overall production of bitumen in ES-SAGD. However, the effect of the resulting multiphase flow on bitumen production is uncertain. The solubility of butane in bitumen may be limited by the L_1L_2 separation at operating conditions for steam-solvent coinjection, such as ES-SAGD, even when a sufficient accumulation of n-butane takes place near a chamber edge. Experimental observations given in Figure 2.9 show that the L_1L_2 separation may occur at a wide range of temperatures at operating pressures in ES-SAGD.

2.3.4 Mixture C (37.02 mol% n-butane + 0.96 mol% bitumen + 62.02 mol% water)

After the multiphase equilibrium measurements for Mixture B, 7.389 g of distilled water was injected into the PVT cell. Four co-existing phases, consisting of L_1, L_2, V, and W phases, were observed over a wide range of temperature-pressure conditions. **Table 2.11** summarizes the

phase-boundary pressures measured for Mixture C at different temperatures. The phase-boundary measurement was also attempted at 50.0°C. However, it was difficult due to water-in-oil and oil-in-water emulsion formation as briefly discussed in the next subsection.

Appendix F shows the measured PV data for Mixture C at different temperatures. Phase boundary pressures were confirmed by visual observation and by the intersections of PV segments for each temperature. The uncertainty in measurement is ± 1.136 MPa (150 psig) for WL_2-WL_1L_2 phase boundaries and ± 0.174 MPa (10.5 psig) for WL_1L_2-WL_1L_2V boundaries, except for the measurements at 80.0°C and 110°C. At these two temperatures, the interface between the L_1 and L_2 phases was unclear from visual observation and PV plots (Appendix F).

Figure 2.12 shows the digital photos taken during the phase equilibrium tests for Mixture C. At the temperature-pressure conditions in this research, the W phase was always denser than the L_1 phase. As can be seen in Figure 2.12, the W phase was transparent, but contained some hydrocarbon droplets that were denser than the water; that is, the droplets likely consisted of bitumen components, e.g., asphaltenes. At 159.9°C and 27.687 MPa, the W and L_2 phases were observed, where the W phase was below the L_2 phase. When the pressure declined to 8.258 MPa, liquid-liquid separation of hydrocarbons happened, resulting in the WL_1L_2 equilibrium. In this WL_1L_2 equilibrium, the L_1 phase was situated between and the W and L_2 phases. The L_2 phase showed a lighter color than the L_1 phase due to a higher fraction of n-butane. With the pressure further decreasing to 4.576 MPa, the four-phase equilibrium of WL_1L_2V was detected, where the V phase appeared on top of the existing phases. The L_2 phase became lighter color than at 8.258 MPa, implying that n-butane extracted a smaller amount of heavy components from the bitumen at WL_1L_2V equilibrium. Again, due to the limited PVT cell volume, the WL_1L_2V phase equilibria persisted all the way up to the maximum cell volume, and the lower phase boundary was not detected.

Figure 2.13 compares the phase boundaries observed with those from the EOS model (Tables 2.5 and 2.6) for Mixture C. The phase labeling in this figure is based on the EOS model as for Figure 2.9. The AARD is 1.1% for the boundary for the presence of the vapor phase, and 33% for the WL-WLL boundary at temperatures from 140.0°C to 159.9°C. The higher-pressure boundaries for the four phases are calculated close to the extension of n-butane's vapor pressure; however, they are higher than the corresponding vapor pressures of n-butane, unlike in Mixture

B (Figure 2.9). This is likely because the higher-pressure boundary for the presence of the V phase for Mixture C (Figure 2.13) is increased by water vapor pressure, compared with that for Mixture B (Figure 2.9). The four-phase region of WL_1L_2V is predicted as a closed loop from the EOS model, near the lower-pressure boundaries measured for the WL_1L_2 region. As mentioned previously, however, no lower-pressure boundary for WL_1L_2V was observed experimentally. The phase transition between three and four phases was not represented by the EOS model at 80.0°C and 110.0°C. The EOS model gives a large deviation in representing the WL_2-WL_1L_2 boundary at lower temperatures. As mentioned previously, the interface between L_1 and L_2 tended to be unclear at lower temperatures. The phase compositions of L_1 and L_2 are calculated to be close to each other near the critical temperature of n-butane in the WLV region (either WL_1V or WL_2V in Figure 2.13).

Figure 2.14 shows the measured volumetric data and volumetric/compositional predictions from the EOS model for Mixture C at 140.0°C. Figure 2.14a demonstrates that a better prediction in the phase saturations was achieved with the EOS model for the four-phase region compared to that for the three-phase region. Figures 2.14b and c indicate that adding water to an n-butane/bitumen mixture resulted in water dissolution into hydrocarbon liquid phases at elevated temperatures. The L_1 phase exhibited a higher water concentration than the L_2 phase. This is because the L_1 phase contained a higher bitumen fraction, that is, a higher level of aromaticity (Venkatramani and Okuno 2015). For the WL_1L_2 equilibrium at 140.0°C (Figure 2.14), the water concentration is calculated to be around 3.5 mol% in the L_1 phase, and around 2.0 mol% in the L_2 phase. The EOS model indicates that the V phase in the four-phase equilibrium is a mixture of n-butane and water.

The phase-composition analysis for Mixture C at 159.9°C is shown in **Figure 2.15**. A higher water concentration in the L_1 phase is calculated at this temperature than at 140.0°C. As simulated in Venkatramani and Okuno (2016), water dissolution in the L_1 phase can reduce the L_1-phase viscosity and increase bitumen production rate in SAGD and ES-SAGD, the extent of which depends on temperature near the chamber edge. Figures 2.14bc and 2.15bc also indicate that Mixture C may be closer to a critical endpoint of L_1=L_2-V at 140.0°C than at 159.9°C. This is likely because of the extraction of bitumen components by n-butane is more significant at the lower temperature. Figures 2.15e and f show detailed variations in pseudocomponents' fractions

in the L_1 and L_2 phases, respectively. It can be seen from Figure 2.15c that the n-butane fraction decreases with decreasing pressure from the three-phase to four-phase zone. However, the L_2 phase extracts lighter pseudocomponents more than heavier pseudocomponents from the bitumen in the four-phase region as shown in Figure 2.15f. This is in line with the experimental observation that the L_2 phase became lighter color as the pressure was decreased (Figure 2.12).

2.3.5 Oil-in-water and Water-in-oil Emulsion

The series of isothermal experiments for Mixture C were conducted from the highest temperature, 159.9°C, and then the temperature was decreased in a step-wise manner. It became more difficult to observe the W phase at lower temperatures mainly because of oil-in-water emulsion caused by the repeated usage of the PVT-cell stirrer.

After the multiphase equilibrium measurements for Mixture B, distilled water was injected into the PVT cell at 50.0°C and 5.617 MPa (800 psig). Without turning on the magnetic stirrer before measurements for Mixture C, W-L_2 phases were clearly observed in the PVT cell at this temperature-pressure condition. After a series of measurements from 159.9°C to 50.0°C, however, there was only one single liquid phase in the PVT cell at the same temperature-pressure condition, 50.0°C and 5.617 MPa.

Then, the pressure was reduced to 0.1 MPa at 50.0°C, and water was observed as shown in **Figure 2.16.** Figure 2.16b is an enlarged photo for the detected water. The existence of oil-in-water emulsion can be also confirmed by the comparison with the clear W phase at 159.9°C given in Figure 2.12. The overall composition is identical in these two figures.

Also, water-in-oil emulsion likely occurred because water came out of the hydrocarbon liquid phases as water-in-oil emulsion, instead of as a separate bulk phase, as the temperature was decreased. This type of water precipitation in the oleic phase was described also in Glandt and Chapman (1995). In this research, water-in-oil emulsion was confirmed by comparing the mass of injected water (7.389 g) and the mass of the W phase after completing measurements (7.347 g).

2.4 Conclusions

This chapter presented an experimental study of multiphase behavior for n-butane/Athabasca-bitumen/water mixtures at temperatures up to 160°C and pressures up to 10 MPa. The data presented in this chapter include liquid densities and multiphase boundaries for 100% bitumen, two mixtures of n-butane/bitumen, and one mixture of n-butane/bitumen/water. Although limited in correlative accuracy, a single thermodynamic model was made to correlate all data measured for all mixtures on the basis of the Peng-Robinson equation of state with the van der Waals mixing rules. Conclusions are as follows:

1. Liquid-liquid separation of hydrocarbons (L_1L_2) was experimentally observed at the butane concentration of 97 mol% in the n-butane/bitumen system with/without water (Mixtures B and C) for a wide range of temperatures at operating pressures for ES-SAGD. This may indicate the limited solubility of butane in bitumen even when a high level of accumulation of butane takes place near a chamber edge in ES-SAGD for Athabasca bitumen.

2. It was observed that the color of the L_2 phase became lighter with decreasing pressure in the LLV region for Mixture B and in the WLLV region for Mixture C. This may indicate the selective extraction of bitumen components by n-butane at lower pressure; the L_2 phase became richer in lighter pseudocomponents rapidly with decreasing pressure in the LLV region for Mixture B and in the WLLV region for Mixture C.

3. The multiphase transition that involves appearance/disappearance of the V phase was observed to occur near the vapor pressure of n-butane or its extension. Such phase transition occurs at a higher pressure in the presence of water (Mixture C), due to its vapor pressure, than in the absence of water (Mixture B) at a given temperature.

4. Water-in-oil emulsion may occur when dissolved water in the oleic phase comes out of the solution at a lower temperature even without significant stirring.

5. Near-miscibility of two liquid phases and oil-in-water emulsion made it difficult to conduct phase boundary measurements in this research. The experimental setup and/or procedure should be improved in this regard.

References:

Agrawal, P., Schoeggl, F.F., Satyro, M.A., Taylor, S.D., and Yarranton, H.W. 2012. Measurement and Modeling of the Phase Behavior of Solvent Diluted Bitumens. *Fluid Phase Equilibria.* **334**: 51-64.

Amani, M.J., Gray, M.R., and Shaw, J.M. 2013. Phase Behavior of Athabasca Bitumen+ Water Mixtures at High Temperature and Pressure. *J. Supercri. Fluid.* **77**: 142-152.

Amani, M.J., Gray, M.R., and Shaw, J.M. 2014. The Phase Behavior of Athabasca Bitumen+Toluene+Water Ternary Mixtures. *Fluid Phase Equilibr.* **370**: 75-84.

Ardali, M., Mamora, D.D., and Barrufet, M. 2010. A Comparative Simulation Study of Addition of Solvents to Steam in SAGD Process. CSUG/SPE paper 138170 presented at Canadian Unconventional Resources and International Petroleum Conference, Calgary, Alberta, Canada, October 19-21.

Ardali, M., Barrufet, M., and Mamora, D.D. 2012. Laboratory Testing of Addition of Solvents to Steam to Improve SAGD Process. Paper SPE 146993 presented at SPE Heavy Oil Conference Canada , Calgary, Alberta, Canada, June 12-14.

Arshad, M. and Li, H. 2015. Multiphase Equilibria of Solvent-Steam-Bitumen System within SAGD Steam-Chamber Boundary. Paper SPE 174444 presented at the SPE heavy oil conference-Canada, Calgary, Alberta, Canada, June 11-13, 2015.

Ashrafi, M., Souraki, Y., Karimaie, H., Torsaeter, O., and Bjorkvik, B.J. 2011. Experimental PVT Property Analyses for Athabasca Bitumen. CSUG/SPE paper 147064 presented at the Canadian Unconventional Resources Conference, Calgary, Alberta, Canada, November 15-17.

Azinfar, B., Zirrahi, M., Hassanzadeh, H., and Abedi, J. 2014. A New Method for the Characterization of Heavy Oil and Bitumen using Distillation Curve Data. Paper SPE 172846 presented at the SPE International Heavy Oil Conference and Exhibition, Mangaf, Kuwait, December 8-10.

Badamchi-Zadeh, A., Yarranton, H.W., Svrcek, W.Y., and Maini, B.B. 2009. Phase Behaviour and Physical Property Measurements for VAPEX Solvents: Part I. Propane and Athabasca bitumen. *J. Can. Petro. Tech.* **48**(01): 54-61.

Bulter, R.M. 1991. *Thermal Recovery of Oil and Bitumen.* Prentice Hall, New Jersey.

Díaz, O.C., Modaresghazani, J., Satyro, M.A., and Yarranton, H.W. 2011. Modeling the Phase Behavior of Heavy Oil and Solvent Mixtures. *Fluid Phase Equilibr.* **304** (1): 74-85.

Díaz, O.C., Schoeggl, F.F., Yarranton, H.W., and Satyro, M.A. 2013. Measurement of Heavy Oil and Bitumen Vapor Pressure for Fluid Characterization. *Ind. & Eng.Chem. Res.* **52**(8): 3027-3035.

Ezeuko, C.C., Wang, J., and Gates, I.D. 2013. Investigation of Emulsion Flow in Steam-Assisted Gravity Drainage. *SPE J.* **18**(03): 440-447.

Glandt, C.A., and Chapman, W.G. 1995. The Effect of Water Dissolution on Oil Viscosity. *SPE Res. Eng.* **10**(01): 59-64.

Govind, P.A., Das, S.K., Srinivasan, S., and Wheeler, T.J. 2008. Expanding Solvent SAGD in Heavy Oil Reservoirs. Paper SPE/PS/CHOA 117571 presented at the 2008 SPE International Thermal Operations and Heavy Oil Symposium, Calgary, Alberta, Canada, October 20-23.

Jindrová, T., Mikyška, J., and Firoozabadi, A. 2015. Phase Behavior Modeling of Bitumen and Light Normal Alkanes and CO2 by PR-EOS and CPA-EOS. *Energy Fuels*. **30**(1): 515-525.

Jha, R.K., Kumar, M., Benson, I., and Hanzlik, E. 2012. New Insights into Steam-Solvent Co-injection Process Mechanism. Paper SPE 159277 presented at 2012 SPE Annual Technical Conference and Exhibition, San Antonio, Texas, October 8-10.

Kariznovi, M., Nourozieh, H., and Abedi, J. 2011. Experimental Apparatus for Phase Behavior Study of Solvent–Bitumen Systems: A Critical Review and Design of A New Apparatus. *Fuel.* **90**(2): 536-546.

Kariznovi, M., Nourozieh, H., and Abedi, J. 2014. Measurement and Correlation of Viscosity and Density for Compressed Athabasca Bitumen at Temperatures Up to 200ºC. *J. Can. Petro. Tech.* **53**(06), 330-338.

Kariznovi, M., Nourozieh, H., and Abedi, J., 2009. Bitumen Characterization and Pseudocomponents Determination for Equation of State Modeling. *Energy Fuels.* **24** (1): 624-633.

Keshavarz, M., Okuno, R., and Babadagli, T. 2014. Efficient Oil Displacement Near the Chamber Edge in ES-SAGD. *J. Petro. Sci. Eng.* **118**: 99-113.

Krejbjerg, K., and Pedersen, K.S. 2006. Controlling VLLE Equilibrium with a Cubic EOS in Heavy Oil Modeling. Paper PETSOC-2006-052 presented at the Canadian International Petroleum Conference, Calgary, Alberta, Canada, June 13-15.

Kumar, A., and Okuno, R. 2016. A New Algorithm for Multiphase Fluid Characterization for Solvent Injection. Accepted for publication in *SPE Journal* on March 8, 2016. SPE-175123-PA.

Leekumjorn, S., and Krejbjerg, K. 2013. Phase Behavior of Reservoir Fluids: Comparisons of PC-SAFT and Cubic EOS Simulations. *Fluid Phase Equilibr.* **359**: 17-23.

Li, H., Yang, D., and Li, X. 2012. Determination of Three-Phase Boundaries of Solvent (s)–CO2–Heavy Oil Systems under Reservoir Conditions. *Energy Fuels.* **27**(1): 145-153.

Li, W., and Mamora, D.D. 2010. Phase Behavior of Steam with Solvent Co-injection under Steam Assisted Gravity Drainage (SAGD) Process. Paper SPE 130807 presented at SPE EUROPEC/EAGE Annual Conference and Exhibition, Barcelona, June 14-17.

Li, W., Mamora, D.D., and Li, Y. 2011c. Solvent-Type and –Ratio Impacts on Solvent-Aided SAGD Process. *SPE Res. Eval.and Eng.* **14** (3): 320-331.

Li, Y.K., Heavy Fraction Characterization and Hypothetical Component Selection for Oil and Gas Mixtures. Computer Modelling Group Research Report R12.04. May 1983.

Li, Z., and Firoozabadi, A. 2010. Modeling Asphaltene Precipitation by n-Alkanes from Heavy Oils and Bitumens Using Cubic-Plus-Association Equation of State. *Energy and Fuels*. **24**(2): 1106-1113.

Ma, M., Chen, S., and Abedi, J. 2016. Predicting the Multiphase Equilibrium and Density of Bitumen with C2H6, C3H8 and CO2 Using the Simplified PC-SAFT Equation of State. *Fuel*. **181**: 652-659.

Mehra, R.K. 1981. The Computation of Multi-Phase Equilibrium in Compositional Reservoir Studies. PHD Dissertation. University of Calgary.

Mohammadzadeh, O., Rezaei, N., and Chatzis, I. 2012. More Insight into the Pore-Level Physics of the Solvent-Aided SAGD (SA-SAGD) Process for Heavy Oil and Bitumen Recovery. Paper SPE 157776 presented at SPE Heavy Oil Conference Canada, Calgary, Alberta, Canada, June 12-14.

Mohebati, M.H., Maini, B.B., and Harding, T.G. 2010. Optimization of Hydrocarbon Additives With Steam in SAGD for Three Major Canadian Oil Sands Deposits. CSUG/SPE paper 138151 presented at Canadian Unconventional Resources and International Petroleum Conference, Calgary, Alberta, Canada, October 19-21.

Nagarajan, N.R., Honarpour, M.M., and Sampath, K. 2006. Reservoir Fluid Sampling and Characterization—Key to Efficient Reservoir Management. Paper SPE 101517 presented at the Abu Dhabi International Petroleum Exhibition and Conference, Abu Dhabi, U.A.E., November 5-8.

Nasr, T.N. and Isaacs, E. 2001. Process for Enhancing Hydrocarbon Mobility Using a Steam Additive. U.S. Patent 6230814.

Nasr, T.N., Beaulieu, G., Golbeck, H., and Heck, G. 2003. Novel Expanding Solvent-SAGD Process "ES-SAGD". *J. Can. Petro. Tech.* **42** (1): 13-16.

Nguyen, D., Phan, J., and Balsamo, V. 2013. Effect of Diluents on Interfacial Properties and SAGD Emulsion Stability: I. Interfacial Rheology. Paper SPE 165405 presented at the SPE Heavy Oil Conference Canada, Calgary, Alberta, Canada, June 11-13.

Noik, C., Dalmazzone, C.S., Goulay, C., and Glenat, P. 2005. Characterisation and Emulsion Behaviour of Athabasca Extra Heavy Oil Produced by SAGD. Paper SPE/PS/CHOA 97748 presented at the 2005 SPE International Thermal Operations and Heavy Oil Symposium, Calgary, Alberta, Canada, November 1-3.

Nourozieh, H., Kariznovi, M., and Abedi, J. 2014a. Measurement and Prediction of Density for the Mixture of Athabasca Bitumen and Pentane at Temperatures up to 200°C. *Energy Fuels.* **28**(5): 2874-2885.

Nourozieh, H., Kariznovi, M., and Abedi, J. 2014b. Phase Behaviour Study of Butane/Athabasca Bitumen Mixtures Applicable for Thermal and Hybrid Solvent Recovery Processes. Paper SPE 170163 presented at the SPE Heavy Oil Conference-Canada, Calgary, Alberta, Canada, June 10-12.

Nourozieh, H., Kariznovi, M., and Abedi, J. 2015a. Modeling and Measurement of Thermo-Physical Properties for Athabasca Bitumen and n-Heptane Mixtures. *Fuel.* **157**: 73-81.

Nourozieh, H., Kariznovi, M., and Abedi, J. 2015b. Measurement and Prediction of Volumetric Properties for Undersaturated Athabasca Bitumen.*Energy Fuels.* **29**(8): 4711-4720.

Nourozieh, H., Kariznovi, M., and Abedi, J. 2015c. Experimental and Modeling Studies of Phase Behavior for Propane/Athabasca Bitumen Mixtures. *Fluid Phase Equilibr.* **397**: 37-43.

Nourozieh, H., Kariznovi, M., and Abedi, J. 2015d. Density and Viscosity of Athabasca Bitumen Samples at Temperatures Up to 200°C and Pressures Up to 10 MPa. *SPE Res. Eval. and Eng.* **18** (03): 375-386.

Panuganti, S.R., Vargas, F.M., Gonzalez, D.L., Kurup, A.S., and Chapman, W.G. 2012. PC-SAFT Characterization of Crude Oils and Modeling of Asphaltene Phase Behavior. *Fuel*. **93**: 658-669.

Péneloux, A., Rauzy, E., and Fréze, R. 1982. A Consistent Correction for Redlich-Kwong-Soave Volumes. *Fluid Phase Equilibr.* **8**(1): 7-23.

Peng, D.Y., and Robinson, D.B. 1976. A New Two-constant Equation of State. *Ind. Eng. Chem. Fund.* **15**(1): 59-64.

Prats, M. 1982. *Thermal Recovery.* SPE Monograph Series Volume 7, Henry L. Doherty Series., New York.

Quiñones-Cisneros, S.E., Dalberg, A., and Stenby, E.H. 2004. PVT Characterization and Viscosity Modeling and Prediction of Crude Oils. *Petro. Sci. Tech.* **22**(9-10): 1309-1325.

Redford, D.A. and McKay, A.S. 1980. Hydrocarbon-Steam Processes for Recovery of Bitumen from Oil Sands. Paper SPE 8823 presented at SPE/DOE Enhanced Oil Recovery Symposium, Tulsa, Oklahoma, USA, April 20-23.

Robinson, D.B., and Peng, D.Y. 1978. The Characterization of the Heptanes and Heavier Fractions for the GPA Peng-Robinson Programs. *Gas Processors Association.*

Saryazdi, F., Motahhari, H., Schoeggl, F.F., Taylor, S.D., and Yarranton, H.W. 2013. Density of Hydrocarbon Mixtures and Bitumen Diluted with Solvents and Dissolved Gases. *Energy Fuels.* **27**(7): 3666-3678.

Svrcek, W.Y., and Mehrotra, A.K. 1982. Gas Solubility, Viscosity and Density Measurements for Athabasca Bitumen. *J. Can. Petro. Tech.* **21**(04): 31-38.

Tavakkoli, M., Panuganti, S.R., Taghikhani,V., Pishvaie, M.R., and Chapman, W.G. 2013. Precipitated Asphaltene Amount at High-Pressure and High-Temperature Conditions. *Energy and Fuels.* **28**(3): 1596-1610.

Venkatramani, A., and Okuno, R. 2015. Characterization of Water-Containing Reservoir Oil Using an EOS for Steam Injection Processes. *J. Nat. Gas Sci. Eng.* **26**: 1091-1106.

Venkatramani, A., and Okuno, R. 2016. Compositional Mechanisms in SAGD and ES-SAGD with Consideration of Water Solubility in Oil. Paper SPE 180737-MS presented at the SPE Canada Heavy Oil Technical Conference, Calgary, Alberta, Canada, June 7-8, 2016.

Yazdani, A., Alvestad, J., Kjonsvik, D., Gilje, E., and Kowalewski, E. 2011. A Parametric Simulation Study for Solvent Co-injection Process in Bitumen Deposits. Paper SPE 148804 presented at the Canadian Unconventional Resources Conference, Calgary, Alberta, Canada, November 15-17.

Zirrahi, M., Hassanzadeh, H., and Abedi, J. 2015a. Prediction of CO2 Solubility in Bitumen Using the Cubic-Plus-Association Equation of State (CPA-EOS). *J. Supercritical Fluids*. **98**: 44-49.

Zirrahi, M., Hassanzadeh, H., and Abedi, J. 2015b. Prediction of Water Solubility in Petroleum Fractions and Heavy Crudes Using Cubic-Plus-Association Equation of State (CPA-EoS). *Fuel*. **159**: 894-899.

Zou, X.Y., Zhang, X., and Shaw, J.A. 2007. Phase Behavior of Athabasca Vacuum Bottoms+ n-Alkane Mixtures. *SPE Prod and Oper*. **22**(02): 265-272.

Zúñiga-Hinojosa, M.A., Justo-García, D.N., Aquino-Olivos, M.A., Román-Ramírez, L.A., and García-Sánchez, F. 2014. Modeling of Asphaltene Precipitation from n-Alkane Diluted Heavy Oils and Bitumens Using the PC-SAFT Equation of State. *Fluid Phase Equilibr*. **376**: 210-224.

Tables and Figures:

Mixture	Butane, mol%	Bitumen, mol%	Distilled Water, mol%	Butane, wt%	Bitumen, wt%	Distilled Water, wt%
A	72.23	27.77	0.00	19.19	80.81	0.00
B	97.24	2.76	0.00	76.29	23.71	0.00
C	37.02	1.05	61.93	54.65	16.97	28.37

Table 2.1 – Compositions of three n-butane/bitumen/water mixtures in this research.

T, °C	P, MPa	ρ, kg/m^3	T, °C	P, MPa	ρ, kg/m^3
15.6	0.101	1010.4	50.1	4.100	992.1
20.0	0.101	1007.7	50.1	7.093	995.1
25.0	0.101	1004.4	50.1	10.106	997.9
30.0	0.101	1001.3	80.4	1.094	974.9
35.0	0.101	998.1	80.4	4.114	977.3
40.0	0.101	994.9	80.4	7.113	979.4
45.0	0.101	991.7	80.4	10.113	982.0
50.0	0.101	988.5	110.0	1.094	953.9
55.0	0.101	985.2	110.0	4.107	957.1
60.0	0.101	982.0	110.0	7.106	960.4
65.0	0.101	978.7	110.0	10.113	962.5
70.0	0.101	975.3	140.2	0.791	931.3
75.0	0.101	971.6	140.2	3.928	936.3
80.0	0.101	967.7	140.2	7.086	939.6
15.6	1.094	1012.7	140.2	10.119	942.7
15.6	4.107	1015.2	160.0	0.798	914.4
15.6	7.113	1016.6	160.0	3.831	922.1
15.6	10.113	1018.8	160.0	6.851	925.1
50.1	1.094	989.4	160.0	9.561	927.2

Table 2.2 – Densities of bitumen at different temperature-pressure conditions. Measurement of density at 0.101 MPa was conducted by the densitometer. Densities of bitumen at pressures above 0.101 MPa were measured by use of a PVT cell.

T, °C	Experimental data		Predictions from EOS model	
	P, MPa	ρ^{sat}, kg/m^3	P, MPa	ρ^{sat}, kg/m^3
140.2	0.337	932.8	0.349	983.6
160.0	0.484	917.9	0.436	978.4

Table 2.3 – Measured and predicted saturation pressures and saturated-liquid densities of the bitumen sample. The vapor phase was only observed at 140.2°C and 160.0°C in the saturation-pressure measurement for bitumen.

T, °C	P, MPa	Volume fraction of liquid phase	Volume fraction of vapor phase
140.2	0.322	0.933	0.067
140.2	0.322	0.887	0.113
140.2	0.315	0.852	0.148
140.2	0.301	0.820	0.180
140.2	0.301	0.791	0.209
140.2	0.288	0.752	0.248
160.0	0.481	0.960	0.041
160.0	0.467	0.858	0.142
160.0	0.467	0.761	0.240
160.0	0.322	0.933	0.067

Table 2.4 – Measured liquid-phase and vapor-phase volume fractions of the bitumen sample at different temperature-pressure conditions.

	MW	T_C, °C	P_C, MPa	ω	V_C, cm^3/mol	C_{PEN}, cm^3/mol	Bitumen, mol%	Mixture A, mol%	Mixture B, mol%	Mixture C, mol%
C_4	58.123	152.0	3.796	0.2014	254.617	-6.148	0.00	72.23	97.24	37.02
water	18.010	373.9	22.064	0.3433	63.071	-0.091	8.64	2.40	0.24	62.02
PC-1	296.939	435.0	2.146	0.8423	612.873	-147.701	48.84	13.57	1.35	0.51
PC-2	662.802	495.1	1.507	0.9429	920.536	-275.005	21.88	6.08	0.60	0.23
PC-3	1082.668	725.0	1.364	1.0225	1,299.294	-447.976	13.40	3.72	0.37	0.14
PC-4	2003.494	1072.9	1.045	1.1486	2,192.365	-936.360	7.24	2.01	0.20	0.08

Table 2.5 –Components' properties of the characterized EOS model and compositions for the fluids discussed in this research. Bitumen was characterized as a mixture of four pseudo components, PC-1, -2, -3, and -4. C_{PEN} is the volume-shift parameter of Péneloux et al. (1982).

	C_4	Water	PC-1	PC-2	PC-3
Water	0.6360				
PC-1	-0.0005	0.2006			
PC-2	-0.0011	0.1694	0.0000		
PC-3	-0.0018	0.1694	0.0000	0.0000	
PC-4	-0.0031	0.1694	0.0000	0.0000	0.0000

Table 2.6 – Binary interaction parameters used for the EOS model.

T, °C	P, MPa	ρ, kg/m^3	T, °C	P, MPa	ρ, kg/m^3
51.1	1.115	901.5	110.8	7.079	856.5
51.1	4.128	903.7	110.8	10.113	860.0
51.1	7.086	904.8	140.1	4.093	830.7
51.1	10.126	905.8	140.1	7.079	833.7
81.1	1.094	872.3	140.1	10.119	837.0
81.1	4.100	876.0	159.0	4.107	814.5
81.1	7.079	878.8	159.0	7.093	818.9
81.1	10.126	880.5	159.0	10.099	824.0
110.8	4.107	853.0			

Table 2.7 – Densities of Mixture A measured at different temperature-pressure conditions by the PVT cell on the basis of constant composition expansion.

T, °C	P, MPa	Volume fraction of liquid phase	Volume fraction of vapor phase
51.1	0.267	0.877	0.123
51.1	0.267	0.845	0.155
51.1	0.260	0.827	0.173
81.1	0.598	0.882	0.119
81.1	0.598	0.848	0.152
81.1	0.591	0.825	0.175
110.8	1.080	0.912	0.089
110.8	1.067	0.852	0.148
110.8	1.060	0.828	0.172
110.8	1.046	0.803	0.197
140.1	1.673	0.838	0.163
140.1	1.660	0.817	0.183
140.1	1.646	0.787	0.213
140.1	1.632	0.759	0.242
159.0	2.046	0.778	0.222
159.0	2.039	0.759	0.242
159.0	2.025	0.746	0.254

Table 2.8 – Measured liquid-phase and vapor-phase volume fractions of Mixture A at different temperature-pressure conditions.

	Experimental data		Predictions from EOS model	
T, °C	P, MPa	ρ^{sat}, kg/m^3	P, MPa	ρ^{sat}, kg/m^3
51.1	0.285	901.4	0.399	867.8
81.1	0.611	872.3	0.837	851.1
110.8	1.105	850.1	1.570	832.4
140.1	1.725	827.1	2.592	811.9
159.0	2.148	811.9	3.400	797.6

Table 2.9 – Measured and predicted saturation pressures and densities at saturation points of Mixture A. Only one liquid phase and liquid-vapor phase equilibria were visually observed within this temperature range for Mixture A.

T, °C	L_2-L_1L_2, MPa	L_1L_2-L_1L_2V, MPa
50.0	1.679	0.517
79.9	2.735	0.983
109.8	4.380	1.761
140.1	9.118	2.946
160.2	16.633	4.033

Table 2.10 – Measured phase-boundary pressures for Mixture B.

T, °C	WL_2-WL_1L_2, MPa	WL_1L_2-WL_1L_2V, MPa
80.0	6.633	1.071
110.0	8.050	1.955
140.0	9.411	3.439
159.9	11.820	4.807

Table 2.11 – Measured phase-boundary pressures for Mixture C.

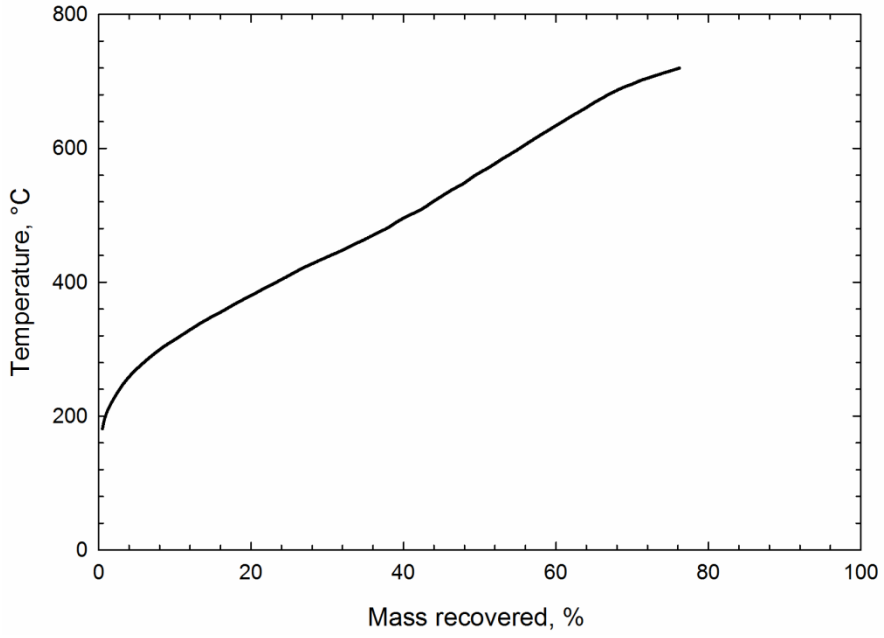

Figure 2.1 – Simulated distillation test results of Athabasca-bitumen sample at temperature up to 720°C.

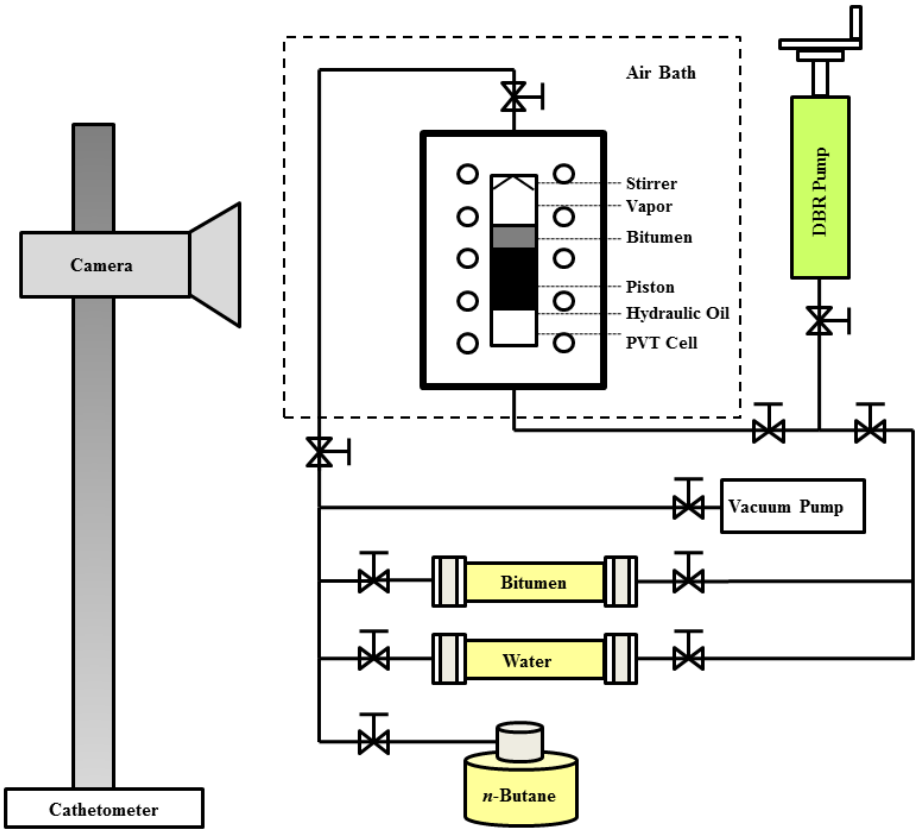

Figure 2.2 – Schematic of the experimental setup.

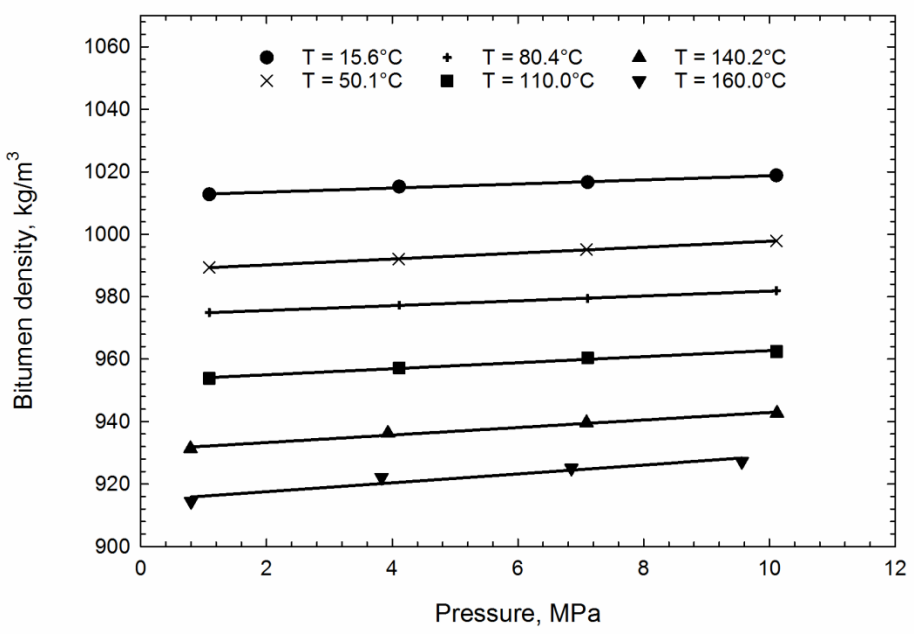

Figure 2.3 – Densities of bitumen measured with PVT cell at different temperatures. Solid lines are the trend lines matched with experimental data to illustrate the effect of temperature and pressure on bitumen density.

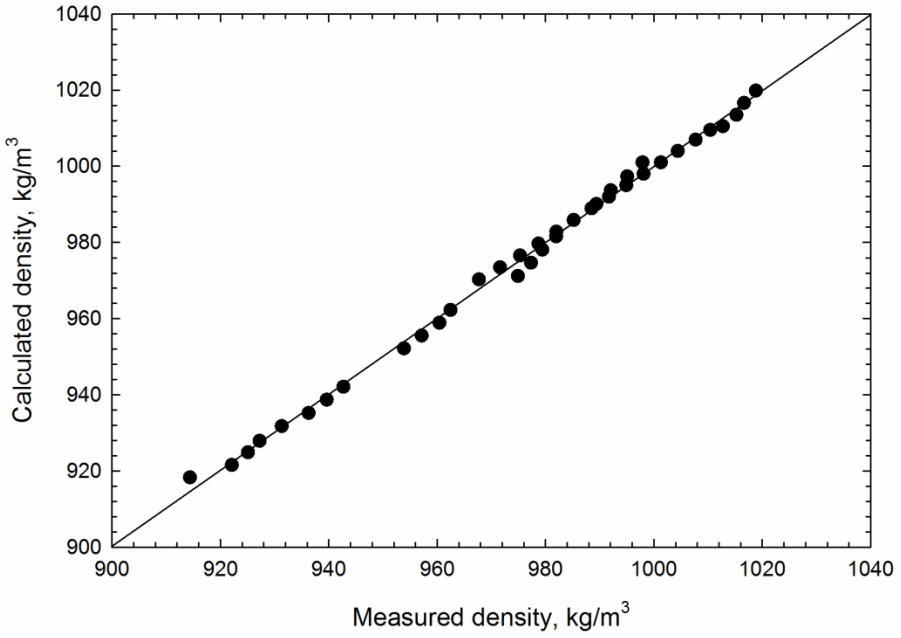

Figure 2.4 – The comparison between the calculated bitumen densities by use of the correlated Tait equation and experimental data.

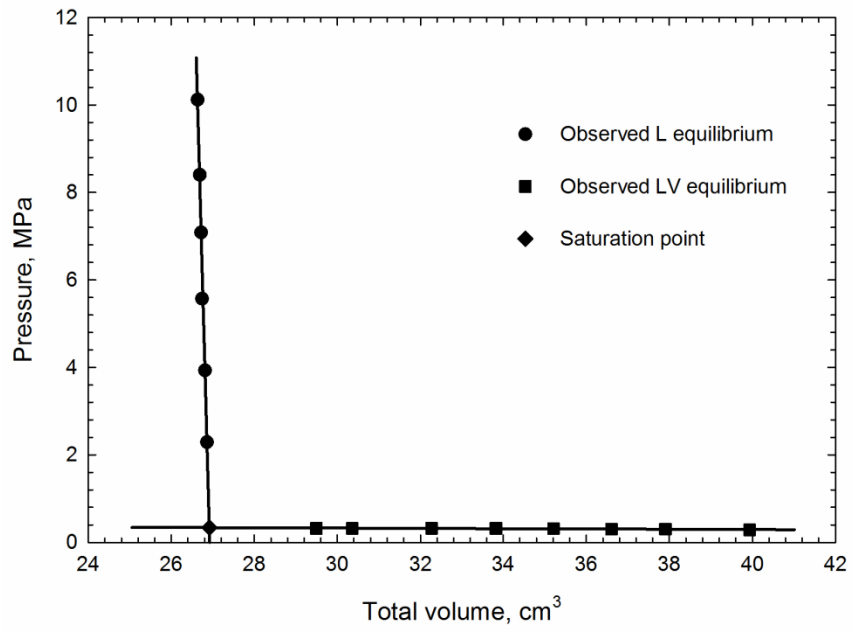

Figure 2.5 – Measured PV data for bitumen at 140.2°C. Only single liquid phase and liquid-vapor phase equilibria were observed at this temperature. The saturation point is determined as the intersection of two PV curves.

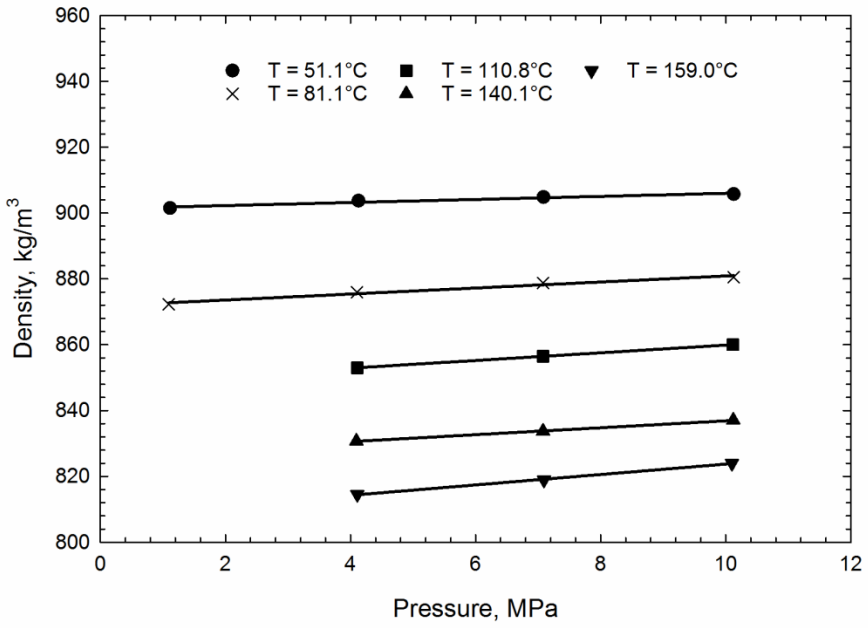

Figure 2.6 – Densities of Mixture A measured at a single liquid phase state. Solid lines are the trend lines matched with experimental data.

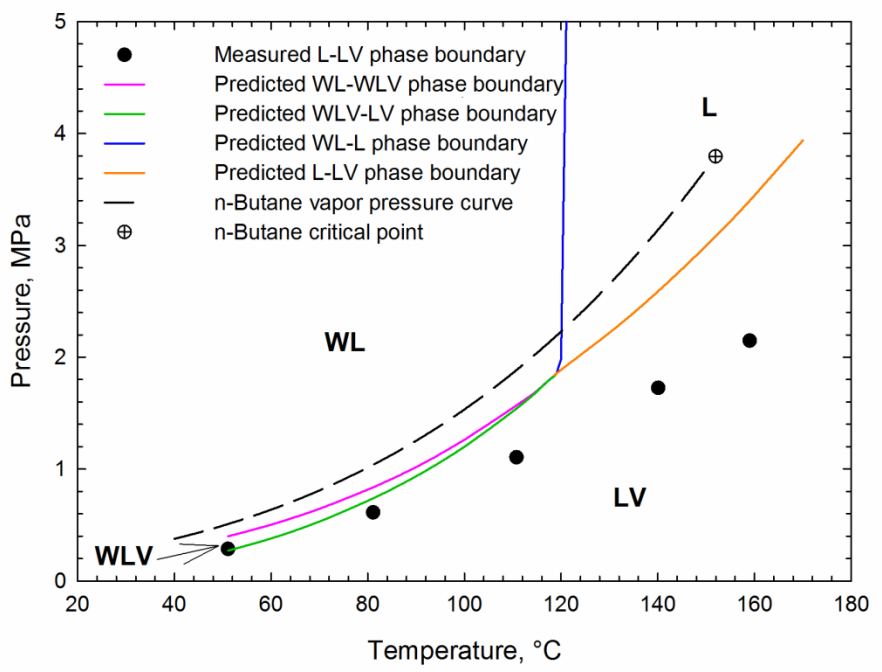

Figure 2.7 – Measured and predicted saturation pressures for Mixture A at different temperatures. The V phase is calculated to be almost pure butane.

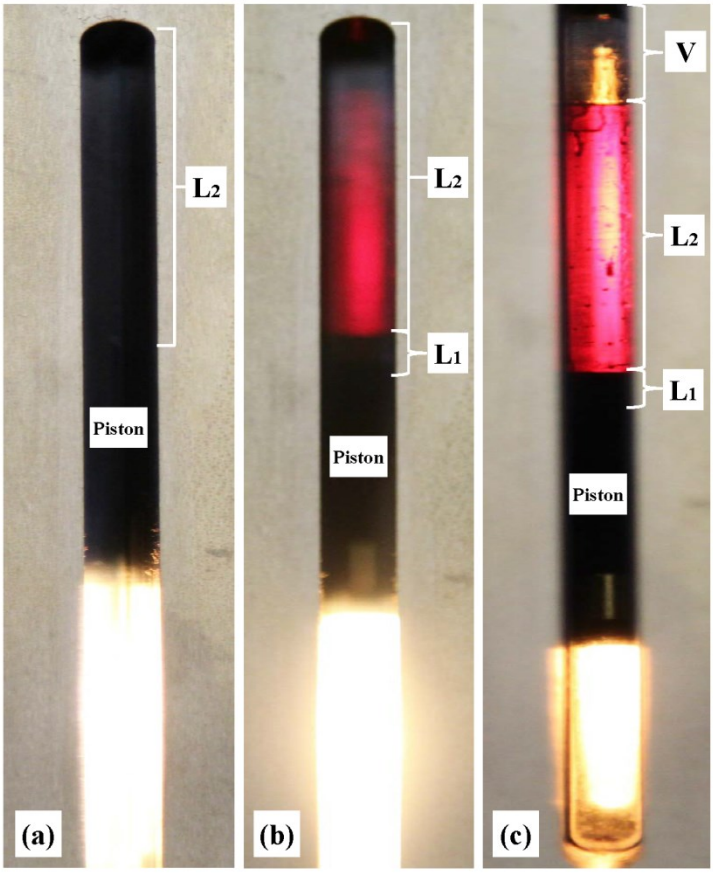

Figure 2.8 – Digital images of multiphase equilibrium captured for Mixture B: (a) Single liquid phase equilibrium at 140.1°C and 11.105 MPa; (b) L_2V equilibrium at 140.1°C and 8.375 MPa; (c) L_1L_2V equilibrium at 140.1°C and 2.921 MPa. L_1 is bitumen-rich phase. L_2 is n-butane-rich phase. Phase boundaries were measured by step-wise pressure reduction and based on visual observation of phases. The color of the L_2 phase became lighter with decreasing pressure, changing from black to red, indicating that n-butane extracted light and intermediate components more than heavier components from bitumen at lower pressures.

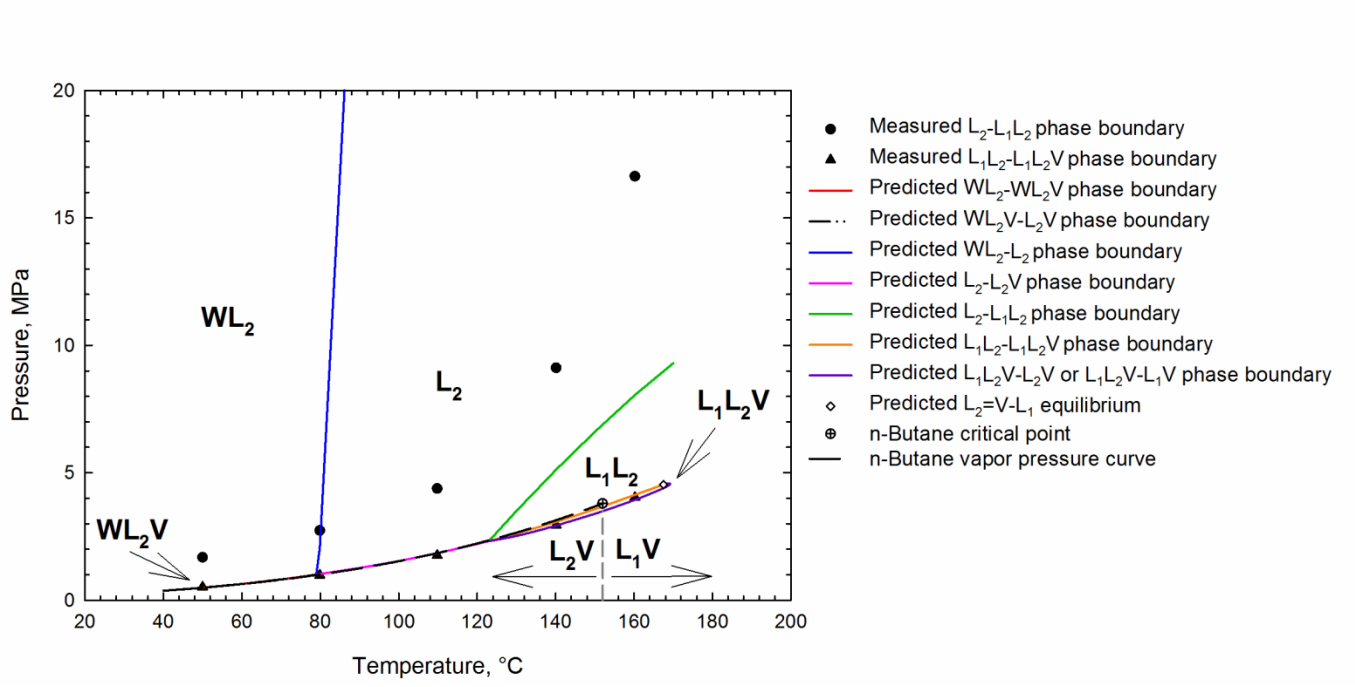

Figure 2.9 – Measured and predicted phase boundaries for Mixture B. The phase labeling in this figure is based on the continuity of phase compositions on phase transitions calculated from the EOS model. The three-phase region of L_1L_2V is predicted as a closed loop from the EOS model, near the higher-pressure boundary observed for three phases. However, the three-phase equilibrium observed at 50.0°C, 79.9°C and 109.8°C are not represented by the EOS model. The lowest temperature for L_1L_2V predicted from the EOS model is around 122.8°C. Higher-pressure boundaries observed for three phases are well correlated with the extension of n-butane's vapor pressure. EOS calculations further indicate that the L_1 and L_2 phases are close to each other near critical temperature of n-butane in the LV two-phase region. This gives the dashed demarcation line between L_1V on the higher-temperature side and L_2V on the lower-temperature side.

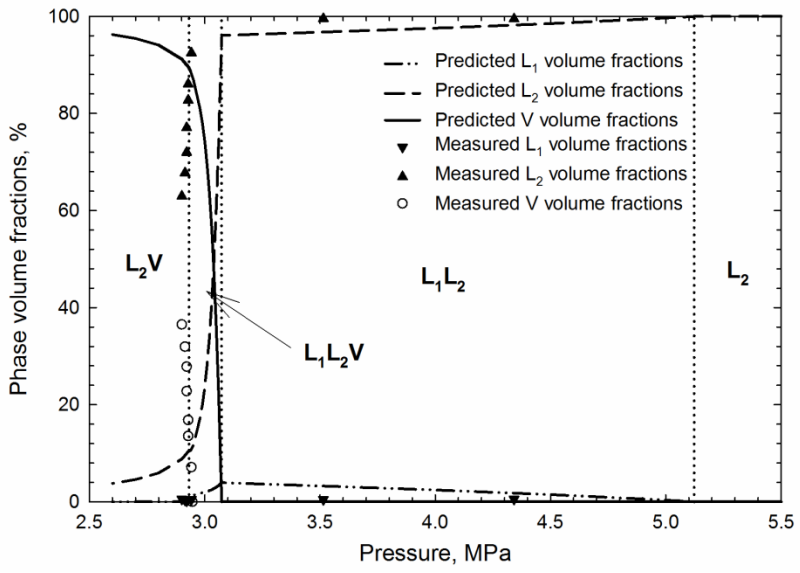
Phase volume fractions, %
Pressure, MPa
Predicted L_1 volume fractions
Predicted L_2 volume fractions
Predicted V volume fractions
Measured L_1 volume fractions
Measured L_2 volume fractions
Measured V volume fractions
L_2V
L_1L_2
L_2
L_1L_2V

a.

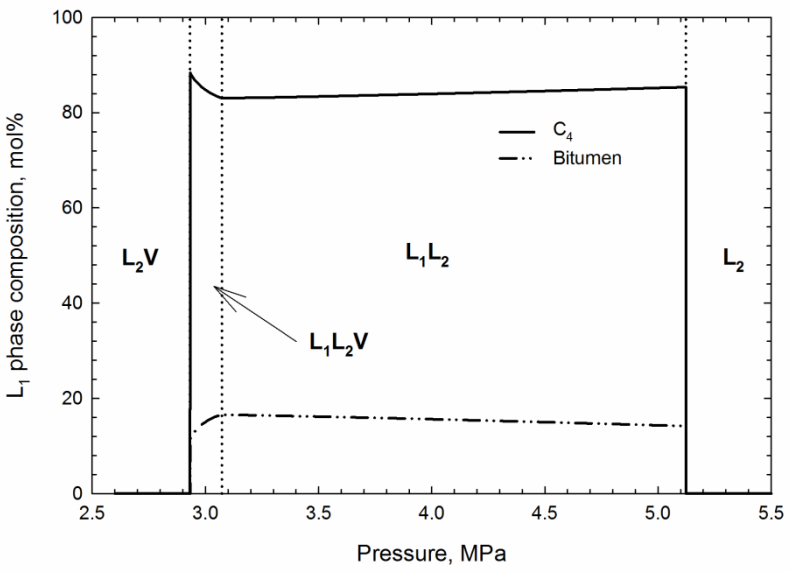
L_1 phase composition, mol%
Pressure, MPa
C_4
Bitumen
L_2V
L_1L_2
L_2
L_1L_2V

b.

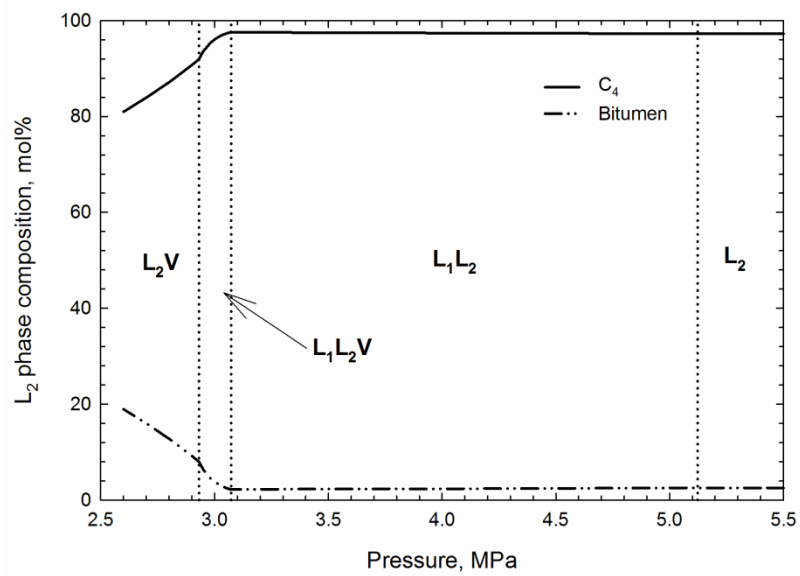
L_2 phase composition, mol%
Pressure, MPa
C_4
Bitumen
L_2V
L_1L_2
L_2
L_1L_2V

c.

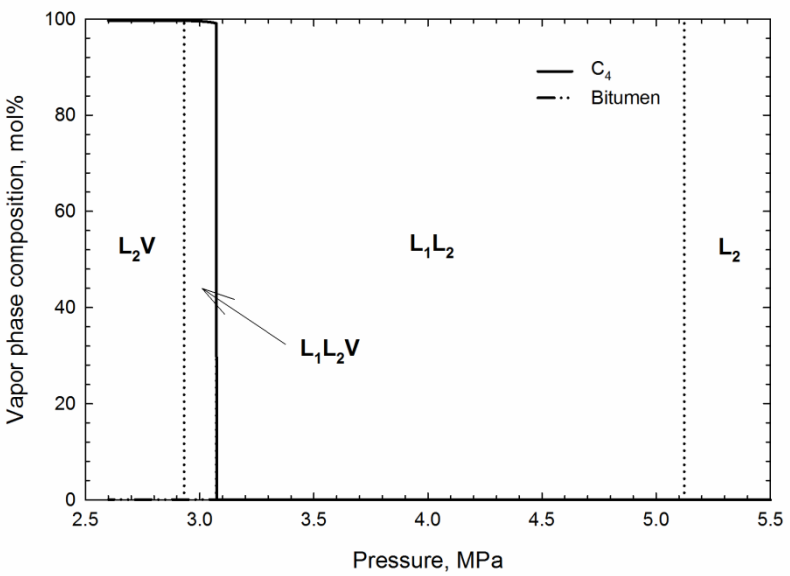
Vapor phase composition, mol%
Pressure, MPa
C_4
Bitumen
L_2V
L_1L_2
L_2
L_1L_2V

d.

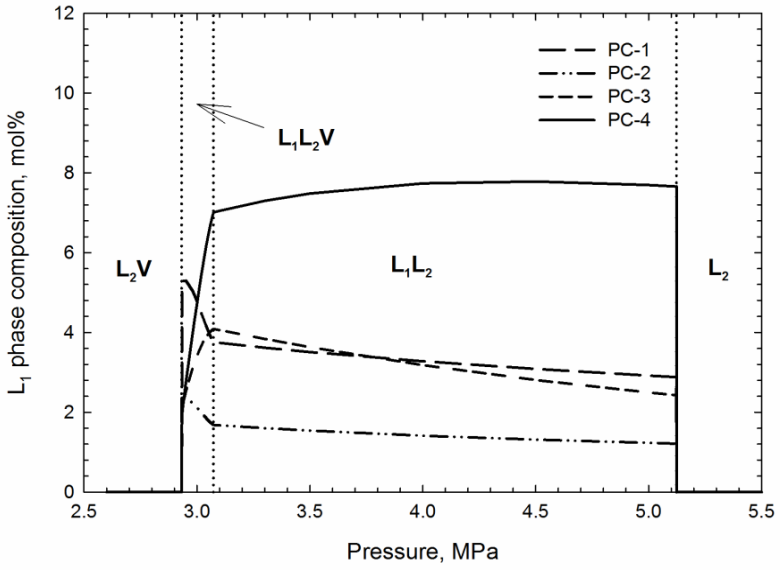

e.

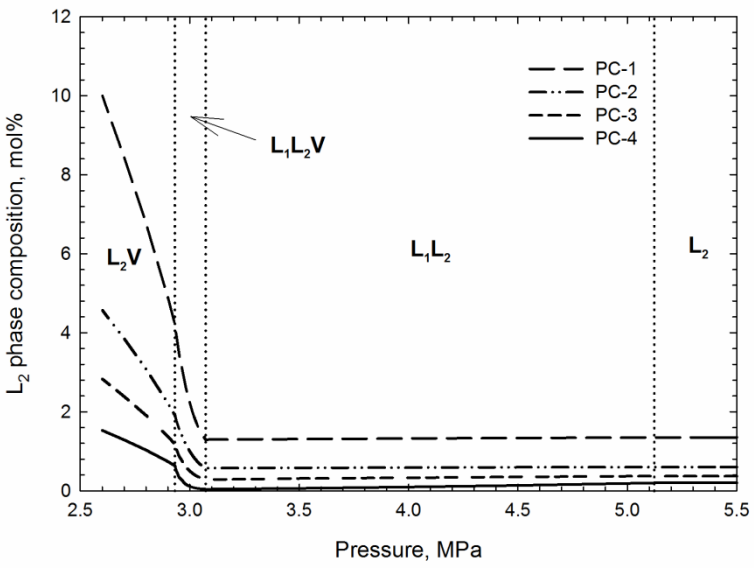

f.

Figure 2.10 – a. Measured and predicted phase saturations of Mixture B at 140.1°C; b-d. Predicted phase compositions for the L_1, L_2, and V phases, respectively; e-f. Detailed compositions predicted for pseudo components in the L_1 and L_2 phases, respectively.

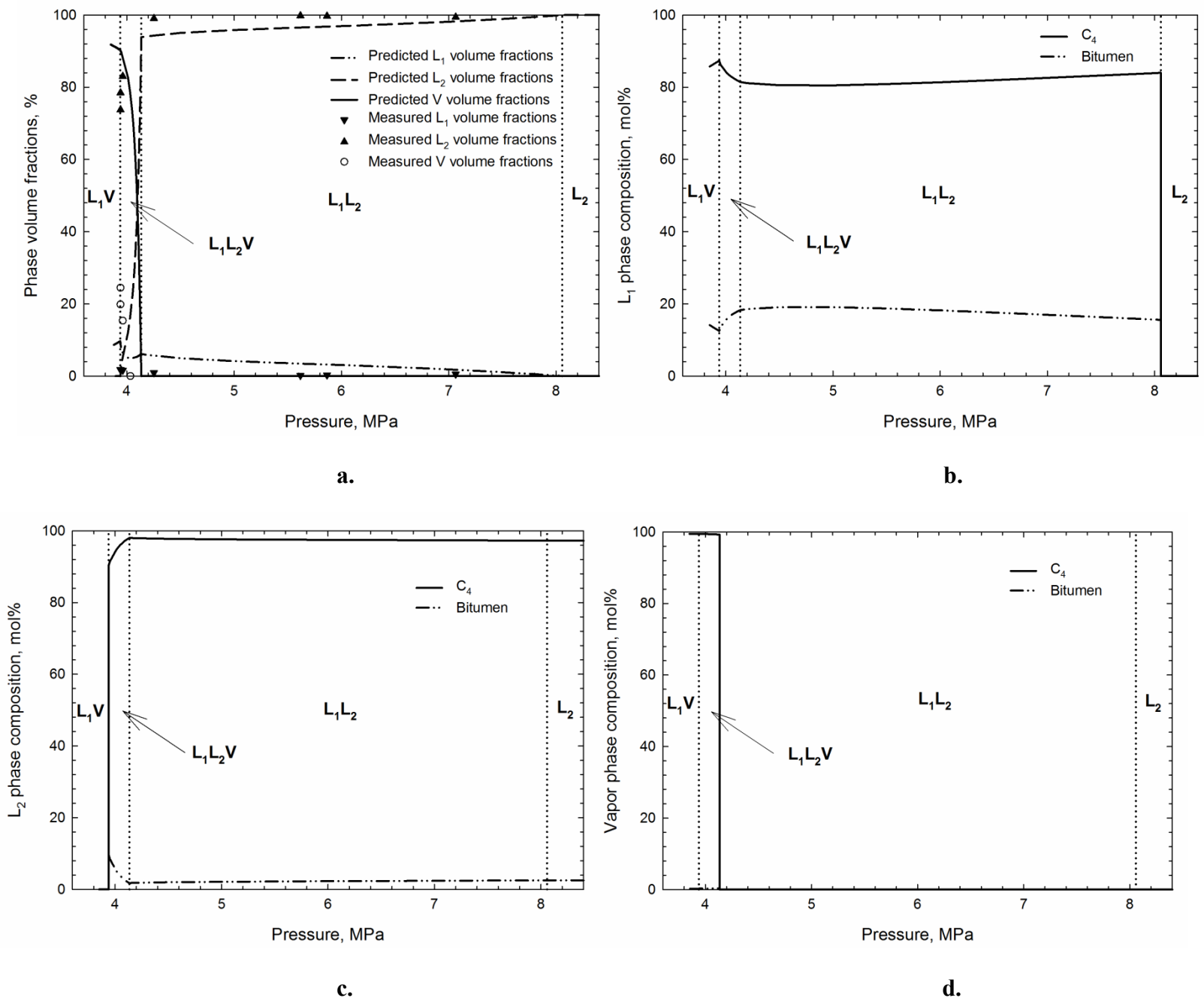

Figure 2.11 – a. Measured and predicted phase saturations of Mixture B at 160.2°C; b-d. Predicted phase compositions for the L_1, L_2, and V phases, respectively.

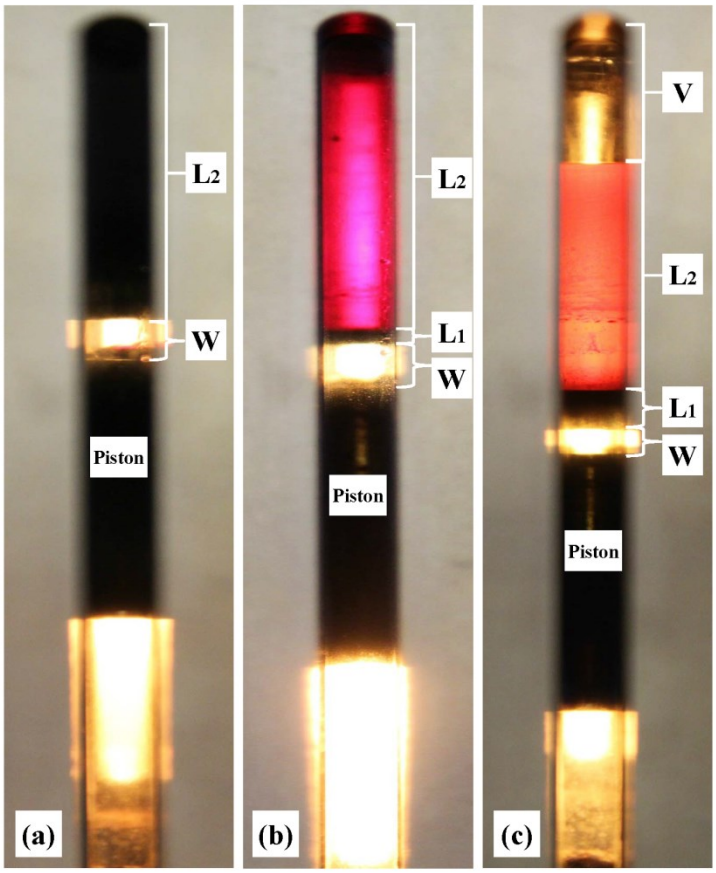

Figure 2.12 – Digital images of multiphase equilibrium captured for Mixture C: (a) WL_2 equilibrium at 159.9°C and 27.687 MPa; (b) WL_1L_2 equilibrium at 159.9°C and 8.258 MPa; (c) WL_1L_2V equilibrium at 159.9°C and 4.576 MPa. L_1 is bitumen-rich phase. L_2 is n-butane-rich phase. The W phase was denser than the L_1 phase at the temperature-pressure conditions in this research.

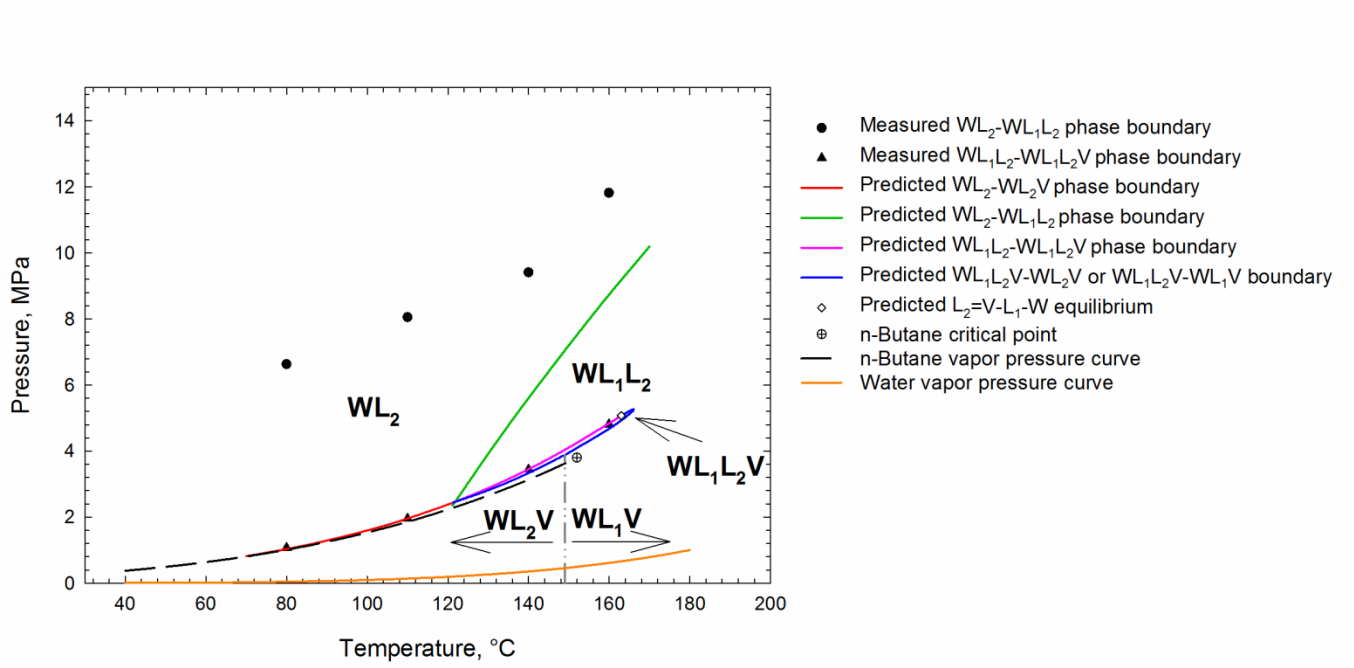

Figure 2.13 – Measured and predicted phase boundaries for Mixture C. The phase labeling in this figure is based on the EOS model. The higher-pressure boundaries for the four phases are observed close to the extension of n-butane's vapor pressure; however, they are higher than the corresponding vapor pressures of n-butane, unlike in Mixture B (Figure 2.9). The four-phase region of WL_1L_2V is predicted as a closed loop from the EOS model, near the lower-pressure boundaries measured for the WL_1L_2 region. However, no lower-pressure boundary for WL_1L_2V was observed experimentally. The phase transition between three and four phases was not represented by the EOS model at 80.0°C and 110.0°C. The EOS model gives a large deviation for the WL_2-WL_1L_2 boundary at lower temperatures; as mentioned previously, the interface between L_1 and L_2 was not clear at lower temperatures. The phase compositions of L_1 and L_2 are calculated to be close to each other near n-butane's critical temperature in the WLV region (WL_1V or WL_2V).

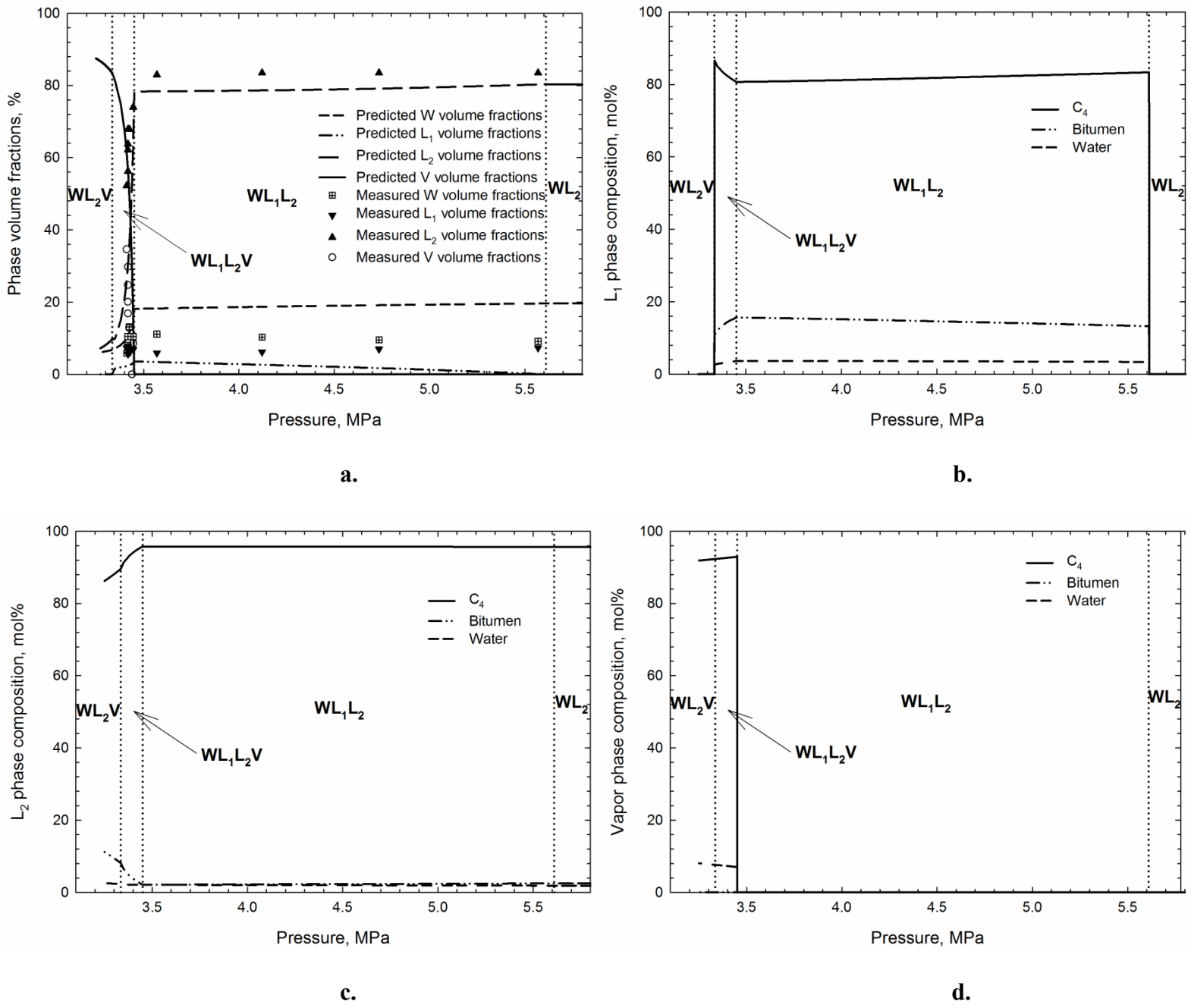

Figure 2.14 – a. Measured and predicted phase saturations of Mixture C at 140.0°C; b-d. Predicted phase compositions for the L_1, L_2, and V phases, respectively.

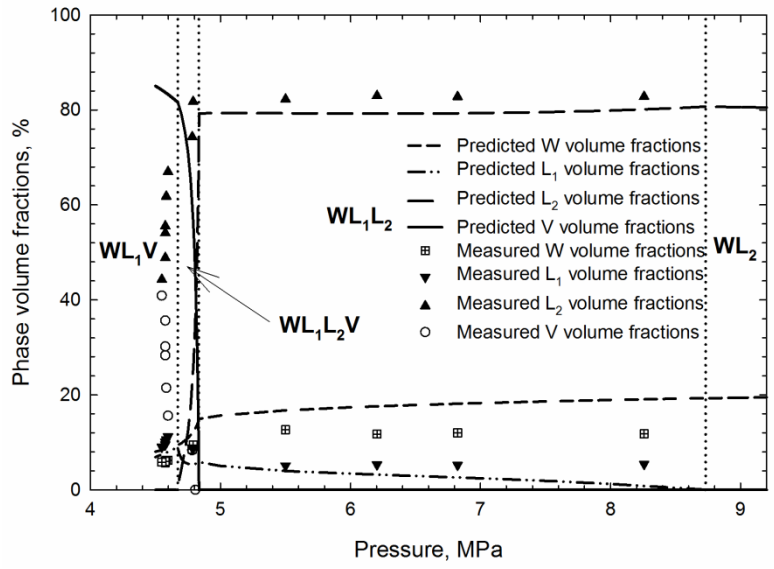
Phase volume fractions, %
Pressure, MPa
Predicted W volume fractions
Predicted L1 volume fractions
Predicted L2 volume fractions
Predicted V volume fractions
Measured W volume fractions
Measured L1 volume fractions
Measured L2 volume fractions
Measured V volume fractions
WL1V
WL1L2
WL2
WL1L2V

a.

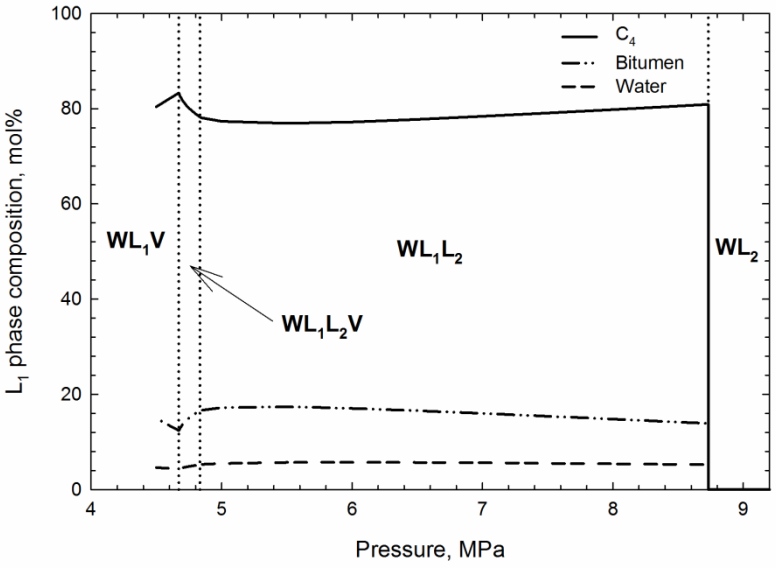
L1 phase composition, mol%
Pressure, MPa
C4
Bitumen
Water
WL1V
WL1L2
WL2
WL1L2V

b.

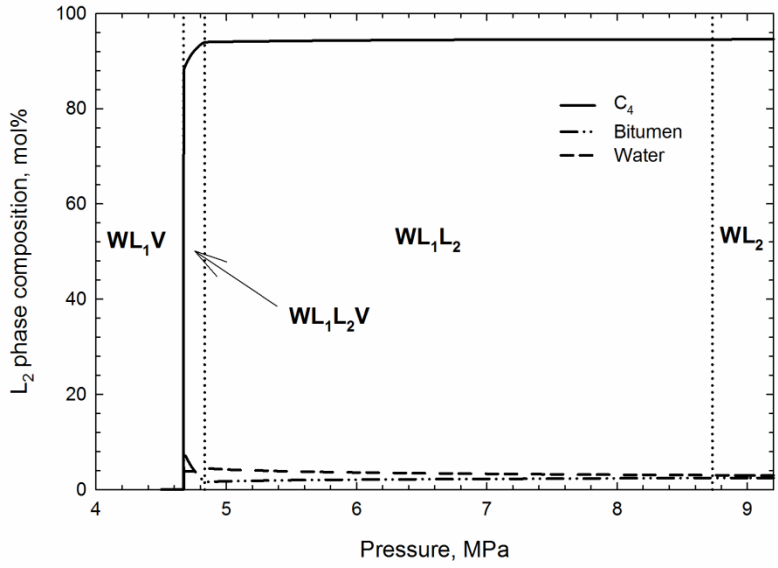
L2 phase composition, mol%
Pressure, MPa
C4
Bitumen
Water
WL1V
WL1L2
WL2
WL1L2V

c.

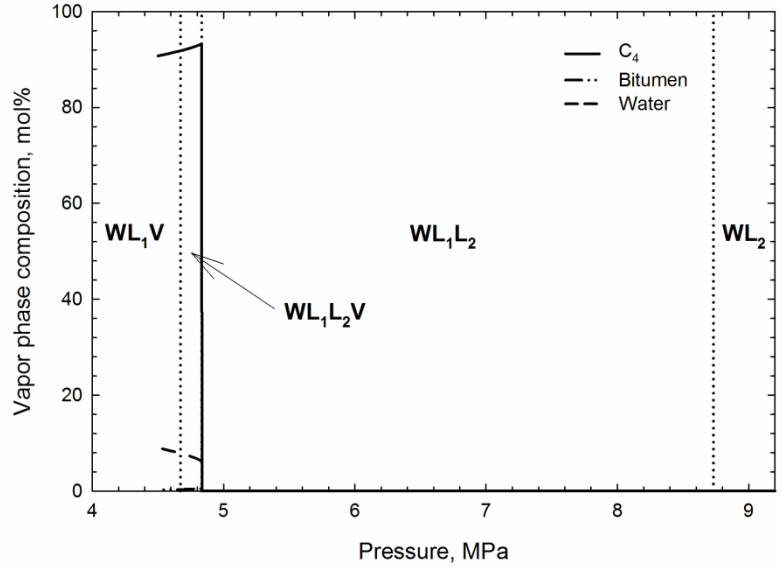
Vapor phase composition, mol%
Pressure, MPa
C4
Bitumen
Water
WL1V
WL1L2
WL2
WL1L2V

d.

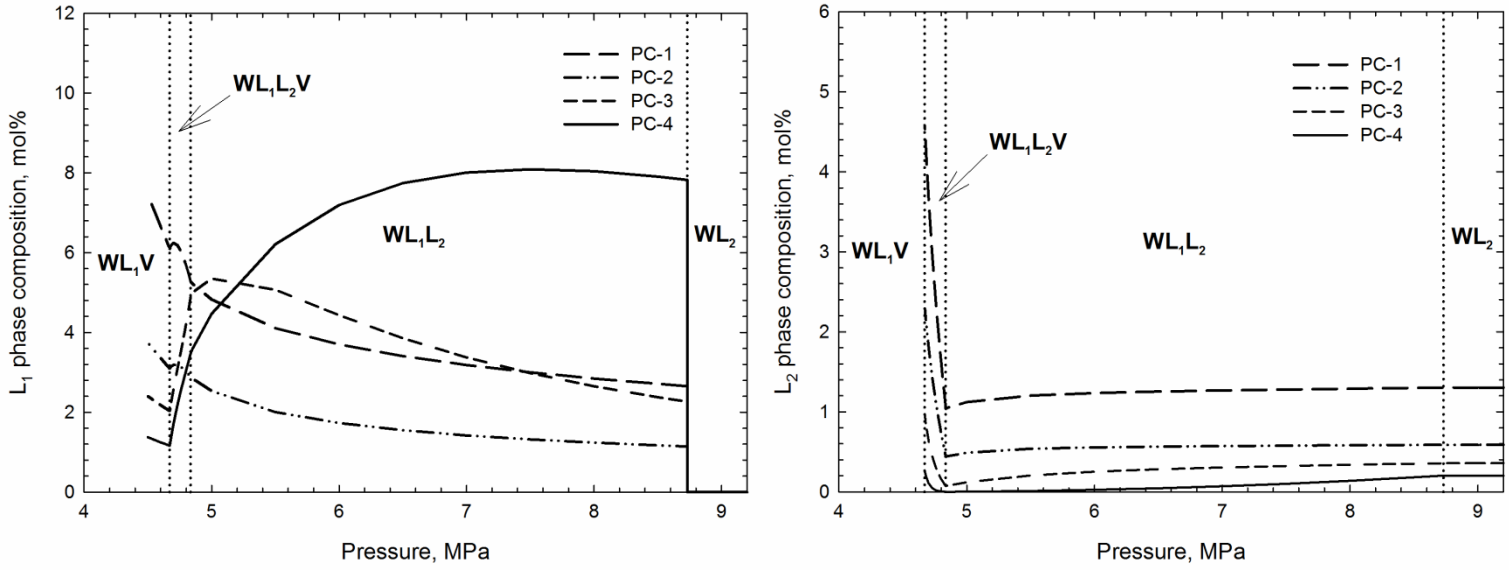

e. **f.**

Figure 2.15 – a. Measured and predicted phase saturations of Mixture C at 159.9°C; b-d. Predicted phase compositions for the L_1, L_2, and V phases, respectively; e-f. Detailed compositions predicted for pseudocomponents in the L_1 and L_2 phases, respectively.

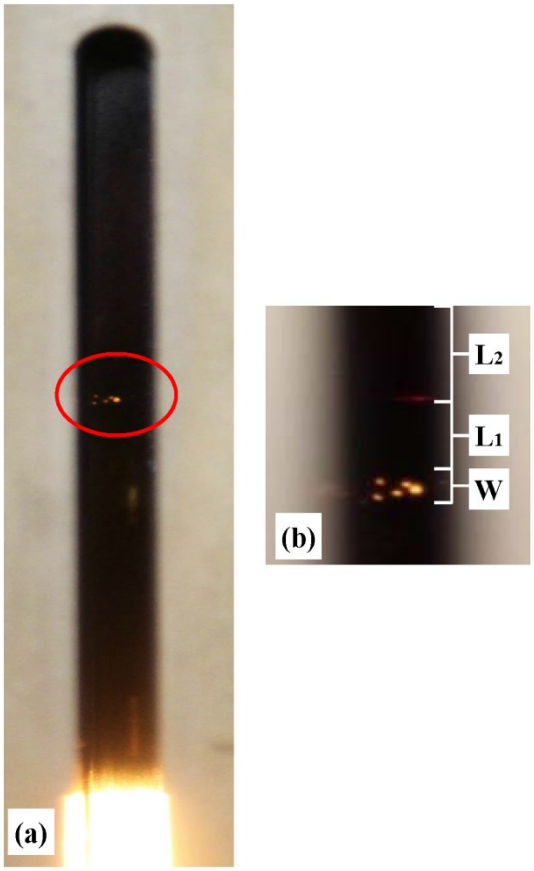

Figure 2.16 – a. Water phase is not transparent due to oil-in-water emulsion at 50.0°C for Mixture C. Shining points indicate the presence of water; b. Enlarged photo of detected water in the PVT cell.

Chapter 3 A Phase-Behavior Study for n-Hexane/Bitumen and n-Octane/Bitumen Mixtures

A version of this chapter has been submitted to SPE Journal for publication and is under review.

Abstract:

Steam-solvent coinjection has been studied as a potential method to improve the efficiency of the conventional steam-assisted gravity drainage (SAGD) for bitumen recovery. This research is part of an experimental program for phase behavior of Athabasca-bitumen/solvent mixtures.

This chapter presents a new set of experimental data for phase equilibrium, viscosity, density, and asphaltene precipitation for 11 mixtures of Athabasca bitumen with n-hexane and 10 mixtures of the same bitumen with n-octane. Phase-boundary measurements were conducted at temperatures up to 160°C and pressures up to 10 MPa. The bitumen sample used in this research was studied in our previous research, in which the same bitumen was not effectively diluted by n-butane due to the coexistence of a butane-rich liquid with a bitumen-rich liquid phase.

In this research, the liquid-liquid separation of hydrocarbons was not observed for n-hexane/bitumen and n-octane/bitumen mixtures for the range of temperatures and pressures tested, even at solvent concentrations higher than 90 mol%. This observation indicates that the amount of solvent available near the edge of a steam chamber may be entirely used for bitumen dilution beyond the chamber edge in coinjection of steam with heavier hydrocarbon solvents, such as n-hexane and n-octane.

Experiments for asphaltene precipitation at atmospheric pressure showed a larger amount of precipitates with n-hexane than with n-octane at a given solvent concentration higher than 50 wt%. For solvent concentrations below 50 wt%, no asphaltene precipitation was observed for both solvents with the bitumen sample tested in this research.

3.1 Introduction

Bitumen is one of the main petroleum resources in Canada, and is highly viscous and immobile at reservoir conditions. Several bitumen recovery technologies [e.g., cyclic steam stimulation and steam-assisted gravity drainage (SAGD)] have been applied for bitumen recovery by decreasing bitumen viscosity at in-situ conditions (Butler 1991).

Coinjection of a small amount of solvent with steam, such as expanding-solvent SAGD (ES-SAGD), has been proposed and pilot-tested to improve the efficiency of SAGD (Nasr and Isaacs 2001; Nasr et al. 2003; Gupta and Gittins 2007). A properly-designed coinjection of solvent with steam can benefit both from the latent heat of the injected vapor and the bitumen dilution by solvent. The incremental oil recovery of steam-solvent coinjection in comparison with steam-only injection has been presented in lab-scale physical experiments, pore-scale experiments, and numerical simulations (e.g., Redford and McKay 1980; Li and Mamora 2010; Mohammadzadeh et al. 2012; Jha et al. 2013). A successful coinjection of steam with solvent can reduce the energy and water consumption while improving displacement efficiency in comparison with SAGD (e.g., Ardali et al. 2012; Keshavarz et al. 2015 a; b).

The efficiency of SAGD and its variants depends largely on the temperature and composition near the edge of a steam chamber at the operating pressures. Various hydrocarbons were tested as potential additives to steam. Li and Mamora (2010) pointed out that a successful coinjection of steam and solvent should be designed to take advantage of the solvent without losing heat of steam. They stated that n-hexane was a better choice for Athabasca reservoirs due to its similar boiling points with steam. Mohabati et al. (2010) found that steam-hexane coinjection could improve SAGD performance for Athabasca bitumen more than for Cold Lake and Lloydminster reservoirs. Yazdani et al. (2011) indicated that n-hexane and n-heptane were preferable for Athabasca bitumen in comparison with propane and n-pentane. Li et al. (2011) stated that heavy liquid solvents, such as C_{12}, were the optimum solvents to be coinjected with steam for Athabasca bitumen.

Several papers reported that lighter hydrocarbon solvents were suitable for coinjection with steam. Ardali et al. (2010) simulated the coinjection of steam and normal hydrocarbons (C_3 to C_7), and concluded that n-butane was the optimum solvent for Cold Lake with no initial solution gas at the operating pressure of 3400 kPa. Govind et al. (2008) observed a lower residual oil saturation and a higher drainage rate simulated for n-butane coinjection at a higher operating pressure (4000 kPa).

Gao et al. (2016) showed in their experimental study that mixtures of Athabasca bitumen with n-butane can exhibit complex multiphase behavior. They observed up to three equilibrium phases for a mixture of bitumen with n-butane between 50°C and 160°C, which consist of the bitumen-

rich liquid (L_1), butane-rich liquid (L_2), and vapor (V) phases. At 140.1°C, for example, the transition from a single-phase liquid to L_1L_2 occurred at 9.1 MPa, and the transition from L_1L_2 to L_1L_2V at 2.9 MPa. The observed liquid-liquid separation of hydrocarbons indicates that n-butane may be not entirely used for diluting bitumen ahead of a steam-chamber edge, even if a high level of accumulation of n-butane takes place there. Also, the effect of the resulting multiphase flow on in-situ bitumen production is uncertain. The experimental results for bitumen/n-butane mixtures by Gao et al. (2006) have arisen the question as to whether liquid-liquid separation of hydrocarbons occurs for heavier solvents, such as hexane and octane, with the same Athabasca bitumen. Those solvents less volatile than butane were concluded to be optimal for steam-solvent coinjection for Athabasca bitumen in various papers; hence, this question will be addressed as one of the main objectives in this chapter.

Phase-behavior models for bitumen developed on the basis of experimental data were used for prediction of fluid behavior at reservoir conditions. For example, cubic EOS's were used by Díaz et al. (2011), Agrawal et al. (2012), and Kumar and Okuno (2016). The perturbed-chain form of the statistical association fluid theory (PC-SAFT) was also applied for bitumen characterization (e.g., Ma et al. 2016; Panuganti et al. 2012; Zúñiga-Hinojosa et al. 2014; Tavakkoli et al. 2013). Several researchers successfully applied cubic-plus-association (CPA) EOS's for bitumen characterization (e.g., Zirrahi et al. 2015a, b; Jindrová et al. 2015; Li and Firoozabadi 2010). Design of solvent type and its concentration in coinjection requires a detailed understanding and reliable prediction of phase behavior for solvent/bitumen mixtures at a wide range of temperature at operating pressures (Nagarajan et al. 2006). However, it is not easy to find in the literature a comprehensive set of PVT data for phase behavior (or phase boundaries), density, and viscosity for the same bitumen sample with different solvents.

Zou et al. (2006) presented multiphase behavior data for Athabasca vacuum bottoms/n-pentane and Athabasca vacuum bottoms/n-heptane mixtures up to 350°C. The denser hydrocarbon-liquid phase in their study was presented to be rich in asphaltene component as shown in the SARA test results. Agrawal et al. (2012) measured the saturation pressure for bitumen+11 wt% pentane and bitumen+30 wt% pentane at temperatures from 90°C to 180°C. Argüelles-Vivas et al. (2012) reported the density and viscosity data for Athabasca-bitumen/pentane mixtures with different solvent weight fractions (5.1%, 10.3% and 15.4%) up to 210°C and 1 MPa. Many papers

presented experimental results for density and viscosity for Athabasca bitumens with n-pentane, n-hexane, n-heptane and n-decane, respectively (Nourozieh et al. 2013; Kariznovi et al. 2013; Nourozieh et al. 2014; Kariznovi et al. 2014b; Nourozieh et al. 2015a, b, d).

Asphlatenes are the heaviest and most polarizable fraction of crude oil, which may cause deposition problems in production wells (Vargas et al. 2009). The amount of asphaltene precipitation and water-in-oil emulsion due to the asphaltene-water interaction are also important for selection of an optimum solvent for steam-solvent coinjection (Hascakir 2016). Various papers reported asphaltene precipitation for solvent-diluted bitumen (e.g., Buenrostro-Gonzalez et al. 2004; Alboudwarej et al. 2003; Sabbagh et al. 2006; Rassamdana et al. 1996; Vargas et al. 2009).

Viscosity data for bitumen and its mixtures with solvent are also essential for in-situ processes and pipeline transportation. Numerous studies for bitumen viscosity were reported in the literature. Mehrotra and Svrcek (1984; 1985a, b, c; 1988) and Svrcek and Mehrotra (1989) presented the viscosity data of different Alberta bitumens at atmospheric pressure. Mehrotra and Svrcek (1986; 1987) reported the viscosity of Athabasca and Cold Lake bitumens at pressures up to 10 MPa and temperatures up to 120°C. Kariznovi et al. (2014a) and Nourozieh et al. (2015c) presented viscosity data for Athabasca bitumen up to 200°C and 10 MPa. Besides experimental studies, various researchers presented correlations for bitumen viscosity (e.g., Mehrotra and Svrcek 1986 and 1987; Naseri et al. 2005; Satyro and Yarranton 2010).

This research is part of a comprehensive study of phase behavior for different solvents with an Athabasca bitumen, for which Gao et al. (2016) presented results for n-butane/Athabasca-bitumen mixtures. There are two main objectives in this research. One is to address the question about the potential liquid-liquid separation for mixtures of Athabasca bitumen with n-hexane and n-octane. The same bitumen sample as the one in Gao et al. (2016) is used for a fair comparison among n-butane, n-hexane, and n-octane. The other objective is to present a new set of experimental data for mixtures of Athabasca bitumen with n-hexane and n-octane, such as phase boundaries, densities, viscosities, and asphaltene precipitation.

Section 2 describes the experimental setup and procedure adopted in this research. Section 3 shows experimental results and correlations for the data using the Peng-Robinson EOS and other

equations. To our knowledge, this is the first time PVT data are reported for n-octane/Athabasca-bitumen mixtures, including saturation pressures and densities at pressures up to 10 MPa and temperatures up to 160°C. A new set of PVT data is also presented for n-hexane/Athabasca-bitumen mixtures. Limited data for viscosity and asphaltene precipitation measurement at atmospheric pressure are reported for n-hexane/Athabasca-bitumen and n-octane/Athabasca-bitumen mixtures.

3.2 Experimental Section

3.2.1 Materials

The same Athabasca bitumen as our previous study (Gao et al. 2016) was used for this chapter. The molecular weight (MW) for the Athabasca bitumen based on freezing-point depression measurement is 635 gram/mole. The water content was measured to be 0.245 wt% in the bitumen sample. Removal of water from the bitumen sample by heating was not attempted in order to prevent light components from being evaporated. The SARA analysis results are presented in **Table 3.1**, for which resins I was eluted from the column with methyl ethyl ketone and resins II was then eluted from the column with tetrahydrofuran. The simulated distillation test was also conducted for the bitumen sample. The boiling-point distribution is shown in **Figure 3.1** and **Appendix A (Table A.1)**. The resulting carbon-number distribution in mass fraction is given in **Table A.2**. The solvents used are n-hexane and n-octane. The purity of n-hexane is 99.9% and that of n-octane is 99.0% (Fisher Scientific, Edmonton, Canada).

3.2.2 Experimental Setup

A Saybolt viscometer (K21410, Koehler, Holtsville, USA) was used to measure the viscosity of Athabasca bitumen sample at atmospheric pressure. The temperature of Saybolt viscometer was controlled by an oil bath with a control accuracy of ±0.03°C. The Furol orifice was factory-calibrated by viscosity standard S600 at 50°C. As presented in ASTM D88 for Saybolt viscometer measurement, the repeatability is 1% by the same operator and the same apparatus.

The viscosity of the bitumen sample was also measured by use of a Cone and Plate viscometer (DV2TRV, Brookfield, Massachusetts, USA) at atmospheric pressure. The temperature of the Cone and Plate viscometer was controlled by oil or water bath with the accuracy of ±1.0°C. The

viscosity measurement accuracy is ±1.0% of a full scale viscosity range at the corresponding rotational speed. The Cone and Plate viscometer was also used for the viscosity measurement for n-hexane/bitumen and n-octane/bitumen mixtures at atmospheric pressure. A full scale viscosity range in cp is calculated as the product of TK, SMC, and 10000/RPM, where TK is 1 for viscometer model DV2TRV, SMC is 9.922 for spindle CPA-52Z and 0.327 for spindle CPA-40Z, and RPM is rotational speed in revolutions per minute.

Phase behavior measurements for n-hexane/Athabasca-bitumen and n-octane/Athabasca-bitumen mixtures were conducted with a conventional PVT apparatus (PVT-ZS-16-2-2-H/AC, DBR, Edmonton, Canada). **Figure 3.2** shows a schematic for the apparatus. Details of the PVT apparatus were presented in Gao et al. (2016). The PVT system consists of a PVT cell, an air bath, a high-pressure positive displacement pump, and a cathetometer. The operation limits of the PVT cell are approximately 100 MPa (15,000 psi) and 199°C. The accuracy of the temperature and pressure control of the PVT system are ±0.1°C and ±0.07 MPa (10.5 psig), respectively. In addition, a high-pressure precision test gauge (700RG31, Fluke, Calgary, Canada) with an accuracy of ±0.007 MPa (1.0 psig) was also connected to the PVT cell for more accurate pressure measurement. The uncertainty in volume measurement is ±0.016 cm^3. The dead volume of this PVT system is 1.754 cm^3.

A digital densitometer (DDM 2910, Rudolph Research Analytical, Hackettstown, USA) was used to measure the reference density for bitumen/solvent mixtures at atmospheric pressure. The accuracy of temperature control is ±0.05°C. The uncertainty of the density measurement by use of this densitometer is ±0.1 kg/m^3.

3.2.3 Experimental Procedure

Experiments were conducted for viscosities with the two viscometers, saturation pressures and densities with the PVT system, and asphaltene precipitation by following ASTM D4124-97. Altogether 21 mixtures were created for the n-hexane/bitumen (HB) and n-octane/bitumen (OB) systems, which are labeled as HB1, HB2, …, HB11, OB1, OB2, …, and OB10 and summarized in **Table 3.2**.

Viscosities of the bitumen were firstly measured by the Saybolt viscometer at atmospheric pressure over the temperature range from 60.0°C to 140.0°C. The viscosity measurement was

conducted by following ASTM D88. After setting the oil bath to a test temperature, bitumen sample was strained into the viscometer until the fluid level was above the overflow rim. A sufficient time was needed for reaching thermal equilibrium. An equilibrium state was deemed to be achieved once the reading of thermometer became steady. Then, the cork was snapped simultaneously with the timer. The corrected efflux time in seconds (i.e. Saybolt Furol viscosity) for 60 mL of sample through the calibrated Furol orifice was measured at different temperatures. The dynamic viscosity of bitumen sample was calculated with the following equations:

$$\mu_{SUS} = 10\mu_{SFS}, \tag{3.1}$$

$$\text{when } \mu_{SUS} < 100, \gamma = 0.226\mu_{SUS} - 195/\mu_{SUS}, \tag{3.2}$$

$$\text{when } \mu_{SUS} > 100, \gamma = 0.220\mu_{SUS} - 135/\mu_{SUS}, \tag{3.3}$$

$$\mu = \gamma\rho, \tag{3.4}$$

where μ_{SFS} is Saybolt Furol viscosity in second, μ_{SUS} is Saybolt Universal viscosity in second, γ is kinematic viscosity in centistokes, μ is dynamic viscosity in centipoise, and ρ is density in g/cm^3.

Viscosities of the bitumen sample at atmospheric pressure were also measured by use of the Cone and Plate viscometer at temperatures from 25.0°C to 100.0°C. The fitted spindle (CPA-52Z) was used with the consideration of the predicted viscosity range of bitumen sample. After setting the rotational speed, the results of viscosity, toque, shear stress, shear rate and accuracy of viscosity measurement were recorded at each test temperature. The measurement was repeated twice at the same temperature due to the large uncertainty in viscosity measurement for highly viscous fluids. Viscosities of n-hexane/bitumen mixtures (Mixtures HB3, HB4, and HB5) and n-octane/bitumen mixtures (Mixtures OB3 and OB4) were also measured by following the same procedure with the Cone and Plate viscometer with the CPA-40Z spindle. The CPA-52Z spindle was used for Mixture OB2 to avoid exceeding the operating limit of the CPA-40Z spindle, which is 32,700 cp.

Saturation pressure measurements were conducted on the basis of the constant composition expansion test method by use of the PVT system. Before each measurement, the PVT cell and inlet tubings were cleaned with toluene and evacuated by a vacuum pump. For the measurement

of each mixture, sufficient amounts of bitumen and solvent were separately injected into two transfer cylinders that were directly connected to the inlet tubing of the PVT cell. Then, the transfer cylinders were placed in the air bath, which was set to 50.0°C for at least 12 hours. After reaching thermal equilibrium, the solvent was firstly injected into the PVT cell. The injected mass of solvent was calculated by use of the volume measured by the cathetometer and density values from the NIST database (Lemmon et al. 2016). The bitumen sample was then injected into the PVT cell without turning on the magnetic stirrer. After injection, the volume of bitumen was determined as the difference between the total volume and the solvent volume as no volume change upon mixing was assumed to occur for a short time period. The composition of this mixture was calculated based on the densities, volumes, and MWs of bitumen and solvent. After that, the temperature of the PVT cell was increased to the highest operating temperature in this research, 160.0°C, for facilitating the mixing of bitumen and solvent. Subsequently, the mixture was vigorously stirred by the magnetic stirrer at 160.0°C for at least 12 hours. During the mixing, the injected bitumen gradually moved downwards as the orientation of the PVT cell was switched to the inverted position. The counter flow of bitumen and solvent occurred under the operation of the magnetic stirrer, which enabled the components to be well mixed.

At each temperature, saturation pressure measurements of bitumen/solvent systems were started from a single-liquid-phase state at a high pressure. Then, the pressure was gradually decreased by step-wise expansion at the rate of 3 cm^3/hr, while the mixture was sufficiently stirred for quickly reaching an equilibrium state. Mixing by the stirrer was observed as circular movement for the fluid inside the PVT cell. After reaching each specified pressure, the magnetic stirrer was switched off and the system was kept static for a sufficient duration. An equilibrium state was deemed to be achieved once the cell pressure became steady. Two to three hours were sufficient for a single liquid phase to reach an equilibrium state at each temperature-pressure condition. The time allowed for equilibration was increased to four to five hours for multiphase equilibrium. Thereafter, the phase equilibrium state of the mixture was visually identified, and the volume of each phase was measured. Then, a saturation pressure was calculated by plotting the total volume (V) with respect to pressure (P), and was determined as the intersection of two PV lines as the PV relationship often showed a clear change in slope when the vapor phase appeared as pressure changed as shown in **Figure 3.3**.

Densities of n-hexane/bitumen and n-octane/bitumen mixtures were measured with the PVT cell based on mass balance at conditions of 50.0°C-160.0°C and 1.0-10.0 MPa. As the mass injected into the closed PVT cell was conserved, the densities at different temperature-pressure conditions were obtained using the reference density that was measured at a known reference condition: i.e.,

$$\rho_2 = \frac{V_1}{V_2}\rho_1 = \frac{H_1}{H_2}\rho_1, \quad (3.5)$$

where ρ_1, V_1 and H_1 are the sample's density (kg/m^3), volume (cm^3), and height in the PVT cell (cm) at the reference conditions, respectively. ρ_2, V_2 and H_2 are the sample's density (kg/m^3), volume (cm^3), and height in the PVT cell (cm) at a given temperature-pressure condition. The reference densities of mixtures were measured with the digital densitometer (DDM 2910, Rudolph Research Analytical, Hackettstown, USA).

The asphaltene precipitation measurements were conducted for n-hexane/bitumen and n-octane/bitumen mixtures following ASTM D4124-97 at 20.4°C and atmospheric pressure. Different amounts of solvents were mixed with 30 g bitumen to make the solvent mass fractions used in this study, which are approximately 0.4, 0.5, 0.6, 0.7, 0.8, and 0.9. The mass of bitumen and solvent were measured by an electronic balance (MXX 412, Denver Instrument, Bohemia, USA). After a mixture was prepared, it was firstly mixed by a glass rod. After that, a magnetic stir (6795-220, Corning, New York, USA) was used for sufficient mixing for 10 hours. Thereafter, the mixture was left for 10 hours for precipitation. Then, the diluted bitumen was filtered by use of a vacuum system with a 0.25 μm pore size filter paper (Grade 5 Whatman filter paper, GE Healthcare Life Sciences, Chicago, USA). After that, the precipitated asphaltene was dried in an oven at a temperature higher than the solvent's boiling point for 10 hours (heating temperature for bitumen/n-hexane mixtures is 116.0°C and for bitumen/n-octane mixtures is 152.2°C). The weight of the dried asphaltene after heating was recorded.

3.3 Results and Discussions

3.3.1 Bitumen

Table 3.3 gives the results of measured Saybolt Furol viscosities and the calculated dynamic viscosities for bitumen sample at atmospheric pressure from 60.0°C to 140.0°C. Dynamic

viscosities of bitumen were determined by Saybolt Furol viscosity and bitumen density calculated by use of the correlated Tait equation presented in Gao et al. (2016). As expected, the viscosity of bitumen sample decreased with increasing temperature at atmospheric pressure, and the effect of temperature on bitumen viscosity is more significant at lower temperatures.

Viscosities of the bitumen sample at atmospheric pressure were also measured by the Cone and Plate viscometer at temperatures from 25.0°C to 100.0°C. The measurement was repeated twice by use of the same spindle and at the conditions of similar rotational speed. The deviations of measured viscosity data at corresponding temperatures are within the uncertainty of measurement. The results of viscosity, torque, shear stress, shear rate and accuracy of measurement were recorded as shown in **Table 3.4**.

Measured viscosities at atmospheric pressure were correlated with the correlation developed by Khan et al. (1984), as follows:

$$\ln(\mu) = \exp[b_1 + b_2 \ln(T + 273.15)], \qquad (3.6)$$

in which μ is bitumen viscosity at atmospheric pressure in centipoise, T is temperature in °C, and b_1 and b_2 are the fitting parameters. **Table 3.5** gives the fitting parameters for the viscosity data measured by the Saybolt viscometer, with which the average absolute relative deviation (AARD) is 3.9%. The fitting parameters of equation 3.6 for the viscosity data measured by the Cone and Plate viscometer were compared with those for the Saybolt viscometer, as summarized in Table 3.5. **Figure 3.4** indicates that the correlation can represent the experimental data.

The bitumen was characterized by the use of the Peng-Robinson (PR) EOS with the van der Waals mixing rules (Peng and Robinson 1976, 1978). For consistency, it was aimed to obtain a single set of parameters for the PR EOS to correlate all data obtained in this chapter for bitumen/hexane and bitumen/octane, and in Gao et al. (2016) for bitumen/butane. The details for bitumen characterization were presented in Gao et al. (2016). Critical properties and binary interaction parameters (BIPs) were finalized primarily for accurate correlation of the phase-boundary data for the presence of the V phase (i.e., bubble points). **Tables 3.6 and 3.7** present the components' parameters for use with the PR EOS.

3.3.2 n-Hexane/Bitumen Mixtures

Saturation pressures were measured for Mixture HB1 at temperatures from 80.8°C to 159.6°C, to address the question as to whether LL separation occurs for this Athabasca bitumen with n-hexane. Only single liquid phase and liquid-vapor phase equilibria were observed through the PVT-cell window within this temperature range below 10 MPa. The total volume and volume of each phase were recorded by use of the cathetometer. **Table 3.8** shows the variation of liquid-phase and vapor-phase volume fractions measured at different pressures for Mixture HB1 (Table 3.2). **Table 3.9** summarizes the results and the comparison with predictions from the EOS model (Tables 3.6 and 3.7). The bubble points were observed at higher pressures than n-hexane's vapor pressures at the test temperatures, and reasonably correlated by the EOS model, as shown in **Figure 3.5**. The AARD is 15% for the bubble points (i.e., boundaries for the presence of the V phase). The EOS model predicts a separate water phase (labeled as W in Figure 3.5) below 108.0°C. Such a phase was not observed in the PVT experiment, although water may have precipitated as invisible water-in-oil emulsion in the bulk oil (L) phase.

Further PVT experiment was conducted for Mixture HB2. This mixture has a higher solvent concentration of 97.53 mol%, which is close to the butane concentration, 97.24 mol%, for the butane/bitumen mixture (Mixture B) studied by Gao et al. (2016). However, only L and LV equilibria were observed below 10 MPa at 159.8°C. The bubble-point pressure was 1.238 MPa at 159.8°C. **Figure 3.6** shows the digital images of a single-liquid phase at 4.199 MPa and LV two phases at 0.931 MPa at 159.8°C for Mixture HB2. No further experiments were conducted at lower temperatures for Mixture HB2, due to the limited availability of the PVT system for this research. It seems unlikely that liquid-liquid separation occurs for this Athabasca bitumen with n-hexane at lower temperatures because the level of miscibility between the two liquid phases, if present, would increase at lower temperatures (Gao et al. 2016).

With the procedure mentioned in the experimental section, densities of Mixture HB1 were measured at different temperature-pressure conditions by use of the PVT cell, as summarized in **Table 3.10 and Figure 3.7**. The reference density was measured at 51.1°C and atmospheric pressure by the densitometer. Figure 3.7 shows that the effect of pressure on density is more pronounced at higher temperatures for Mixture HB1.

Densities measured for Mixture HB1 were firstly compared with the values calculated with the following equation assuming no volume change on mixing:

$$\frac{1}{\rho_m} = \frac{w_s}{\rho_s} + \frac{1-w_s}{\rho_B}, \quad (3.7)$$

where ρ_m is the mass density of solvent/bitumen mixture. w_s is the weight fraction of solvent. ρ_s and ρ_B are the mass densities of solvent and bitumen, respectively. The values for ρ_s at different conditions were obtained from the NIST database (Lemmon et al. 2016). The ρ_B values were calculated from the correlated Tait equation presented in Gao et al. (2016). The resulting AARD is 13%, which indicates that volume change on mixing should be taken into account for Mixture HB1. Therefore, an excess-volume mixing rule

$$\frac{1}{\rho_m} = \frac{w_s}{\rho_s} + \frac{1-w_s}{\rho_B} - w_s(1-w_s)[\frac{1}{\rho_s} + \frac{1}{\rho_B}]\gamma \quad (3.8)$$

was used to correlate the data. In equation 3.8, γ is the parameter between solvent and bitumen for this model. The best-fitted γ, 0.2520, was obtained by regression to the measured densities (Table 3.10). It gives the AARD of 0.3%, which is much lower than that from equation 3.7. The predicted densities by use of the EOS model give an AARD of 12% with respect to the experimental data (Table 3.10).

Viscosities of n-hexane/bitumen mixtures (Mixtures HB3, HB4, and HB5 given in Table 3.2) at atmospheric pressure were measured by use of the Cone and Plate viscometer at temperatures from 25.0°C to 90.0°C as shown in **Table 3.11**. **Figure 3.8** shows a substantial reduction of bitumen viscosity by dilution with n-hexane.

Centeno et al. (2011) summarized a total of 26 mixing rules. Viscosities measured for n-hexane/bitumen mixtures were evaluated with four models: Arrhenius, Cragoe, power law, and Lederer. These models were used for heavy oil/solvent mixtures by Nourozieh et al. (2015 a b). These equations are given as follows:

Arrhenius: $\mu_m = {\mu_s}^{x_s} \times {\mu_B}^{(1-x_s)}$, (3.9)

where μ_m is the viscosity of a solvent/bitumen mixture, x_s is the mole fraction of solvent, and μ_s and μ_B are the viscosities of solvent and bitumen, respectively.

Cragoe: $\frac{1}{\ln(2000\mu_m)} = \frac{w_s}{\ln(2000\mu_s)} + \frac{1-w_s}{\ln(2000\mu_B)}$, (3.10)

where w_s is the weight fraction of solvent.

Power law: $\mu_m = [x_s{\mu_s}^n + (1 - x_s){\mu_B}^n]^{1/n}$, (3.11)

where n is the adjustable parameter in this model, and should be obtained through regression for a minimum AARD.

Lederer: $ln\mu_m = \left(1 - \frac{\theta\varphi_B}{\theta\varphi_B+\varphi_s}\right) ln\mu_s + \left(\frac{\theta\varphi_B}{\theta\varphi_B+\varphi_s}\right) ln\mu_B$, (3.12)

where θ is the adjustable parameter between 0.0 and 1.0 in this model, and should be obtained through regression for a minimum AARD. φ_s is the volume fraction of solvent.

Following the research by Nourozieh et al. (2015b), the fraction of solvent was considered as mole, weight, and volume fractions for each of equations 3.9, 3.10, and 3.11. Then, the total AARDs were calculated for all data for Mixtures HB3, HB4, and HB5 as shown in **Table 3.12**. Table 3.12 also shows the values for n and θ used for equations 3.11 and 3.12 in this research. Results show that the power-law model with weight fraction results in a more-accurate correlation than the other models for Mixtures HB3, HB4, and HB5. The power-law model with volume fraction gave the best results for n-hexane/bitumen mixtures in Nourozieh et al. (2015b).

Asphaltene precipitation measurements were conducted at ambient condition for bitumen diluted with n-hexane (Mixtures HB6, HB7, HB8, HB9, HB10, and HB11 given in Table 3.2). The measured asphaltene precipitation fractional yields are shown in **Table 3.13. Figure 3.9** presents the fractional yields obtained in this research, along with the data presented in the literature (Alboudwarej et al. 2003). The Athabasca bitumen used in this study yielded more asphaltene than the other bitumens, due to the higher asphaltene content (Table 3.1) in comparison with 14.6 wt% asphaltene content for Athabasca bitumen and 15.1 wt% for Lloydminster bitumen in Alboudwarej et al. (2003). No precipitated asphaltene was observed for the concentrations of n-hexane 39.97 wt% (83.10 mol%) and 50.01 wt% (88.08 mol%) at 20.4°C and atmospheric pressure in this research.

The results shown in Table 3.13 indicate that asphaltene precipitation may have happened in the PVT experiment for Mixture HB1 and HB2, considering the high n-hexane concentration. Asphaltene precipitates may have resided in the oleic phase as dispersed particles as described in Agrawal et al. (2012). However, it was not possible to observe asphaltene precipitation with the current PVT setup, which is not equipped with a solid-detection unit.

3.3.3 n-Octane/Bitumen Mixtures

Saturation pressures of Mixture OB1 were measured at 140.7°C and 159.0°C. Only single liquid phase and liquid-vapor phase equilibria were observed through the PVT-cell window within this temperature range. **Table 3.14** shows the variation of liquid-phase and vapor-phase volume fractions measured at different pressures for Mixture OB1. **Table 3.15** summarizes the results and the comparison with predictions from the EOS model (Tables 3.6 and 3.7). The EOS model reasonably correlates the data as shown in **Figure 3.10**. The AARD is 20% for the bubble points. As in section 3.2, the W phase predicted below 90.0°C by the EOS model was not observed in the PVT experiment. However, it is possible that water droplets have resided as water-in-oil emulsion in the L phase below a temperature limit of water-in-oil solubility.

Densities of Mixture OB1 were measured at different temperature-pressure conditions by use of the PVT cell, as summarized in **Table 3.16 and Figure 3.11**. The reference density was measured at 50.2°C and atmospheric pressure by the densitometer (section 3.2.2). Thereafter, measured densities for Mixture OB1 were compared with the calculated values by use of equations 3.7 and 3.8. The AARD is 3.5% with equation 3.7 and 0.2% with equation 3.8. The best-fitted γ for equation 3.8 is 0.0966 for Mixture OB1. The predicted densities by use of the EOS model give an AARD of 2.7% in comparison with experimental data (Table 3.16).

Viscosities of n-octane/bitumen mixtures (Mixtures OB2, OB3, and OB4 given in Table 3.2) at atmospheric pressure were also measured by use of the Cone and Plate viscometer at the temperature from 25.0°C to 90.0°C as shown in **Table 3.17** and Figure 3.8. Measured viscosities of n-octane/bitumen mixtures were also compared with equations 3.9, 3.10, 3.11, and 3.12. The total AARDs for Mixtures OB2, OB3, and OB4 with equations 3.9-3.12 are presented in **Table 3.18**. For Mixtures OB2, OB3, and OB4, the best-fitted model is the power law correlation with weight fraction.

Asphaltene precipitation measurements were also conducted at ambient condition for Mixtures OB5, OB6, OB7, OB8, OB9, and OB10 given in Table 3.2. **Table 3.19** showed the measured asphaltene precipitation fractional yields**.** No precipitated asphaltene was observed for the concentrations of n-octane 40.24 wt% (78.95 mol%) and 50.10 wt% (84.83 mol%) at 20.4°C and atmospheric pressure. Figure 3.9 showed a lower fractional yield for n-octane/bitumen mixtures compared with n-hexane-diluted-bitumen, which is consistent with data presented in the literature (e.g., Rassamdana et al. 1996; Akbarzadeh et al. 2005).

3.4 Conclusions

This chapter presented an experimental study of phase equilibrium, viscosity, density, and asphaltene precipitation for 11 mixtures of Athabasca bitumen with n-hexane and 10 mixtures of the same bitumen with n-octane. The bitumen sample used in this research is the same as the one used in our previous research (Gao et al. 2016) for multiphase behavior of bitumen/n-butane mixtures. One of the main questions addressed in this study is whether liquid-liquid separation of hydrocarbons occurs for mixtures of Athabasca bitumen with n-hexane or n-octane at conditions relevant to steam-solvent coinjection. Conclusions are as follows:

- The liquid-liquid immiscibility of hydrocarbons was not observed for n-hexane/bitumen and n-octane/bitumen mixtures for the range of temperatures and pressures in this research, even at solvent concentrations over 90 mol%. This is in contrast to the previous research by Gao et al. (2016), in which the same bitumen was not effectively diluted by n-butane due to the coexistence of a butane-rich liquid with a bitumen-rich liquid phase. In coinjection of steam with heavier hydrocarbon solvents, such as n-hexane and n-octane, the amount of solvent available near the edge of a steam chamber may be entirely used for diluting bitumen ahead of the edge.

- Results from the viscosity measurements at atmospheric pressure showed that n-hexane yields more reduction of the bitumen-phase viscosity than n-octane. In asphaltene precipitation experiments at atmospheric pressure, a larger amount of precipitates was observed with n-hexane than with n-octane at a given solvent concentration above 50 wt%. Below the solvent concentration of 50 wt%, no asphaltene precipitation was observed for both solvents with the Athabasca bitumen sample used in this research.

- The viscosity data obtained for n-hexane/bitumen and n-octane/bitumen mixtures in this research were well correlated by the power-law correlation with weight fraction. Representation of the density data obtained for n-hexane/bitumen and n-octane/bitumen mixtures requires the excess volume mixing rule.

References:

Agrawal, P., Schoeggl, F.F., Satyro, M.A., Taylor, S.D., and Yarranton, H.W. 2012. Measurement and Modeling of the Phase Behavior of Solvent Diluted Bitumens. *Fluid Phase Equilibr.* **334:** 51-64.

Alboudwarej, H., Akbarzadeh, K., Beck, J., Svrcek, W.Y., and Yarranton, H.W. 2003. Regular Solution Model for Asphaltene Precipitation from Bitumens and Solvents. *AIChE J.* **49**(11): 2948-2956.

Ardali, M., Mamora, D.D., and Barrufet, M. 2010. A Comparative Simulation Study of Addition of Solvents to Steam in SAGD Process. CSUG/SPE paper 138170 presented at Canadian Unconventional Resources and International Petroleum Conference, Calgary, Alberta, Canada, October 19-21.

Ardali, M., Barrufet, M., and Mamora, D.D. 2012. Laboratory Testing of Addition of Solvents to Steam to Improve SAGD Process. Paper SPE 146993 presented at SPE Heavy Oil Conference Canada, Calgary, Alberta, Canada, June 12-14.

Argüelles-Vivas, F.J., Babadagli, T., Little, L., Romaniuk, N., and Ozum, B. 2012. High Temperature Density, Viscosity, and Interfacial Tension Measurements of Bitumen–Pentane–Biodiesel and Process Water Mixtures. *J. Chem. Eng. Data*, **57**(10): 2878-2889.

Arshad, M. and Li, H. 2015. Multiphase Equilibria of Solvent-Steam-Bitumen System within SAGD Steam-Chamber Boundary. Paper SPE 174444 presented at the SPE Heavy Oil Conference-Canada, Calgary, Alberta, Canada, June 11-13, 2015.

Azinfar, B., Zirrahi, M., Hassanzadeh, H., and Abedi, J. 2015. A Method for Characterization of Bitumen. *Fuel.* **153**: 240-248.

Buenrostro-Gonzalez, E., Lira-Galeana, C., Gil-Villegas, A., and Wu, J. 2004. Asphaltene Precipitation in Crude Oils: Theory and Experiments. *AIChE J*. **50**(10): 2552-2570.

Bulter, R.M. 1991. Thermal Recovery of Oil and Bitumen. Prentice Hall, New Jersey.

Centeno, G., Sánchez-Reyna, G., Ancheyta, J., Muñoz, J.A., and Cardona, N. 2011. Testing Various Mixing Rules for Calculation of Viscosity of Petroleum Blends. *Fuel*. **90**(12): 3561-3570.

Díaz, O.C., Modaresghazani, J., Satyro, M.A., and Yarranton, H.W. 2011. Modeling the Phase Behavior of Heavy Oil and Solvent Mixtures. *Fluid Phase Equilibr.* **304** (1): 74-85.

Gao, J., Okuno, R., and Li, H. A. 2016. An Experimental Study of Multiphase Behavior for n-Butane/Bitumen/Water Mixtures. Accepted for publication in *SPE J.* on Sep 8, 2016. SPE-180736-PA.

Govind, P.A., Das, S.K., Srinivasan, S., and Wheeler, T.J. 2008. Expanding Solvent SAGD in Heavy Oil Reservoirs. Paper SPE/PS/CHOA 117571 presented at the 2008 SPE International Thermal Operations and Heavy Oil Symposium, Calgary, Alberta, Canada, October 20-23.

Gupta, S.C., and Gittins, S.D. 2007. Effect of Solvent Sequencing and Other Enhancements on Solvent Aided Process. *J. Can. Petrol. Tech.* **46**(09).

Hascakir, B. 2016. How to Select the Right Solvent for Solvent-Aided Steam Injection Processes. *J. Petrol. Sci. Eng.*

Hosseininejad Mohebati, M., Maini, B.B., and Harding, T.G. 2012. Numerical-Simulation Investigation of the Effect of Heavy-Oil Viscosity on the Performance of Hydrocarbon Additives in SAGD. *SPE Res. Eval. and Eng*. **15**(02): 165-181.

Jha, R.K., Kumar, M., Benson, I., and Hanzlik, E. 2013. New Insights into Steam-Solvent Co-Injection Process Mechanism. *SPE J.* **18**(05): 867-877.

Jindrová, T., Mikyška, J., and Firoozabadi, A. 2015. Phase Behavior Modeling of Bitumen and Light Normal Alkanes and CO2 by PR-EOS and CPA-EOS. *Energy Fuels*. **30**(1): 515-525.

Kariznovi, M., Nourozieh, H., and Abedi, J. 2009. Bitumen Characterization and Pseudocomponents Determination for Equation of State Modeling. *Energy Fuels*. **24** (1): 624-633.

Kariznovi, M., Nourozieh, H., Guan, J.G.J., and Abedi, J. 2013. Measurement and Modeling of Density and Viscosity for Mixtures of Athabasca Bitumen and Heavy N-alkane. *Fuel*. **112**: 83-95.

Kariznovi, M., Nourozieh, H., and Abedi, J. 2014a. Measurement and Correlation of Viscosity and Density for Compressed Athabasca Bitumen at Temperatures Up to 200ºC. *J. Can. Petro. Tech.* **53**(06): 330-338.

Kariznovi, M., Nourozieh, H., and Abedi, J. 2014b. Volumetric Properties of Athabasca Bitumen+ n-Hexane Mixtures. *Energy Fuels*. **28**(12): 7418-7425.

Keshavarz, M., Okuno, R., and Babadagli, T. 2015a. Optimal Application Conditions for Steam/Solvent Coinjection. *SPE Res. Eval. and Eng*. **18**(01): 20-38.

Keshavarz, M., Okuno, R., and Babadagli, T. 2015b. A Semi-Analytical Solution to Optimize Single-Component Solvent Coinjection with Steam during SAGD. *Fuel*. **144**: 400-414.

Khan, M.A.B., Mehrotra, A.K., and Svrcek, W.Y. 1984. Viscosity Models for Gas-Free Athabasca Bitumen. *J. Can. Pet. Tech*. **23**(3): 47-53.

Krejbjerg, K., and Pedersen, K.S. 2006. Controlling VLLE Equilibrium with a Cubic EOS in Heavy Oil Modeling. Paper PETSOC-2006-052 presented at the Canadian International Petroleum Conference, Calgary, Alberta, Canada, June 13-15.

Kumar, A., and Okuno, R. 2016. A New Algorithm for Multiphase Fluid Characterization for Solvent Injection. *SPE J.* SPE-175123-PA.

Lemmon E.W., McLinden M.O. and Friend D.G., "Thermophysical Properties of Fluid Systems" in NIST Chemistry WebBook, NIST Standard Reference Database Number 69, Eds. P.J.

Linstrom and W.G. Mallard, National Institute of Standards and Technology, Gaithersburg MD, 20899, http://webbook.nist.gov, (retrieved August 28, 2016).

Li, Y.K., Heavy Fraction Characterization and Hypothetical Component Selection for Oil and Gas Mixtures. Computer Modelling Group Research Report R12.04. May 1983.

Li, W., and Mamora, D.D. 2010. Phase Behavior of Steam with Solvent Co-injection under Steam Assisted Gravity Drainage (SAGD) Process. Paper SPE 130807 presented at SPE EUROPEC/EAGE Annual Conference and Exhibition, Barcelona, June 14-17.

Li, W., Mamora, D.D., and Li, Y. 2011. Solvent-Type and –Ratio Impacts on Solvent-Aided SAGD Process. *SPE Res. Eval. and Eng.* **14**(3): 320-331.

Li, Z., and Firoozabadi, A. 2010. Modeling Asphaltene Precipitation by n-Alkanes from Heavy Oils and Bitumens Using Cubic-Plus-Association Equation of State. *Energy and Fuels*. **24**(2): 1106-1113.

Ma, M., Chen, S., and Abedi, J. 2016. Predicting the Multiphase Equilibrium and Density of Bitumen with C2H6, C3H8 and CO2 Using the Simplified PC-SAFT Equation of State. *Fuel.* **181**: 652-659.

Mehra, R.K. 1981. The Computation of Multi-Phase Equilibrium in Compositional Reservoir Studies. PHD Dissertation. University of Calgary.

Mehrotra, A.K., and Svrcek, W.Y. 1985a. Viscosity, Density and Gas Solubility Data for Oil Sand Bitumens. Part I: Athabasca Bitumen Saturated with CO and C2H6. *AOSTRA J. Res*. **1**(4): 263-268.

Mehrotra, A.K., and Svrcek, W.Y. 1985b. Viscosity, Density and Gas Solubility Data for Oil Sand Bitumens. Part II: Peace River Bitumen Saturated with N2, CO, CH4, CO2 and C2H6. *AOSTRA J. Res*. **1**(4): 269-279.

Mehrotra, A.K., and Svrcek, W.Y. 1985c. Viscosity, Density and Gas Solubility Data for Oil Sand Bitumens. Part III: Wabasca Bitumen Saturated with N2, CO, CH4, CO2 and C2H6. *AOSTRA J. Res*. **2**(2): 83-93.

Mehrotra, A.K., and Svrcek, W.Y. 1986. Viscosity of Compressed Athabasca Bitumen. *Can. J. Chem. Eng.* **64**(5): 844-847.

Mehrotra, A.K., and Svrcek, W.Y. 1987. Viscosity of Compressed Cold Lake Bitumen. *Can. J. Chem. Eng.* **65**(4): 672-675.

Mehrotra, A.K., and Svrcek, W.Y. 1988. Properties of Cold Lake Bitumen Saturated with Pure Gases and Gas Mixtures. *Can. J. Chem. Eng.* **66**(4): 656-665.

Mohammadzadeh, O., Rezaei, N., and Chatzis, I. 2012. More Insight into the Pore-Level Physics of the Solvent-Aided SAGD (SA-SAGD) Process for Heavy Oil and Bitumen Recovery. Paper SPE 157776 presented at SPE Heavy Oil Conference Canada, Calgary, Alberta, Canada, June 12-14.

Nagarajan, N.R., Honarpour, M.M., and Sampath, K. 2006. Reservoir Fluid Sampling and Characterization—Key to Efficient Reservoir Management. Paper SPE 101517 presented at the Abu Dhabi International Petroleum Exhibition and Conference, Abu Dhabi, U.A.E., November 5-8.

Naseri, A., Nikazar, M., and Dehghani, S.M. 2005. A Correlation Approach for Prediction of Crude Oil Viscosities. *J. Petrol. Sci. Eng.* **47**(3), 163-174.

Nasr, T.N. and Isaacs, E. 2001. Process for Enhancing Hydrocarbon Mobility Using a Steam Additive. U.S. Patent 6230814.

Nasr, T.N., Beaulieu, G., Golbeck, H., and Heck, G. 2003. Novel Expanding Solvent-SAGD Process "ES-SAGD". *J. Can. Petro. Tech.* **42**(1): 13-16.

Nourozieh, H., Kariznovi, M., Guan, J.G., and Abedi, J. 2013. Measurement of Thermophysical Properties and Modeling for Pseudo-Binary Mixtures of N-decane and Athabasca Bitumen. *Fluid Phase Equilibr*. **347**: 62-75.

Nourozieh, H., Kariznovi, M., and Abedi, J. 2014. Measurement and Prediction of Density for the Mixture of Athabasca Bitumen and Pentane at Temperatures up to 200ºC. *Energy Fuels*. **28**(5): 2874-2885.

Nourozieh, H., Kariznovi, M., and Abedi, J. 2015a. Viscosity Measurement and Modeling for Mixtures of Athabasca Bitumen/n-Pentane at Temperatures up to 200ºC. *SPE J*. **20**(02): 226-238.

Nourozieh, H., Kariznovi, M., and Abedi, J. 2015b. Viscosity Measurement and Modeling for Mixtures of Athabasca Bitumen/Hexane. *J. Petro. Sci. Eng.* **129**: 159-167.

Nourozieh, H., Kariznovi, M., and Abedi, J. 2015c. Density and Viscosity of Athabasca Bitumen Samples at Temperatures Up to 200ºC and Pressures Up to 10 MPa. *SPE Res. Eval. and Eng.*

Nourozieh, H., Kariznovi, M., and Abedi, J. 2015d. Modeling and Measurement of Thermo-Physical Properties for Athabasca Bitumen and N-heptane Mixtures. *Fuel*. **157**: 73-81.

Panuganti, S.R., Vargas, F.M., Gonzalez, D.L., Kurup, A.S., and Chapman, W.G. 2012. PC-SAFT Characterization of Crude Oils and Modeling of Asphaltene Phase Behavior. *Fuel.* **93**: 658-669.

Péneloux, A., Rauzy, E., and Fréze, R. 1982. A Consistent Correction for Redlich-Kwong-Soave Volumes. *Fluid Phase Equilibr.* **8**(1): 7-23.

Peng, D.Y., and Robinson, D.B. 1976. A New Two-constant Equation of State. *Ind. Eng. Chem. Fund.* **15**(1): 59-64.

Quiñones-Cisneros, S.E., Dalberg, A., and Stenby, E.H. 2004. PVT Characterization and Viscosity Modeling and Prediction of Crude Oils. *Petro. Sci. Tech.* **22**(9-10): 1309-1325.

Rassamdana, H., Dabir, B., Nematy, M., Farhani, M., and Sahimi, M. 1996. Asphalt Flocculation and Deposition: I. The Onset of Precipitation. *AIChE J.* **42**(1): 10-22.

Redford, D.A. and McKay, A.S. 1980. Hydrocarbon-Steam Processes for Recovery of Bitumen from Oil Sands. Paper SPE 8823 presented at SPE/DOE Enhanced Oil Recovery Symposium, Tulsa, Oklahoma, USA, April 20-23.

Robinson, D.B., and Peng, D.Y. 1978. The Characterization of the Heptanes and Heavier Fractions for the GPA Peng-Robinson Programs. *Gas Processors Association.*

Sabbagh, O., Akbarzadeh, K., Badamchi-Zadeh, A., Svrcek, W.Y., and Yarranton, H.W. 2006. Applying the PR-EoS to Asphaltene Precipitation from N-alkane Diluted Heavy Oils and Bitumens. *Energy fuels*. **20**(2): 625-634.

Satyro, M.A., and Yarranton, H.W. 2010. Expanded Fluid-Based Viscosity Correlation for Hydrocarbons Using an Equation of State. *Fluid Phase Equilibria*. **298**(1): 1-11.

Svrcek, W.Y., and Mehrotra, A.K. 1989. Properties of Peace River Bitumen Saturated with Field Gas Mixtures. *J. Can. Petro. Tech.* **28**(02).

Tavakkoli, M., Panuganti, S.R., Taghikhani,V., Pishvaie, M.R., and Chapman, W.G. 2013. Precipitated Asphaltene Amount at High-Pressure and High-Temperature Conditions. *Energy and Fuels*. **28**(3): 1596-1610.

Vargas, F.M., Gonzalez, D.L., Creek, J.L., Wang, J., Buckley, J., Hirasaki, G.J., and Chapman, W.G. 2009. Development of a General Method for Modeling Asphaltene Stability. *Energy Fuels*. **23**(3): 1147-1154.

Venkatramani, A., and Okuno, R. 2015. Characterization of Water-Containing Reservoir Oil Using an EOS for Steam Injection Processes. *J. Nat. Gas Sci. Eng.* **26**: 1091-1106.

Venkatramani, A., and Okuno, R. 2016. Compositional Mechanisms in SAGD and ES-SAGD with Consideration of Water Solubility in Oil. Accepted for publication in *SPE Res. Eval. and Eng.-Res. Eng.* on August 1, 2016. SPE-180737-PA.

Yazdani, A., Alvestad, J., Kjonsvik, D., Gilje, E., and Kowalewski, E. 2011. A Parametric Simulation Study for Solvent Co-injection Process in Bitumen Deposits. Paper SPE 148804 presented at the Canadian Unconventional Resources Conference, Calgary, Alberta, Canada, November 15-17.

Zirrahi, M., Hassanzadeh, H., and Abedi, J. 2015a. Prediction of CO2 Solubility in Bitumen Using the Cubic-Plus-Association Equation of State (CPA-EOS). *J. Supercritical Fluids*. **98**: 44-49.

Zirrahi, M., Hassanzadeh, H., and Abedi, J. 2015b. Prediction of Water Solubility in Petroleum Fractions and Heavy Crudes Using Cubic-Plus-Association Equation of State (CPA-EoS). *Fuel*. **159**: 894-899.

Zou, X.Y., Zhang, X., and Shaw, J.A. 2007. Phase Behavior of Athabasca Vacuum Bottoms+ N-alkane Mixtures. *SPE Prod. Oper*. **22**(02): 265-272.

Zúñiga-Hinojosa, M.A., Justo-García, D.N., Aquino-Olivos, M.A., Román-Ramírez, L.A., and García-Sánchez, F. 2014. Modeling of Asphaltene Precipitation from n-Alkane Diluted Heavy Oils and Bitumens Using the PC-SAFT Equation of State. *Fluid Phase Equilibr.* **376**: 210-224.

Tables and Figures:

Hydrocarbons	Mass%
Saturates	28.6
Aromatics	30.7
Resins Ⅰ	20.8
Resins Ⅱ	1.8
Asphaltene	18.0

Table 3.1 – SARA test results for Athabasca-bitumen sample. This is the same bitumen as the one studied by Gao et al. (2016).

Mixtures	Solvent, mol%	Dead bitumen, mol%	Water in bitumen mol%	Solvent, wt%	Dead bitumen, wt%	Water in bitumen wt%	Measurement
HB1	88.27	10.72	1.01	52.67	47.21	0.13	PVT
HB2	97.53	2.26	0.21	85.38	14.59	0.04	PVT
HB3	27.50	66.24	6.26	5.31	94.44	0.25	viscosity
HB4	44.47	50.74	4.79	10.58	89.18	0.24	viscosity
HB5	53.81	42.21	3.99	14.69	85.08	0.23	viscosity
HB6	81.83	16.60	1.57	39.97	59.87	0.16	asphaltene precipitation
HB7	87.12	11.76	1.11	50.01	49.86	0.13	asphaltene precipitation
HB8	90.40	8.77	0.83	58.20	41.69	0.11	asphaltene precipitation
HB9	93.68	5.78	0.55	68.66	31.26	0.08	asphaltene precipitation
HB10	96.15	3.51	0.33	78.71	21.24	0.06	asphaltene precipitation
HB11	98.39	1.48	0.14	90.01	9.96	0.03	asphaltene precipitation
OB1	93.71	5.75	0.54	74.49	25.45	0.07	PVT
OB2	17.35	75.52	7.13	3.95	95.79	0.26	viscosity
OB3	36.08	58.40	5.52	9.96	89.80	0.24	viscosity
OB4	45.84	49.49	4.67	14.23	85.55	0.23	viscosity
OB5	77.46	20.60	1.95	40.24	59.60	0.16	asphaltene precipitation
OB6	83.67	14.92	1.41	50.10	49.76	0.13	asphaltene precipitation
OB7	88.48	10.53	0.99	60.07	39.82	0.11	asphaltene precipitation
OB8	92.25	7.08	0.67	69.99	29.93	0.08	asphaltene precipitation
OB9	95.34	4.26	0.40	80.04	19.91	0.05	asphaltene precipitation
OB10	97.87	1.95	0.18	90.00	9.97	0.03	asphaltene precipitation

Table 3.2 – Compositions and measurement type for the mixtures discussed in this research. The bitumen sample used in this study is dead bitumen containing a small amount of water.

Removal of water from the bitumen sample by heating was not attempted in order to prevent light components from being evaporated.

T, °C	μ_{SFS}, s	μ, cp
60.0	998.3	2158.4
65.0	697.8	1504.0
70.0	488.8	1050.2
75.0	350.2	750.0
80.0	257.5	549.7
85.0	189.5	403.2
90.0	142.5	302.0
95.0	113.6	240.1
100.0	93.1	195.9
105.0	74.9	157.0
110.0	63.9	133.5
115.0	54.5	113.3
120.0	40.6	84.0
125.0	34.4	70.9
130.0	30.3	62.0
135.0	26.5	54.1
140.0	22.1	44.7

Table 3.3 – Saybolt Furol viscosities (μ_{SFS}) measured by use of Saybolt viscometer and dynamic viscosities (μ) calculated from 60.0°C to 140.0°C at atmospheric pressure. Dynamic viscosities of bitumen were determined by Saybolt Furol viscosity and the calculated bitumen densities by use of the correlated Tait equation in Gao et al. (2016).

First Measurement						
T, °C	**Speed, RPM**	**Torque, %**	**Shear stress, dyne/cm^2**	**Shear rate, 1/s**	**μ, cp**	**Accuracy, cp**
25.0	1	98.2	1949	2	97430	992.2
30.0	2	99.4	1972	4	49310	496.1
40.0	6	89	1766	12	14720	165.4
50.0	18	93.4	1853	36	5148	55.12
60.0	40	85.2	1691	80	2113	24.81
70.0	100	98	1945	200	972.4	9.92
80.0	180	90.8	1802	360	500.5	5.51
90.0	200	56.6	1123	400	280.8	4.96
100.0	200	34.4	682.6	400	170.7	4.96
Second Measurement						
T, °C	**Speed, RPM**	**Torque, %**	**Shear stress, dyne/cm^2**	**Shear rate, 1/s**	**μ, cp**	**Accuracy, cp**
25.0	0.9	91	1806	1.8	100300	1102
30.0	1.8	92	1826	3.6	50710	551.2
40.0	6	90.2	1790	12	14920	165.4
50.0	18	95.3	1891	36	5253	55.12
60.0	40	86.5	1717	80	2146	24.81
70.0	90	88.9	1764	180	980.1	11.02
80.0	180	91.6	1818	360	504.9	5.51
90.0	200	57.6	1143	400	285.8	4.96
100.0	200	36	714.4	400	178.6	4.96

Table 3.4 – Measured bitumen viscosities from 25.0°C to 100.0°C at atmospheric pressures by use of Cone and Plate viscometer. After setting the rotational speed at each test temperature, the torque, shear stress, shear rate, viscosity and accuracy were recorded from the viscometer. The accuracy is 1.0% of full-scale viscosity range at the corresponding rotational speed.

Coefficients	Saybolt viscometer	Cone and Plate viscometer 1st measurement	Cone and Plate viscometer 2nd measurement
b_1	21.5036	23.3463	23.4760
b_2	-3.3511	-3.6691	-3.6914
AARD, %	3.9	2.7	3.6

Table 3.5 – The fitting parameters for the correlation equation 3.6 (Khan et al. 1984) for bitumen viscosities at atmospheric pressure measured with the Saybolt viscometer and Cone and Plate viscometer.

	MW	T_C, °C	P_C, MPa	ω	V_C, cm^3/mol	C_{PEN}, cm^3/mol	Bitumen, mol%
C_6	86.176	234.5	3.025	0.3010	368.570	-3.111	0.00
C_8	114.230	295.6	2.492	0.3980	485.407	3.879	0.00
water	18.010	373.9	22.064	0.3433	63.071	-0.091	8.64
PC-1	296.939	435.0	2.146	0.8423	612.873	-147.701	48.84
PC-2	662.802	495.1	1.507	0.9429	920.536	-275.005	21.88
PC-3	1082.668	725.0	1.364	1.0225	1,299.294	-447.976	13.40
PC-4	2003.494	1072.9	1.045	1.1486	2,192.365	-936.360	7.24

Table 3.6 – Components' properties of the characterized EOS model and the bitumen sample composition. Bitumen was characterized as a mixture of four pseudo components, PC-1, -2, -3, and -4. C_{PEN} is the volume-shift parameter of Péneloux et al. (1982).

	C_6	C_8	Water	PC-1	PC-2	PC-3
C_8	0.0000					
Water	0.5790	0.5270				
PC-1	0.0036	0.0008	0.2006			
PC-2	0.0115	0.0057	0.1694	0.0000		
PC-3	0.0217	0.0133	0.1694	0.0000	0.0000	
PC-4	0.0426	0.0308	0.1694	0.0000	0.0000	0.0000

Table 3.7 – Binary interaction parameters used for the EOS model.

T, °C	P, MPa	Volume fraction of liquid phase	Volume fraction of vapor phase
80.8	0.177	0.899	0.101
80.8	0.170	0.868	0.132
80.8	0.170	0.840	0.160
111.1	0.412	0.957	0.043
111.1	0.405	0.920	0.080
111.1	0.405	0.896	0.104
111.1	0.398	0.869	0.131
111.1	0.398	0.836	0.164
140.8	0.846	0.951	0.049
140.8	0.839	0.918	0.082
140.8	0.832	0.881	0.119
140.8	0.818	0.852	0.148
159.6	1.232	0.955	0.045
159.6	1.218	0.929	0.071
159.6	1.191	0.890	0.110
159.6	1.177	0.857	0.143
159.6	1.163	0.819	0.181

Table 3.8 – Measured liquid-phase and vapor-phase volume fractions for Mixture HB1 at different temperature-pressure conditions.

T, °C	Experimental data		Predictions from EOS model	
	P, MPa	ρ^{sat}, kg/m^3	P, MPa	ρ^{sat}, kg/m^3
80.8	0.209	845.0	0.178	747.2
111.1	0.426	813.0	0.423	719.6
140.8	0.880	784.4	0.715	690.6
159.6	1.290	754.5	0.974	669.6

Table 3.9 – Measured and predicted saturation pressures and densities at saturation points of Mixture HB1. Only single liquid phase and liquid-vapor phase equilibria were observed within this temperature range for Mixture HB1.

T, °C	P, MPa	ρ, kg/m^3	T, °C	P, MPa	ρ, kg/m^3
51.1	1.122	878.6	111.1	7.093	828.6
51.1	4.093	884.2	111.1	10.133	834.3
51.1	7.093	889.3	140.8	1.101	783.9
51.1	10.133	892.6	140.8	4.107	790.9
80.8	1.129	846.9	140.8	7.113	796.6
80.8	4.128	853.4	140.8	10.133	801.7
80.8	7.113	859.5	159.6	4.114	760.2
80.8	10.140	865.1	159.6	7.100	766.6
111.1	1.136	814.8	159.6	10.126	772.7
111.1	4.128	820.9			

Table 3.10 – Densities of Mixture HB1 measured at different temperature-pressure conditions by the PVT cell on the basis of constant composition expansion.

n-Hexane/Bitumen Mixture HB3						
T, °C	**Speed, RPM**	**Torque, %**	**Shear stress, dyne/cm^2**	**Shear rate, 1/s**	**μ, cp**	**Accuracy, cp**
25	0.3	96.8	237.4	2.25	10550	109
30	0.4	80.4	197.2	3	6573	81.75
40	1.1	88	215.8	8.25	2616	29.73
50	2.5	91.2	223.7	18.75	1193	13.08
60	4.5	82.7	202.8	33.75	601	7.27
70	8.5	84.9	208.2	63.75	326.6	3.85
80	15	89	218.3	112.5	194	2.18
90	25	91.7	224.9	187.5	119.9	1.31
n-Hexane/Bitumen Mixture HB4						
T, °C	**Speed, RPM**	**Torque, %**	**Shear stress, dyne/cm^2**	**Shear rate, 1/s**	**μ, cp**	**Accuracy, cp**
25	1.4	88.7	217.5	10.5	2072	23.36
30	1.9	83.7	205.3	14.25	1441	17.21
40	3.7	84.3	206.7	27.75	745	8.84
50	7	88.9	204.8	48.75	415.3	5.03
60	11	84.5	207.2	82.5	251.2	2.97
70	17	81.5	199.9	127.5	156.8	1.92
80	28	87.8	215.3	210	102.5	1.17
90	40	94.3	231.3	300	77.09	0.82
n-Hexane/Bitumen Mixture HB5						
T, °C	**Speed, RPM**	**Torque, %**	**Shear stress, dyne/cm^2**	**Shear rate, 1/s**	**μ, cp**	**Accuracy, cp**
25	3.2	88.1	216.1	24	900.3	10.22
30	4.2	85	208.5	31.5	661.8	7.79
40	8	89.6	219.7	60	366.2	4.09
50	12	81.6	200.1	90	222.4	2.73
60	20	86.6	212.4	150	141.6	1.64
70	28	84.3	206.7	210	98.45	1.17
80	40	82.1	201.4	300	67.12	0.82
90	55	91.4	224.2	412.5	54.34	0.59

Table 3.11 – Viscosities of n-hexane/bitumen mixtures (HB3, 4, and 5 given in Table 3.2) measured at different temperatures and atmospheric pressure by use of Cone and Plate viscometer.

Model	AARD, % mole fraction	AARD, % weight fraction	AARD, % volume fraction
Arrhenius	81.77	397.17	190.81
Cragoe	97.65	24.75	47.2
Power Law	46.20 (n=0.1002)	7.67 (n=-0.1885)	15.01 (n=-0.1321)
Lederer	-	-	37.75 (θ=0.4072)

Table 3.12 – Calculated AARDs of different models for prediction and correlation of the viscosities measured for n-hexane/bitumen mixtures (HB3, 4, and 5 given in Table 3.2). Nourozieh et al. (2015b) presented for Athabasca-bitumen/n-hexane mixtures that the coefficients for the power law with mole fraction, weight fraction, and volume fraction were 0.0186, -0.3365, -0.2049, respectively. They also presented the coefficient for Lederer's correlation to be 0.2869 in their research.

Mixtures	$M_{bitumen}$, g	$M_{solvent}$, g	Solvent weight fraction	$M_{asphaltene}$, g	Fractional yield
HB6	30.230	20.125	0.3997	0.000	0.0000
HB7	29.425	29.433	0.5001	0.000	0.0000
HB8	29.970	41.720	0.5820	2.168	0.0723
HB9	29.920	65.540	0.6866	3.204	0.1071
HB10	29.885	110.455	0.7871	4.279	0.1432
HB11	29.550	266.223	0.9001	4.944	0.1673

Table 3.13 – Results of asphaltene precipitation measurements for n-hexane/bitumen mixtures HB6, 7, 8, 9, 10 given in Table 3.2.

T, °C	P, MPa	Volume fraction of liquid phase	Volume fraction of vapor phase
140.7	0.156	0.883	0.117
140.7	0.150	0.867	0.133
140.7	0.143	0.845	0.155
159.0	0.219	0.876	0.124
159.0	0.212	0.865	0.135
159.0	0.205	0.853	0.147
159.0	0.191	0.797	0.203

Table 3.14 – Measured liquid-phase and vapor-phase volume fractions for Mixture OB1 at different temperature-pressure conditions.

	Experimental data		Predictions from EOS model	
T, °C	P, MPa	ρ^{sat}, kg/m^3	P, MPa	ρ^{sat}, kg/m^3
140.7	0.198	687.7	0.227	669.0
159.0	0.247	673.0	0.311	650.7

Table 3.15 – Measured and predicted saturation pressures and densities at saturation points of Mixture OB1. Only single liquid phase and liquid-vapor phase equilibria were observed within this temperature range for Mixture OB1.

T, °C	P, MPa	ρ, kg/m^3	T, °C	P, MPa	ρ, kg/m^3
50.2	1.101	768.4	110.5	7.100	727.0
50.2	4.107	772.2	110.5	10.113	731.5
50.2	7.106	775.5	140.7	1.094	690.0
50.2	10.092	779.6	140.7	4.100	694.0
80.2	1.101	744.1	140.7	7.100	699.8
80.2	4.114	747.8	140.7	10.099	705.1
80.2	7.106	751.7	159.0	1.101	674.3
80.2	10.119	756.5	159.0	4.100	678.6
110.5	1.094	718.5	159.0	7.100	682.5
110.5	4.100	721.5	159.0	10.099	686.8

Table 3.16 – Densities of Mixture OB1 measured at different temperature-pressure conditions by the PVT cell on the basis of constant composition expansion.

n-Octane/Bitumen Mixture OB2						
T, °C	**Speed, RPM**	**Torque, %**	**Shear stress, dyne/cm^2**	**Shear rate, 1/s**	**μ, cp**	**Accuracy, cp**
25	7	86.5	1717	14	12260	141.7
30	12	90	1786	24	7441	82.68
40	30	91.4	1814	60	3023	33.07
50	60	82.3	1633	120	1361	16.54
60	130	86.6	1718	260	661	7.63
70	200	71.8	1425	400	356.2	4.96
80	200	43.4	861.2	400	215.3	4.96
90	200	28.1	557.6	400	139.4	4.96
n-Octane/Bitumen Mixture OB3						
T, °C	**Speed, RPM**	**Torque, %**	**Shear stress, dyne/cm^2**	**Shear rate, 1/s**	**μ, cp**	**Accuracy, cp**
25	0.6	92.2	226.1	4.5	5025	54.5
30	0.9	90.4	221.7	6.75	3285	36.33
40	2	85.4	209.4	15	1396	16.35
50	4	84.4	207	30	690	8.18
60	8	90.8	222.7	60	371.1	4.09
70	14	93.8	230	105	219.1	2.34
80	20	85.1	208.7	150	139.1	1.64
90	30	85.1	208.7	225	92.76	1.09
n-Octane/Bitumen Mixture OB4						
T, °C	**Speed, RPM**	**Torque, %**	**Shear stress, dyne/cm^2**	**Shear rate, 1/s**	**μ, cp**	**Accuracy, cp**
25	2.5	82.8	203.1	18.75	1083	13.08
30	3.5	85.5	209.7	26.25	798.8	9.34
40	6	88.5	217	45	482.3	5.45
50	10	88.5	217	75	289.4	3.27
60	17	94.4	231.5	127.5	181.6	1.92
70	25	93	228.1	187.5	121.6	1.31
80	37	90	220.7	277.5	79.54	0.88
90	50	89.5	219.5	375	58.53	0.65

Table 3.17 – Viscosities of n-octane/bitumen mixtures measured at different temperatures and atmospheric pressure by use of Cone and Plate viscometer.

Model	AARD, % mole fraction	AARD, % weight fraction	AARD, % volume fraction
Arrhenius	58.07	310.21	176.49
Cragoe	91.93	37.29	36.5
Power Law	55.33 (n=0.0093)	29.17 (n=-0.2292)	34.25 (n=-0.1812)
Lederer	-	-	54.55 (θ=0.2973)

Table 3.18 – Calculated AARDs of different models for prediction and correlation of the viscosities measured for n-octane/bitumen mixtures, OB 2, 3, and 4.

Mixtures	$M_{bitumen}$, g	$M_{solvent}$, g	Solvent weight fraction	$M_{asphaltene}$, g	Fractional yield
OB5	29.680	19.985	0.4024	0.000	0.0000
OB6	30.115	30.240	0.5010	0.000	0.0000
OB7	30.070	45.240	0.6007	1.878	0.0625
OB8	29.890	69.720	0.6999	3.394	0.1135
OB9	29.470	118.160	0.8004	4.064	0.1379
OB10	29.610	266.480	0.9000	4.569	0.1543

Table 3.19 – Asphaltene precipitation measurement results for n-octane/bitumen mixtures OB5, 6, 7, 8, 9, and 10.

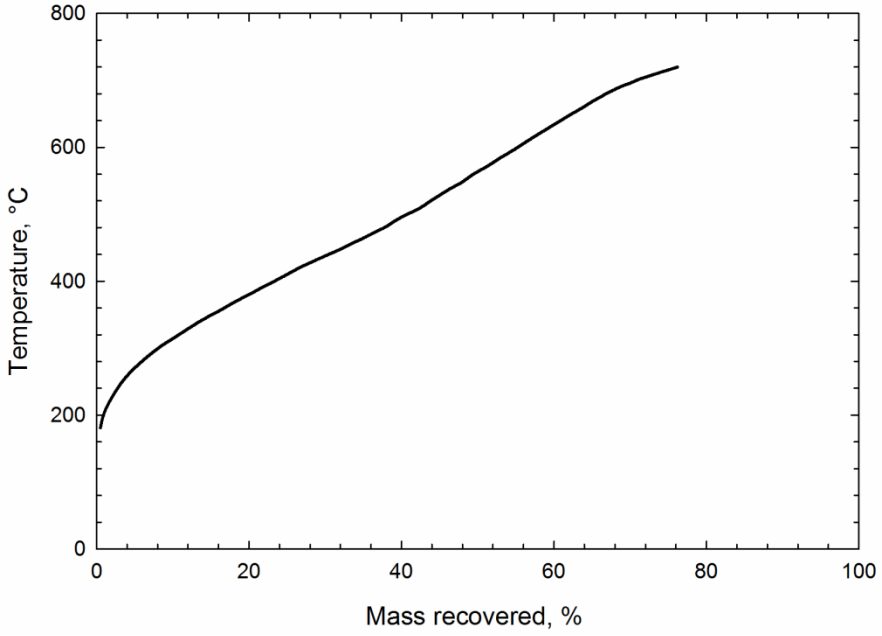

Figure 3.1 – Simulated distillation test results of Athabasca-bitumen sample at temperature up to 720°C.

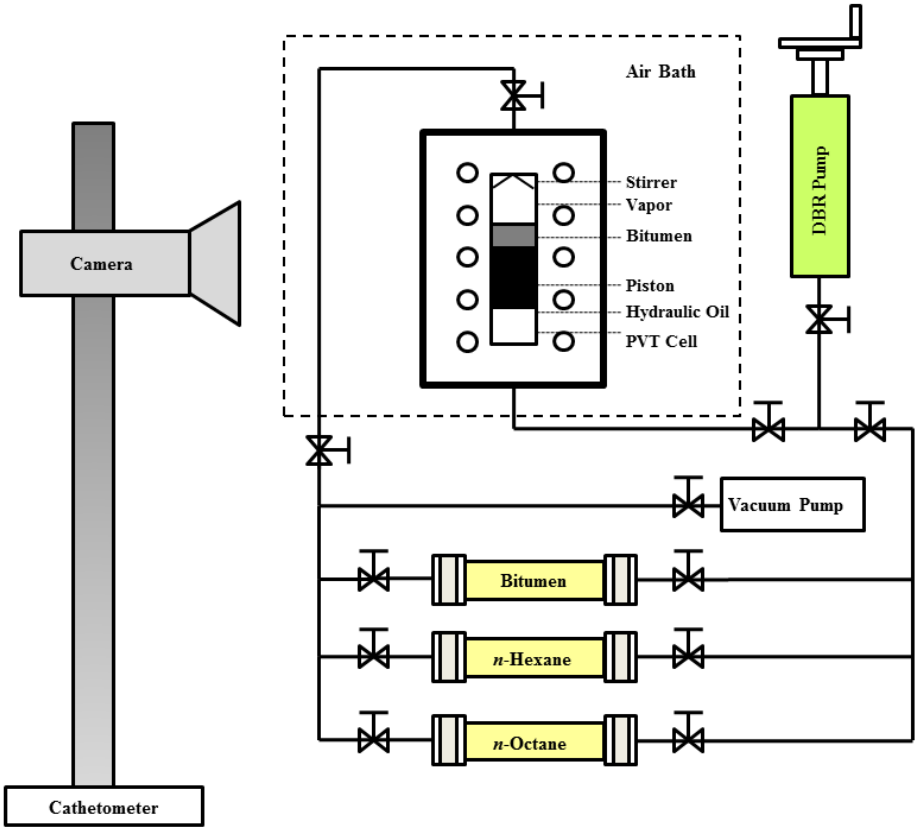

Figure 3.2 – Schematic of the phase behavior experimental setup.

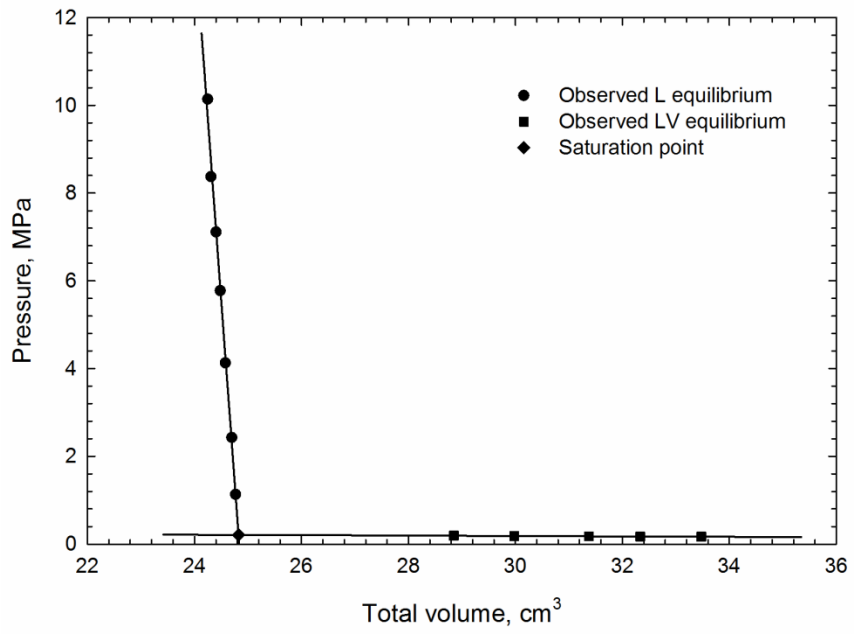

Figure 3.3 – Measured PV data for n-hexane/bitumen (Mixture HB1) at 80.8°C. Only single liquid phase and liquid-vapor phase equilibria were observed at this temperature. The saturation point is determined as the intersection of two PV lines.

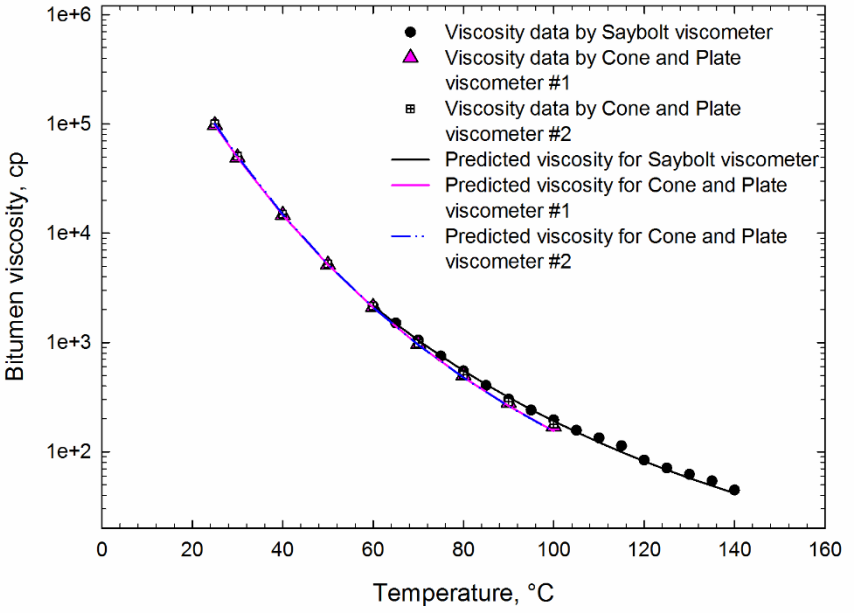

Figure 3.4 – The comparison between the correlated bitumen viscosity and experimental data measured by Saybolt viscometer and Cone and Plate viscometer. The predicted viscosities were calculated with equation 3.6 at corresponding temperatures with the fitting parameters presented in Table 3.5.

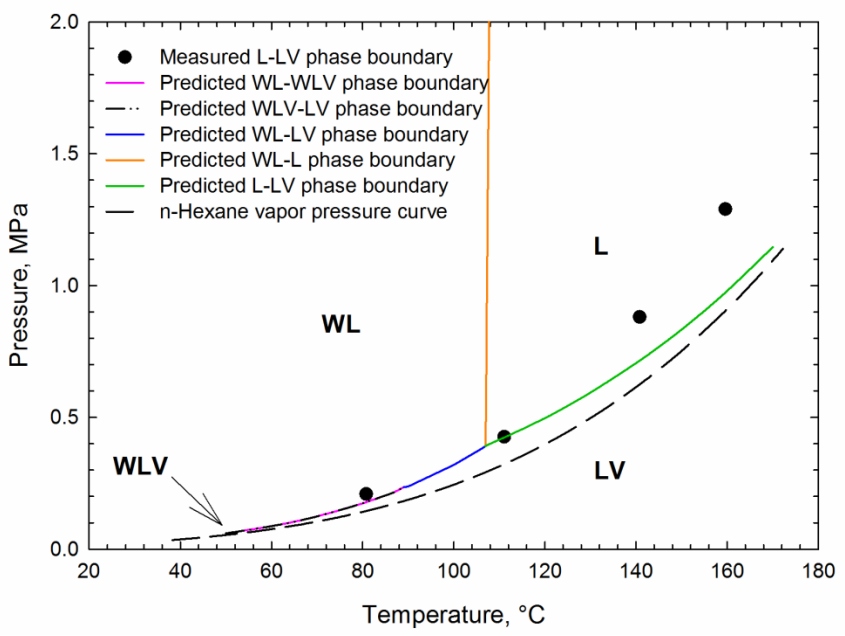

Figure 3.5 – Measured and predicted saturation pressures for Mixture HB1 at different temperatures. The V-phase composition is calculated to be nearly 100% n-hexane.

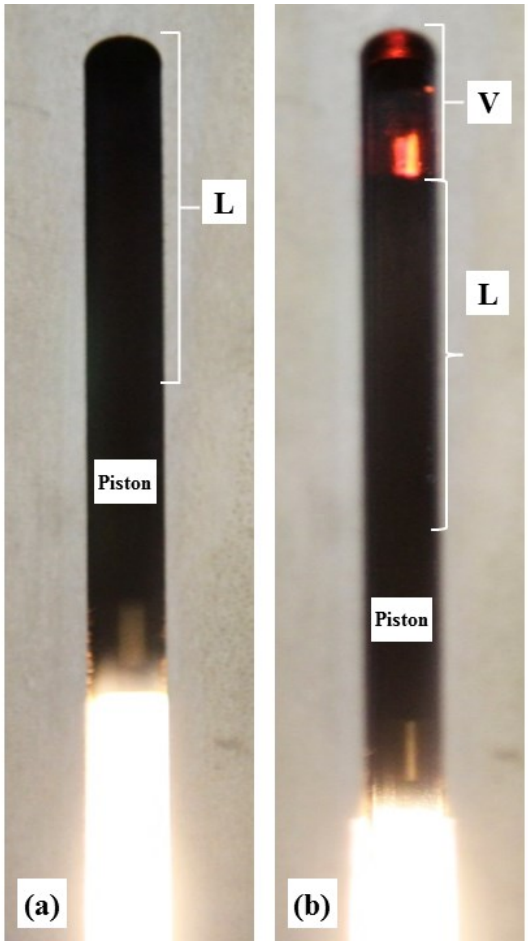

Figure 3.6 – Digital images captured for Mixture HB2: (a) Single liquid phase equilibrium at 159.8°C and 4.199 MPa; (b) LV equilibrium at 159.8°C and 0.931 MPa.

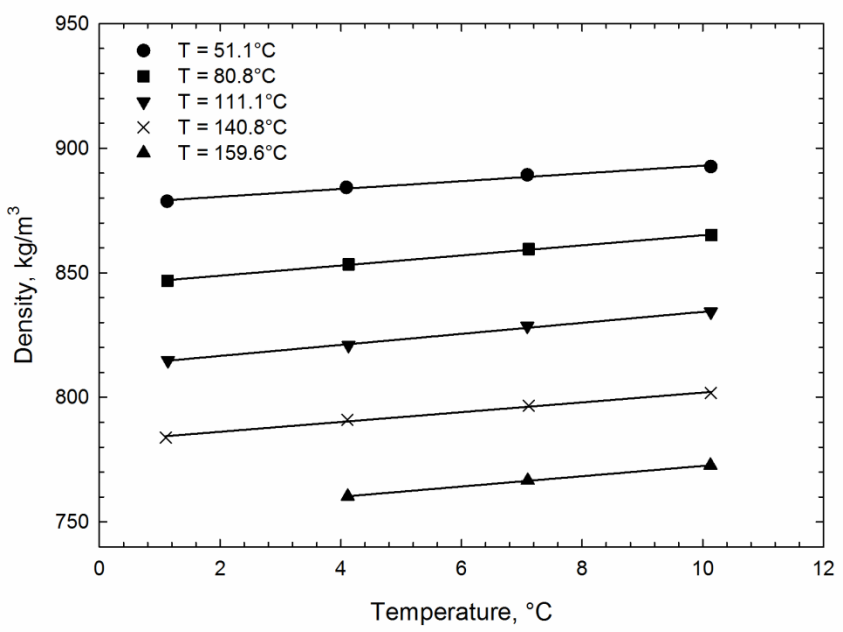

Figure 3.7 – Densities of Mixture HB1 measured with PVT cell at different temperatures. Solid lines are the trend lines matched with experimental data to illustrate the effect of temperature and pressure on density.

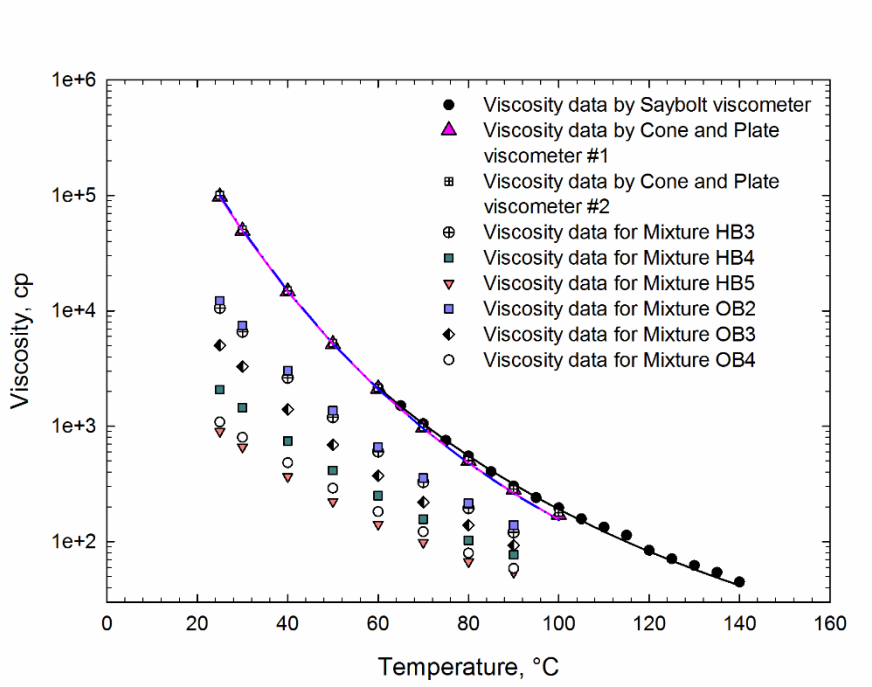

Figure 3.8 – Measured viscosity data for n-hexane/bitumen and n-octane/bitumen mixtures by use of Cone and Plate viscometer. In comparison of bitumen diluted with n-hexane and n-octane, lighter hydrocarbon solvent results in more reduction on bitumen viscosity.

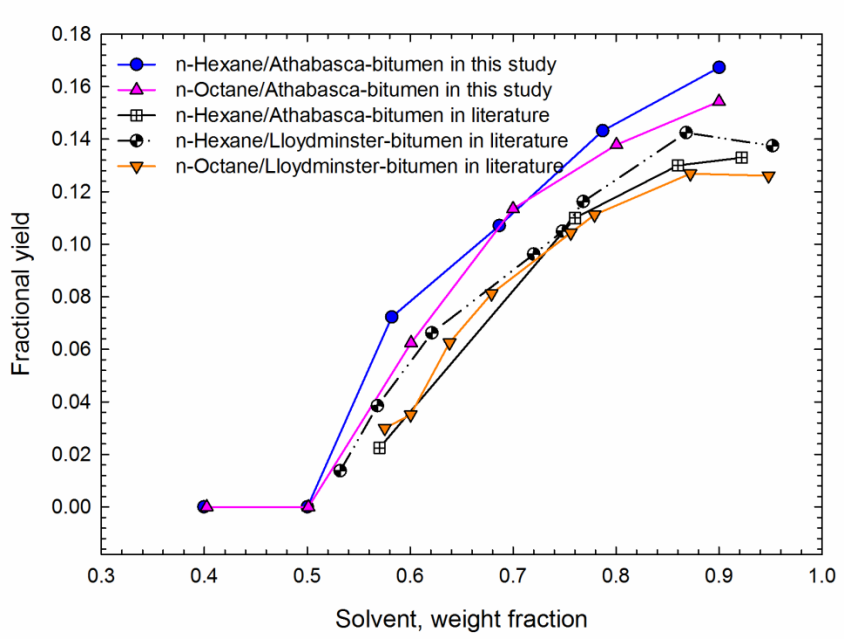

Figure 3.9 – Comparison of measured asphaltene precipitation data with the data by Alboudwarej et al. (2003).

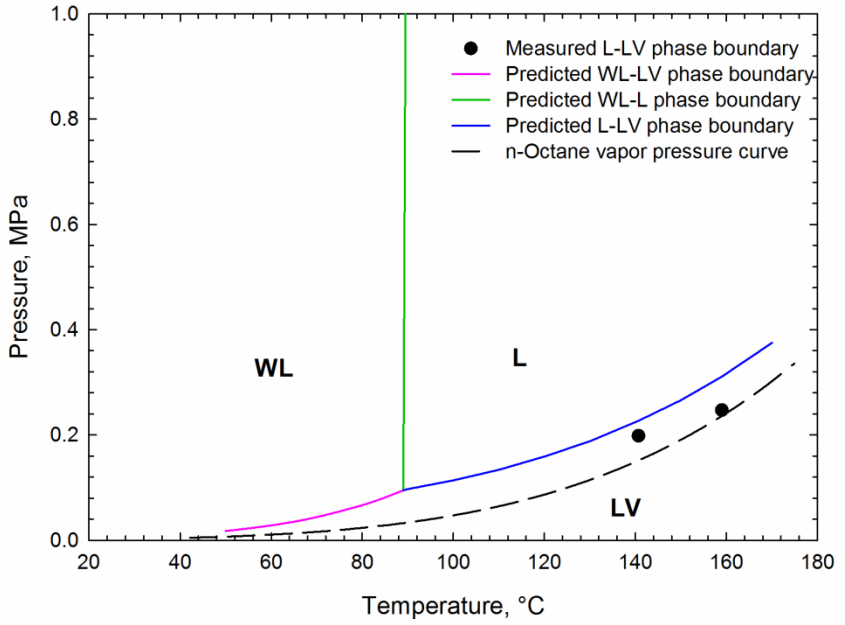

Figure 3.10 – Measured and predicted saturation pressure of Mixture OB1 at different temperatures. The V-phase composition is calculated to be nearly 100% n-octane.

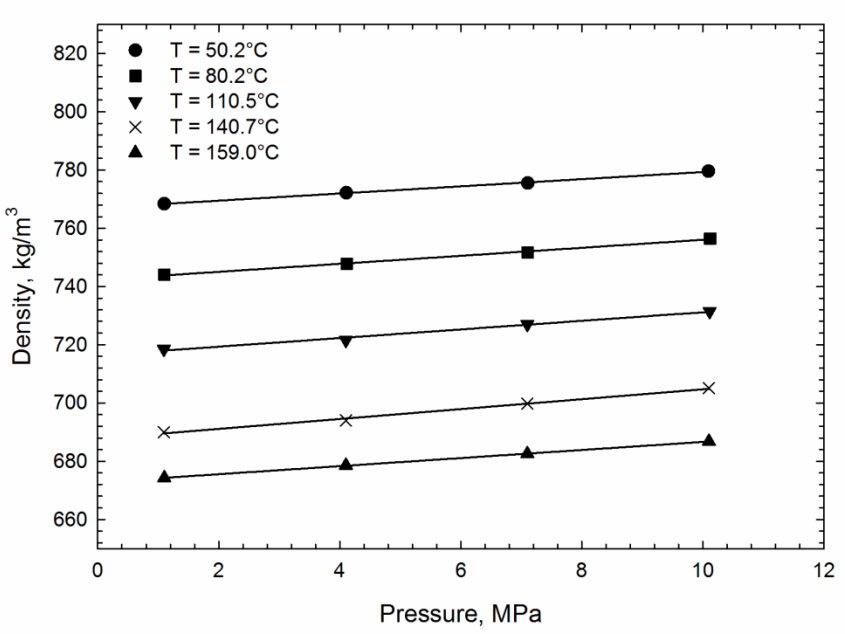

Figure 3.11 – Densities of Mixture OB1 measured with the PVT cell at different temperatures. Solid lines are the trend lines matched with experimental data to illustrate the effect of temperature and pressure on density.

Chapter 4 Conclusions and Recommendations

4.1 Conclusions

In this study, multiphase boundary measurements were conducted for n-butane/bitumen, n-hexane/bitumen and n-octane/bitumen mixtures at pressures up to 10 MPa and temperatures up to 160°C. A ternary mixture of n-butane/bitumen/water was measured to study the effect of adding water on phase behavior of butane/bitumen mixture. Viscosity measurement and asphaltene precipitation measurement were conducted for n-hexane/bitumen and n-octane/bitumen mixtures at ambient pressure to study the effect of solvent type on bitumen mobility for steam-solvent coinjection. Conclusions are as follows:

- Liquid-liquid separation of hydrocarbons was observed for n-butane/bitumen binary mixture, which did not happen for mixtures of bitumen with heavier solvents, such as n-hexane and n-octane, with similar solvent concentrations in the system. Bitumen was not effectively diluted by n-butane due to the coexistence of a butane-rich liquid with a bitumen-rich liquid phase, which may result in limited solubility of butane in oleic-phase flow along the edge of a steam chamber. Limited mobility of bitumen at in-situ conditions may be another consequence of liquid-liquid immiscibility due to the limited volume fraction of bitumen-rich liquid phase and limited solubility of bitumen components in solvent-rich liquid phase. The dilution effect is more pronounced for Athabasca bitumen mixed with heavier hydrocarbon-solvents in this study.

- Results from multiphase flash calculations and observation of the red color of butane-rich liquid phase indicate that n-butane was able to extract a significant amount of light and medium components from the bitumen in the solvent-rich liquid phase, while the bitumen was substantially diluted by n-butane in the bitumen-rich liquid phase.

- Up to four co-existing phases were observed for one n-butane/bitumen/water ternary mixture. In comparison with the n-butane/bitumen mixture without water, adding water into the system resulted in a higher pressure boundary for the multiphase

transition of the vapor phase due to water vapor pressure, and water dissolution into both hydrocarbon-liquid phases. Water-in-oil and oil-in-water emulsion were observed in this study, which could also be considered as one of the effects of adding water for n-butane/bitumen system at in-situ conditions.

- For n-butane-diluted-bitumen, multiphase transition that involves appearance/disappearance of vapor phase was observed to occur near the vapor pressure of n-butane or its extension.

- Results from the viscosity measurements at atmospheric pressure showed that n-hexane yields more reduction of the bitumen-phase viscosity than n-octane. In asphaltene precipitation experiments at atmospheric pressure, a larger amount of precipitates was observed with n-hexane than with n-octane at a given solvent concentration above 50 wt%.

- For steam and solvent coinjection, the highly size-asymmetric mixtures, consisting of bitumen, solvent and water, can result in complex phase behavior at reservoir conditions. Design of optimum solvent type and its concentration should take these factors into account: bitumen properties, reservoir conditions, multiphase behavior, viscosity and asphaltene precipitation.

4.2 Recommendations

In this study, phase-behavior measurements were conducted by use of a conventional PVT apparatus with a visual cell. A phase equilibrium state was determined on the basis of visual observation for phases with distinct colors. For example, the phase equilibrium state transitions of L_2-L_1L_2-L_1L_2V were observed for n-butane/bitumen (Mixture B in Chapter 2). However, asphaltene precipitation may have happened and existed as a dispersed phase at the temperature-pressure conditions in the measurement. However, the asphaltene-rich phase was not observed in the PVT cell in our study due to the limitation of current PVT setup. Asphaltene-rich phase may be in black color and exist at the bottom of the PVT cell, which is not possible to be visually identified through PVT cell window. Solid particles of asphaltene precipitation were observed when we were cleaning the PVT cell after measurement for Mixture C at atmospheric temperature and pressure. As presented in Abedi et al. (1999), X-ray beam is a validated way for

detecting solid particles, such as asphaltene precipitation, because solid particles can greatly reduce the intensity of transmitted X-rays even if present at low mass fraction. X-ray beam technology may be a potential way to improve the current apparatus setup for asphaltene-rich phase measurement in our future study.

As shown in Chapter 2, the PR-EOS model is developed primarily for accurate correlation of the phase-boundary data for the presence of the vapor phase, which shows large deviations on prediction of phase boundaries for liquid phases, like L-LL and WL-WLL. The absence of prediction on asphaltene-rich phase may be another reason for the deviations on predicting phase boundaries for liquid phases. Therefore, association models, such as PC-SAFT and CPA models, are potential alternatives to the PR-EOS with the consideration of association energy and volume for asphaltene component in bitumen.

For the study on bitumen mobility, experimental data on viscosity measurement and asphaltene precipitation measurement for diluted bitumen at high temperatures and pressures are scarce in the literature. Systematic sets of data at high temperatures and pressures may help researchers have a detailed understanding of bitumen mobility at reservoir conditions. Capillary viscometer may be a potential methodology for the viscosity measurement at high pressures as shown in **Appendix I**. Jamaluddin et al. (2001) summarized different technologies for asphaltene precipitation measurement at high temperatures and pressures.

In this study, liquid-liquid immiscibility of hydrocarbons was observed for n-butane/bitumen mixtures. However, it is not certain how the multiphase behavior affects the oil drainage rate at reservoir conditions. As presented in the literature for the study of CO_2-EOR, solvent-rich liquid phase and vapor phase were lumped together, and both of them were identified as vapor phase for the three-phase flow simulation in current commercial software, which may cause incorrect results on oil recovery predictions (Guler et al. 2001). Nourpour Aghbash and Ahmadi (2012) also indicated that the ignorance of solvent-rich liquid phase in simulation work may lead to erroneous prediction of breakthrough time, oil recovery and amount of CO_2 sequestered. Therefore, a simulation study with modified relative permeability models for multiphase flow may be required in order to have a detailed understanding of the effect of multiphase flow for steam and solvent coinjection.

References:

Abedi, S.J., Cai, H.Y., Seyfaie, S., and Shaw, J.M. 1999. Simultaneous Phase Behaviour, Elemental Composition and Density Measurement Using X-ray Imaging. *Fluid Phase Equilibria.* **158**: 775-781.

Guler, B., Wang, P., Delshad, M., Pope, G.A., and Sepehrnoori, K. 2001. Three-and Four-phase Flow Compositional Simulations of CO_2/NGL EOR. Paper SPE 71485 presented at SPE Annual Technical Conference and Exhibition, New Orleans, Louisiana, USA, September 30-October 3.

Jamaluddin, A.K.M., Creek, J., Kabir, C.S., McFadden, J.D., D'Cruz, D., Joseph, M.T., Joshi, N., and Ross, B. 2001. A Comparison of Various Laboratory Techniques to Measure Thermodynamic Asphaltene Instability. Paper SPE 72154 presented at SPE Asia Pacific Improved Oil Recovery Conference, Kuala Lumpur, Malaysia, October 8-9.

Nourpour Aghbash, V., and Ahmadi, M. 2012. Evaluation of CO_2-EOR and Sequestration in Alaska West Sak Reservoir Using Four-Phase Simulation Model. Paper SPE 153920 presented at SPE Western Regional Meeting, Bakersfield, California, USA, March 21-23.

Zou, X.Y., Zhang, X., and Shaw, J.A. 2007. Phase Behavior of Athabasca Vacuum Bottoms+ N-alkane Mixtures. *SPE Prod. Oper*. **22**(02): 265-272.

Appendices:

Appendix A. Simulated distillation test results of the bitumen sample.

Mass %	Temperature, °C	Temperature, °F	Mass %	Temperature, °C	Temperature, °F
0.5	181.0	357.8	32	448.1	838.6
1	203.4	398.1	33	453.8	848.8
2	226.4	439.5	34	459.3	858.7
3	244.3	471.7	35	464.5	868.1
4	258.6	497.5	36	470.4	878.7
5	270.3	518.5	37	476.2	889.2
6	280.7	537.3	38	481.9	899.4
7	290.3	554.5	39	489.3	912.7
8	299.2	570.6	40	495.9	924.6
9	307.1	584.8	41	501.6	934.9
10	314.2	597.6	42	506.8	944.2
11	321.6	610.9	43	513.7	956.7
12	328.9	624.0	44	521.4	970.5
13	336.1	637.0	45	528.6	983.5
14	343.0	649.4	46	535.8	996.4
15	349.4	660.9	47	542.2	1008.0
16	355.4	671.7	48	548.6	1019.5
17	361.9	683.4	49	556.8	1034.2
18	368.4	695.1	50	563.9	1047.0
19	374.4	705.9	51	570.2	1058.4
20	380.3	716.5	52	577.3	1071.1
21	386.4	727.5	53	584.7	1084.5
22	392.4	738.3	54	591.4	1096.5
23	398.2	748.8	55	598.4	1109.1
24	404.3	759.7	56	605.8	1122.4
25	410.4	770.7	57	613.1	1135.6
26	416.6	781.9	58	620.2	1148.4
27	422.5	792.5	59	627.1	1160.8
28	427.7	801.9	60	634.1	1173.4
29	432.9	811.2	61	640.9	1185.6
30	438.0	820.4	62	648.0	1198.4
31	443.0	829.4	63	654.4	1209.9

Table A.1 – Simulated distillation test results of Athabasca bitumen sample at temperature up to 720°C. This is the same bitumen as the one studied by Gao et al. (2016).

Mass %	Temperature, °C	Temperature, °F	Mass %	Temperature, °C	Temperature, °F
64	661.2	1222.2	71	701.1	1294.0
65	668.4	1235.1	72	704.9	1300.8
66	674.7	1246.5	73	708.7	1307.7
67	681.2	1258.2	74	712.3	1314.1
68	686.7	1268.1	75	715.8	1320.4
69	692.0	1277.6	76	719.3	1326.7
70	696.1	1285.0	76.2	720.0	1328.0

Table A.1 (Continued) – Simulated distillation test results of Athabasca bitumen sample at temperature up to 720°C. This is the same bitumen as the one studied by Gao et al. (2016).

Hydro-carbons	Mass fraction	Hydro-carbons	Mass fraction	Hydro-carbons	Mass fraction	Hydro-carbons	Mass fraction
C_1	<0.0001	C_{26}	0.0178	C_{51}	0.0064	C_{76}	0.0040
C_2	<0.0001	C_{27}	0.0166	C_{52}	0.0064	C_{77}	0.0045
C_3	<0.0001	C_{28}	0.0174	C_{53}	0.0059	C_{78}	0.0041
C_4	<0.0001	C_{29}	0.0179	C_{54}	0.0059	C_{79}	0.0042
C_5	<0.0001	C_{30}	0.0177	C_{55}	0.0058	C_{80}	0.0042
C_6	<0.0001	C_{31}	0.0155	C_{56}	0.0054	C_{81}	0.0047
C_7	0.0001	C_{32}	0.0154	C_{57}	0.0054	C_{82}	0.0042
C_8	0.0004	C_{33}	0.0130	C_{58}	0.0053	C_{83}	0.0043
C_9	0.0012	C_{34}	0.0128	C_{59}	0.0053	C_{84}	0.0048
C_{10}	0.0023	C_{35}	0.0110	C_{60}	0.0049	C_{85}	0.0044
C_{11}	0.0040	C_{36}	0.0107	C_{61}	0.0049	C_{86}	0.0050
C_{12}	0.0068	C_{37}	0.0121	C_{62}	0.0049	C_{87}	0.0046
C_{13}	0.0101	C_{38}	0.0118	C_{63}	0.0049	C_{88}	0.0047
C_{14}	0.0115	C_{39}	0.0085	C_{64}	0.0044	C_{89}	0.0053
C_{15}	0.0146	C_{40}	0.0083	C_{65}	0.0049	C_{90}	0.0048
C_{16}	0.0156	C_{41}	0.0081	C_{66}	0.0045	C_{91}	0.0050
C_{17}	0.0171	C_{42}	0.0080	C_{67}	0.0045	C_{92}	0.0056
C_{18}	0.0190	C_{43}	0.0093	C_{68}	0.0045	C_{93}	0.0051
C_{19}	0.0190	C_{44}	0.0086	C_{69}	0.0041	C_{94}	0.0053
C_{20}	0.0201	C_{45}	0.0070	C_{70}	0.0041	C_{95}	0.0054
C_{21}	0.0195	C_{46}	0.0069	C_{71}	0.0041	C_{96}	0.0055
C_{22}	0.0201	C_{47}	0.0068	C_{72}	0.0046	C_{97}	0.0056
C_{23}	0.0184	C_{48}	0.0071	C_{73}	0.0043	C_{98}	0.0057
C_{24}	0.0182	C_{49}	0.0070	C_{74}	0.0039	C_{99}	0.0058
C_{25}	0.0171	C_{50}	0.0065	C_{75}	0.0043	C_{100+}	0.2427

Table A.2 – Carbon number distribution up to C_{100} for Athabasca bitumen sample obtained through simulated distillation test.

Appendix B. Bitumen characterization by use of CPA model.

An attempt of applying a CPA model on the basis of Soave-Redlich-Kwong EOS was made for the bitumen characterization using commercial PVT software. Three pseudocomponents were used to represent the bitumen sample: saturates; aromatics + resins; and asphaltenes. The weight fraction of each pseudocomponent was obtained from the SARA test as presented in the experimental section. The molecular weights of saturates and asphaltene components were assumed to be 460 g/mole and 1700 g/mole, respectively, as reported in the literature (Gonzalez et al. 2007; Akbarzadeh et al. 2005). Thereafter, the molecular weight of the pseudo component for aromatics + resins was calculated to be 629 g/mole based on the molecular weight of bitumen sample, which is 635 g/mole.

The PVTsim Nova software was applied in this study (Michelsen, M.L. and Mollerup, J.M. 2004). Input parameters of Tc', a_0, b, c_1, association energy, association volume for each pseudocomponent are required for CPA model. The properties of Tc', a_0, b, and c_1 for pseudocomponents were calculated by use of the extrapolation by assuming the pseudocomponents as n-alkanes as showed in **Figure 1a-d**. The association term was not considered in the saturate pseudocomponent. Therefore, the association energy and volume for aromatics + resins are the only four adjustable parameters for regression, if the binary interaction parameters are all assumed to be zero. A multiphase region is found to be more sensitive to the association parameters of pseudocomponents. Therefore, the measured LL-LLV boundary data for n-butane/bitumen (Mixture B in Chapter 2) were used for the primary consideration for regression. **Table 1** presents the CPA model parameters for bitumen pseudocomponents.

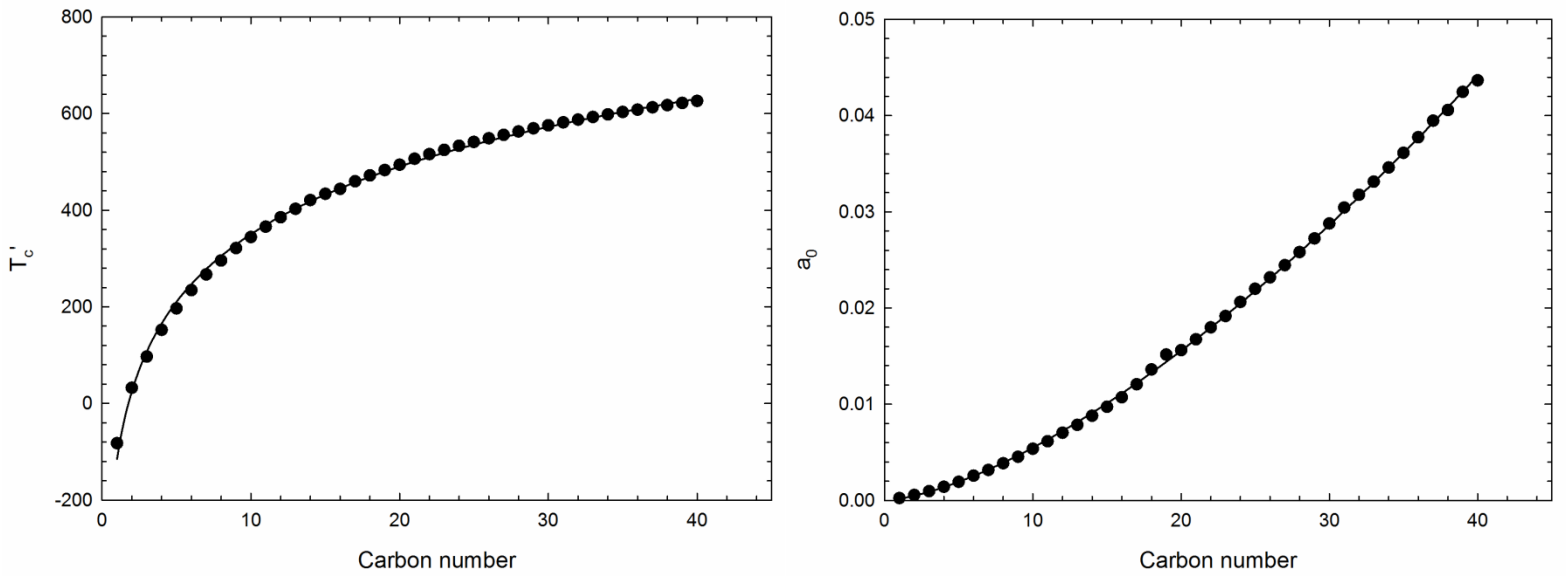

a. Tc'-CN **b. a_0-CN**

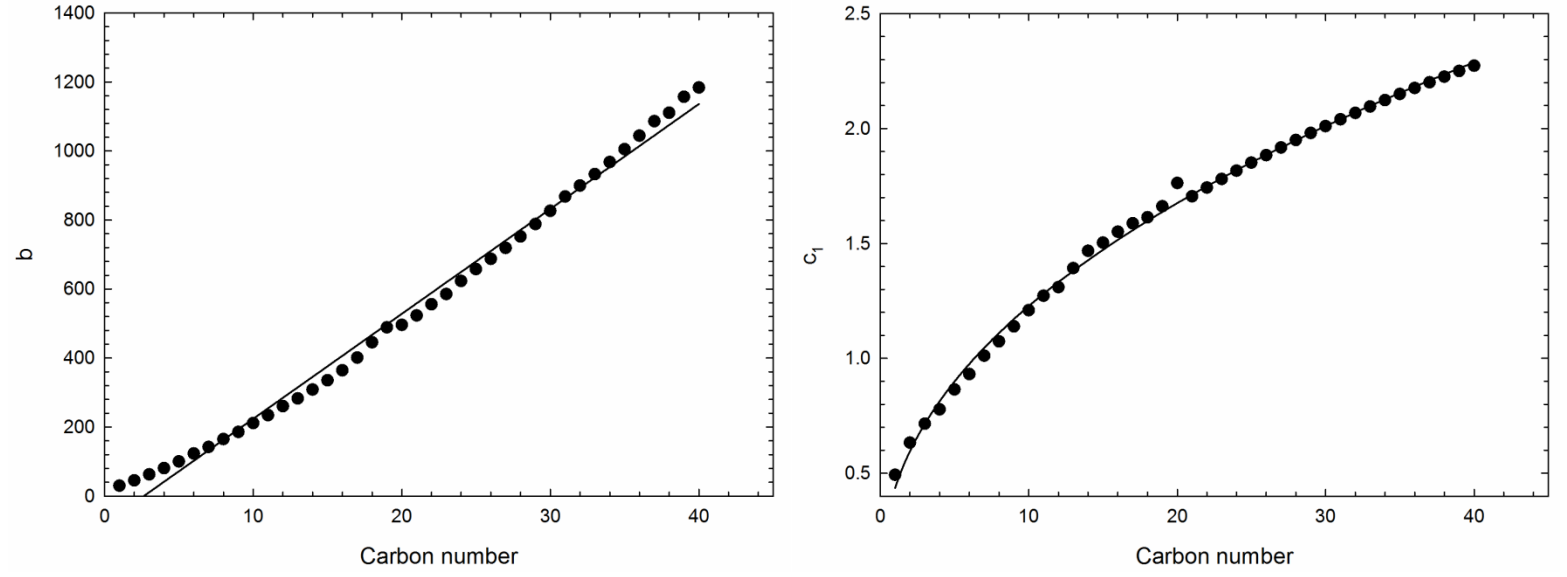

c. b-CN **d. c_1-CN**

Figure 1. Extrapolation curve for CPA model parameters for n-alkanes. a. Tc'-CN diagram. The fitted curve equation is Tc' = 202.08ln(CN)-114.84; b. a_0-CN diagram. The fitted curve equation is a_0 = 0.0002(CN)^1.4652; c. b-CN diagram. The fitted curve equation is b = 30.407CN-80.047; d. c_1-CN diagram. The fitted curve equation is c_1 = 0.4467(CN)^0.441.

	MW	T_C', °C	a_0, kPa $(m^3/mol)^2$	b, cm^3/mol	c_1	ε, kPa m^3/mol	β
Saturates	460	591.734	0.034	923.384	2.088	0.000	0.0000
Aromatics+Resins	629	654.410	0.053	1288.268	2.394	14.341	0.0339
Asphaltene	1700	854.293	0.225	3599.200	3.703	11.466	0.0337

Table 1 –Components' parameters of the characterized CPA model. Three pseudocomponents were used to represent the bitumen sample based on the SARA test result. Two-site molecular was assumed for the bitumen pseudocomponents with association term.

The characterized CPA model was used for matching measured phase boundary data in this study. The asphaltene component is considered as a separate pseudocomponent in the CPA model in order to predict the asphaltene-rich phase formation. As bitumen is characterized with a different methodology from the one we used for the PR-EOS model as presented in Chapter 2, two scenarios were compared to check the validity of the characterization: a CPA model with association terms for water and bitumen pseudocomponents; the CPA model without association terms for water and bitumen pseudocomponents.

Figure 2 indicates a better prediction could be achieved by the CPA model without association term for n-butane/bitumen (Mixture A in Chapter 2). These two scenarios both could obtain smaller deviations for matching measured L-LV boundary data in comparison with the PR-EOS model presented in Chapter 2. **Figure 3** shows that the CPA model without association is not able to predict LL-LLV boundary for n-butane/bitumen (Mixture B in Chapter 2). In stark contrast, the CPA model with consideration of association terms for water and bitumen pseudocomponents can achieve good prediction results for LL-LLV boundary compared with the measured boundary data. The three-phase region is predicted as a closed loop. The lowest temperature for LLV equilibrium predicted from CPA model is approximately 107.8°C, which is 122.8°C for the PR-EOS model presented in Chapter 2. The three phases observed at 50.0°C and 79.9°C are not represented by the CPA model. However, the CPA model could not well correlate the L-LL boundary for Mixture B as shown in Figure 3. The comparison of two scenarios for matching bitumen saturation pressure was shown in **Figure 4**. The CPA models

with or without association could not match the measured bitumen saturation pressure data well. The predicted bitumen saturation pressures are much smaller than experimental data. This may indicate that the characterization methodology used for CPA model in this study should be improved. Meanwhile, the cross association between bitumen pseudocomponents may have to be included as reported in the literature (Li and Firoozabadi 2010), which could not be achieved by PVTsim Nova.

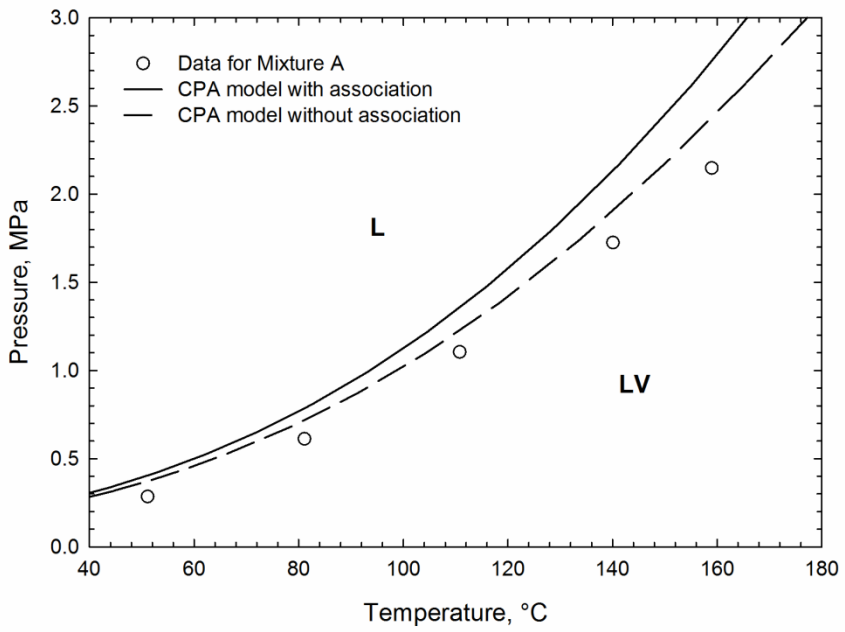

Figure 2. Measured and predicted saturation pressures of Mixture A at different temperatures by use of CPA model.

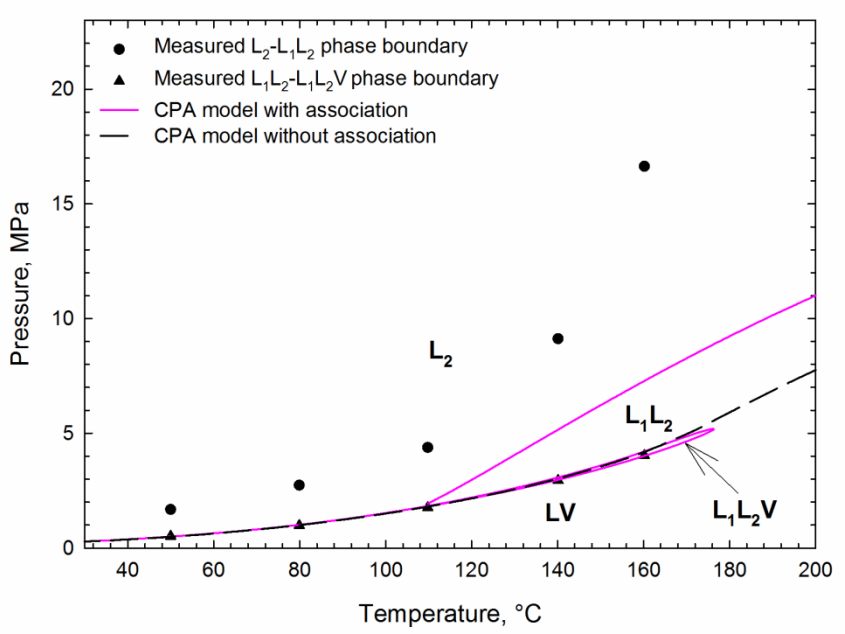

Figure 3. Measured and predicted phase boundaries of Mixture B at different temperatures by use of CPA model.

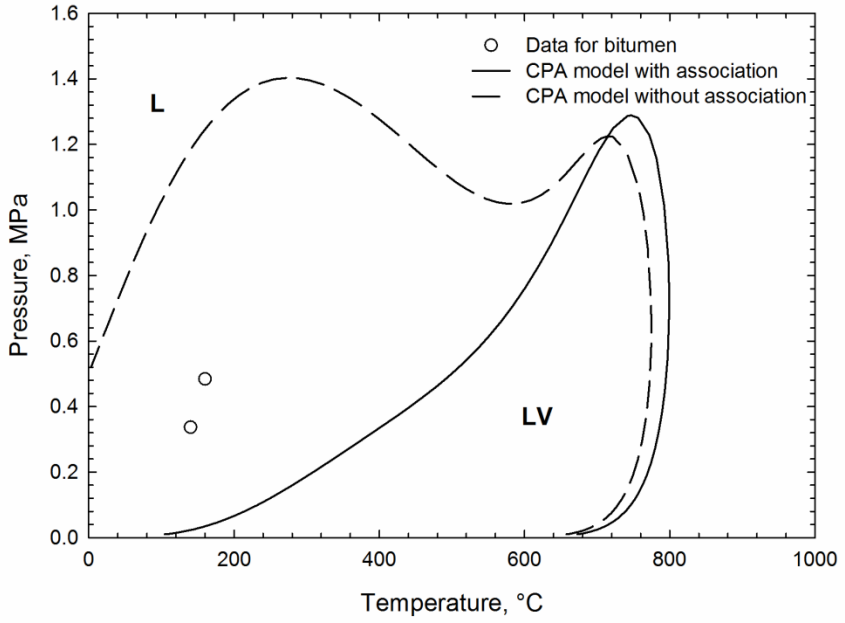

Figure 4. Measured and predicted saturation pressures of bitumen at different temperatures by use of CPA model.

References:

Akbarzadeh, K., Alboudwarej, H., Svrcek, W.Y., and Yarranton, H.W. 2005. A Generalized Regular Solution Model for Asphaltene Precipitation from n-Alkane Diluted Heavy Oils and Bitumens. *Fluid Phase Equilibria.* **232**(1): 159-170.

Gonzalez, D.L., Hirasaki, G.J., Creek, J., and Chapman, W.G. 2007. Modeling of Asphaltene Precipitation due to Changes in Composition Using the Perturbed Chain Statistical Associating Fluid Theory Equation of State. *Energy and Fuels.* **21**(3): 1231-1242.

Li, Z., and Firoozabadi, A. 2010. Modeling Asphaltene Precipitation by n-Alkanes from Heavy Oils and Bitumens Using Cubic-Plus-Association Equation of State. *Energy and Fuels*. **24**(2): 1106-1113.

Michelsen, M.L. and Mollerup, J.M. *Thermodynamic Models: Fundamentals & Computational Aspects*. Tie-Line Publications: Holte, 2004.

Appendix C. PV data measured for the bitumen sample.

T, °C	P,	V_{total},	Phase	V_L,	V_g,	T, °C	P,	V_{total},	Phase	V_L,	V_g,
140.2	10.119	26.632	1	26.632		140.2	0.287	39.935	2	30.017	9.902
140.2	8.403	26.688	1	26.688		160.0	9.561	27.076	1	27.076	
140.2	7.086	26.719	1	26.719		160.0	8.196	27.100	1	27.100	
140.2	5.569	26.743	1	26.743		160.0	6.851	27.139	1	27.139	
140.2	3.928	26.814	1	26.814		160.0	5.328	27.179	1	27.179	
140.2	2.287	26.862	1	26.862		160.0	3.831	27.227	1	27.227	
140.2	0.791	26.957	1	26.957		160.0	2.714	27.282	1	27.282	
140.2	0.543	27.124	1	27.124		160.0	1.577	27.330	1	27.330	
140.2	0.418	27.465	1	27.465		160.0	0.798	27.457	1	27.457	
140.2	0.350	28.677	1	28.677		160.0	0.632	27.544	1	27.544	
140.2	0.322	29.494	2	*	*	160.0	0.501	28.051	2	*	*
140.2	0.322	30.358	2	*	*	160.0	0.481	28.828	2	*	*
140.2	0.322	32.269	2	30.057	2.164	160.0	0.481	29.724	2	*	*
140.2	0.322	33.823	2	30.009	3.813	160.0	0.481	30.572	2	*	*
140.2	0.315	35.210	2	30.009	5.217	160.0	0.481	32.182	2	30.802	1.300
140.2	0.301	36.605	2	30.009	6.588	160.0	0.467	36.058	2	30.905	5.106
140.2	0.301	37.906	2	30.009	7.936	160.0	0.467	40.680	2	30.913	9.736

*Note: * refers to the scenario that the LV equilibrium could be visually observed but the interface is to fuzzy to be identified.*

Appendix D. PV data measured for the n-butane/bitumen (Mixture A in Chapter 2).

T, °C	P,	V_{total},	Phase	V_L,	V_g,	T, °C	P,	V_{total},	Phase	V_L,	V_g,
51.1	10.126	38.421	1	38.421		110.8	2.301	40.855	1	40.855	
51.1	8.465	38.445	1	38.445		110.8	1.094	41.061	2	*	*
51.1	7.086	38.461	1	38.461		110.8	1.080	44.541	2	40.599	3.942
51.1	5.700	38.484	1	38.484		110.8	1.067	46.825	2	39.910	6.915
51.1	4.128	38.508	1	38.508		110.8	1.060	48.236	2	39.957	8.279
51.1	2.349	38.564	1	38.564		110.8	1.046	49.639	2	39.846	9.793
51.1	1.115	38.603	1	38.603		140.1	10.119	41.576	1	41.576	
51.1	0.267	43.963	2	38.538	5.425	140.1	8.568	41.656	1	41.656	
51.1	0.267	45.041	2	38.070	6.971	140.1	7.079	41.743	1	41.743	
51.1	0.260	46.095	2	38.118	7.977	140.1	5.755	41.854	1	41.854	
81.1	10.126	39.523	1	39.523		140.1	4.093	41.893	1	41.893	
81.1	8.396	39.555	1	39.555		140.1	2.294	42.052	1	42.052	
81.1	7.079	39.602	1	39.602		140.1	1.673	48.751	2	40.829	7.922
81.1	5.810	39.666	1	39.666		140.1	1.660	49.925	2	40.790	9.135
81.1	4.100	39.729	1	39.729		140.1	1.646	51.764	2	40.758	11.006
81.1	2.101	39.832	1	39.832		140.1	1.632	53.738	2	40.758	12.980
81.1	1.094	39.896	1	39.896		159.0	10.099	42.234	1	42.234	
81.1	0.598	44.692	2	39.394	5.298	159.0	8.630	42.330	1	42.330	
81.1	0.598	45.961	2	38.958	7.002	159.0	7.093	42.496	1	42.496	
81.1	0.591	47.395	2	39.109	8.287	159.0	5.796	42.575	1	42.575	
110.8	10.113	40.466	1	40.466		159.0	4.107	42.726	1	42.726	
110.8	8.568	40.554	1	40.554		159.0	2.963	42.773	1	42.773	
110.8	7.079	40.633	1	40.633		159.0	2.046	53.135	2	41.337	11.799
110.8	5.838	40.704	1	40.704		159.0	2.039	54.277	2	41.170	13.107
110.8	4.107	40.799	1	40.799		159.0	2.025	55.220	2	41.218	14.003

*Note: * refers to the scenario that the LV equilibrium could be visually observed but the interface is to fuzzy to be identified.*

Appendix E. PV data measured for the n-butane/bitumen (Mixture B in Chapter 2).

T, °C	P,	V_{total},	Phase	V_{L1},	V_{L2},	V_g,
50.0	13.622	28.606	1		28.606	
50.0	11.616	28.741	1		28.741	
50.0	9.651	28.923	1		28.923	
50.0	7.582	29.058	1		29.058	
50.0	5.128	29.272	1		29.272	
50.0	3.645	29.399	1		29.399	
50.0	2.039	29.557	1		29.557	
50.0	1.425	29.597	2	*	*	
50.0	1.142	29.629	2	*	*	
50.0	0.805	29.676	2	*	*	
50.0	0.639	29.692	2	*	*	
50.0	0.529	30.152	2	*	*	
50.0	0.515	30.961	2	*	*	
50.0	0.508	32.174	2	*	*	
50.0	0.501	33.783	3	*	*	*
50.0	0.494	35.844	3	*	*	6.780
50.0	0.487	38.286	3	*	*	9.262
50.0	0.481	40.696	3	*	*	11.450
79.9	13.636	30.327	1		30.327	
79.9	11.850	30.564	1		30.564	
79.9	9.458	30.818	1		30.818	
79.9	7.368	31.048	1		31.048	
79.9	5.259	31.333	1		31.333	
79.9	3.824	31.524	1		31.524	
79.9	2.101	31.746	2	*	*	
79.9	1.694	31.817	2	*	*	
79.9	1.322	31.880	2	*	*	
79.9	0.991	32.879	3	*	*	*
79.9	0.984	33.490	3	*	*	*
79.9	0.977	34.742	3	*	*	*
79.9	0.970	36.051	3	*	*	*
79.9	0.963	37.755	3	*	*	6.566
79.9	0.956	40.086	3	*	*	8.881
79.9	0.956	42.314	3	*	*	11.291

Table E.1 – PV data measured for the n-butane/bitumen (Mixture B in Chapter 2).
*Note: * is the condition that the interface between phases could be visually observed but is not able to be measured clearly through cathetometer.*

T, °C	P,	V_{total},	Phase	V_{L1},	V_{L2},	V_g,
79.9	0.949	45.429	3	*	*	14.478
79.9	0.942	48.212	3	*	*	17.436
79.9	0.942	50.638	3	*	*	19.917
79.9	0.936	54.174	3	*	*	23.659
109.8	13.629	32.634	1		32.634	
109.8	12.367	32.824	1		32.824	
109.8	11.030	33.062	1		33.062	
109.8	9.616	33.300	1		33.300	
109.8	8.279	33.498	1		33.498	
109.8	6.865	33.807	1		33.807	
109.8	5.569	34.092	1		34.092	
109.8	4.845	34.211	1		34.211	
109.8	3.983	34.402	2	*	*	
109.8	3.459	34.623	2	*	*	
109.8	2.907	34.814	2	*	*	
109.8	2.046	35.147	2	*	*	
109.8	1.770	35.749	3	*	*	*
109.8	1.756	36.915	3	*	*	*
109.8	1.756	37.945	3	*	*	*
109.8	1.749	39.547	3	*	*	*
109.8	1.742	40.926	3	0.119	33.860	6.947
109.8	1.728	43.661	3	0.127	33.639	9.896
109.8	1.728	45.889	3	0.063	33.464	12.362
109.8	1.722	51.122	3	0.095	32.838	18.189
109.8	1.715	55.165	3	0.071	32.394	22.700
109.8	1.708	58.487	3	0.032	31.958	26.497
109.8	1.687	63.489	3	0.048	31.324	32.118
109.8	1.680	67.453	3	0.024	30.943	36.487
140.1	23.033	34.084	1		34.084	
140.1	20.696	34.449	1		34.449	
140.1	19.027	34.734	1		34.734	
140.1	17.124	34.956	1		34.956	
140.1	15.890	35.226	1		35.226	
140.1	13.856	35.646	1		35.646	

Table E.1 (Continued) – PV data measured for the n-butane/bitumen (Mixture B in Chapter 2).
*Note: * is the condition that the interface between phases could be visually observed but is not able to be measured clearly through cathetometer.*

T, °C	P,	V_{total},	Phase	V_{L1},	V_{L2},	V_g,
140.1	12.291	35.852	1		35.852	
140.1	11.105	36.154	1		36.154	
140.1	9.685	36.518	1		36.518	
140.1	8.375	36.923	2	*	*	
140.1	7.272	37.382	2	*	*	
140.1	5.590	38.223	2	*	*	
140.1	4.872	38.675	2	*	*	
140.1	4.342	39.103	2	0.206	38.897	
140.1	3.514	39.808	2	0.190	39.618	
140.1	2.942	42.290	3	0.182	39.101	3.007
140.1	2.928	44.470	3	0.182	38.268	6.019
140.1	2.928	45.984	3	0.214	38.039	7.732
140.1	2.921	48.355	3	0.087	37.262	11.006
140.1	2.921	50.622	3	0.095	36.445	14.082
140.1	2.914	52.787	3	0.166	35.763	16.857
140.1	2.901	55.387	3	0.301	34.867	20.218
160.2	27.356	36.328	1		36.328	
160.2	24.233	36.804	1		36.804	
160.2	21.613	37.311	1		37.311	
160.2	19.965	37.525	1		37.525	
160.2	17.662	38.033	1		38.033	
160.2	16.311	38.405	2	*	*	
160.2	15.566	38.627	2	*	*	
160.2	14.270	38.968	2	*	*	
160.2	12.774	39.452	2	*	*	
160.2	10.078	40.633	2	*	*	
160.2	9.002	41.101	2	*	*	
160.2	7.065	42.559	2	0.238	42.322	
160.2	5.865	43.868	2	0.127	43.741	
160.2	5.617	44.232	2	0.079	44.153	
160.2	4.252	47.380	2	0.436	46.944	
160.2	3.962	52.794	3	0.856	43.842	8.096
160.2	3.942	54.071	3	0.936	42.423	10.713
160.2	3.942	55.490	3	0.999	40.932	13.559

Table E.1 (Continued) – PV data measured for the n-butane/bitumen (Mixture B in Chapter 2). *Note: * is the condition that the interface between phases could be visually observed but is not able to be measured clearly through cathetometer.*

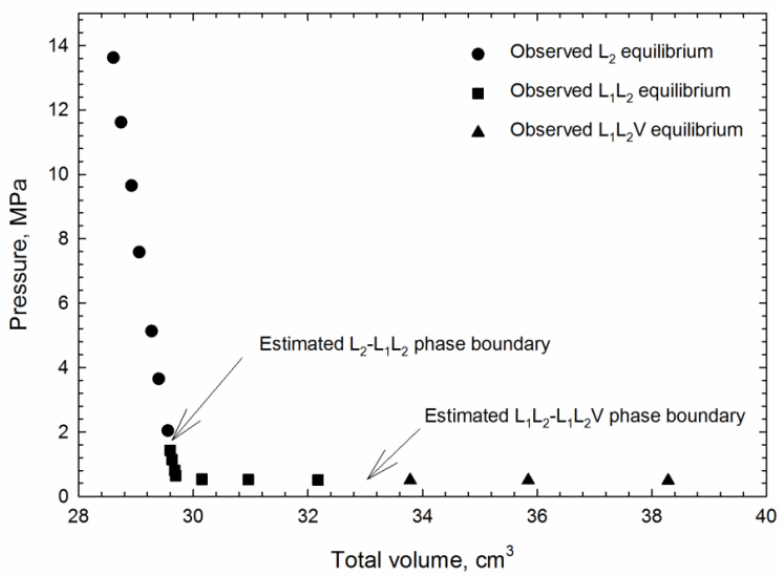

a. = 50.0°C

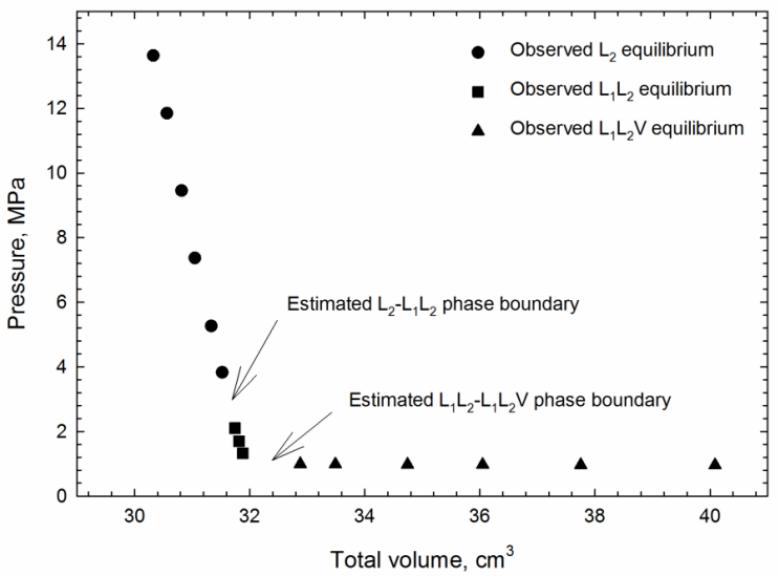

b. = 79.9°C

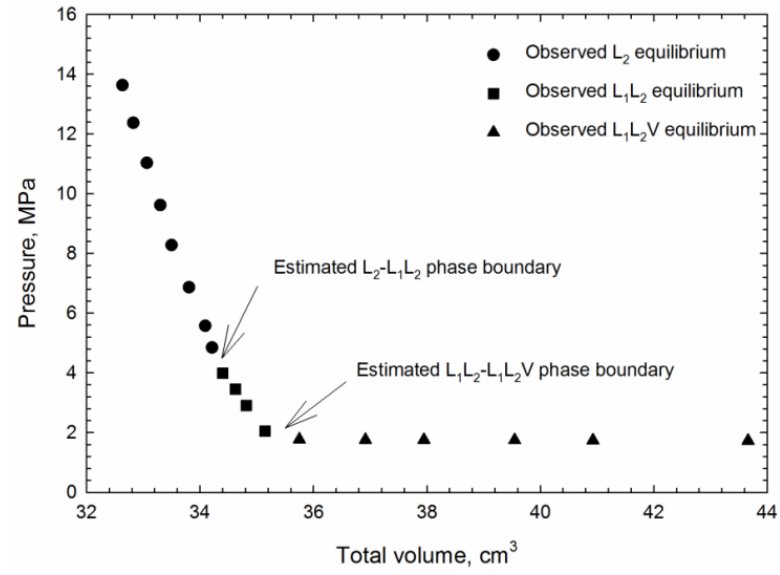

c. = 109.8°C

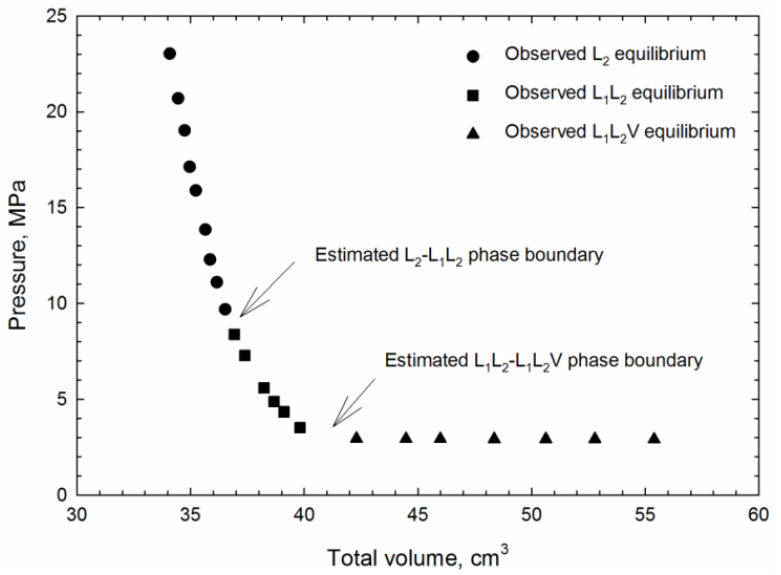

d. = 140.1°C

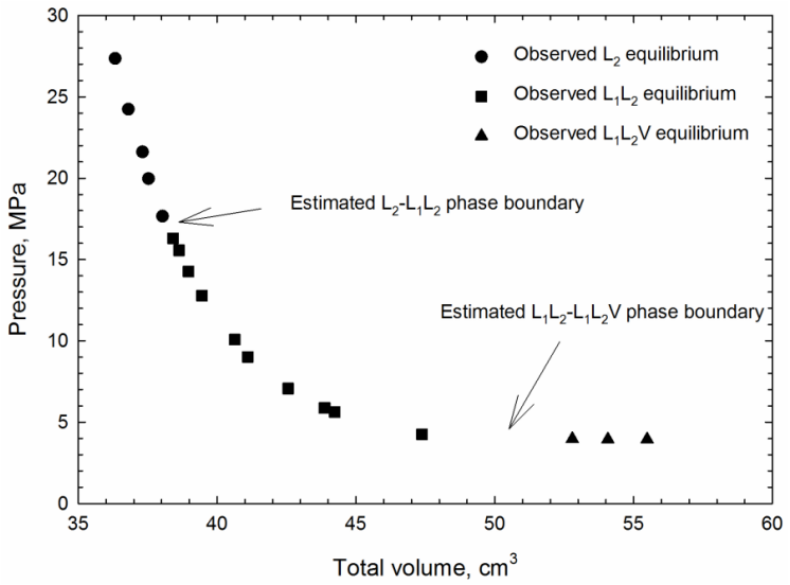

e. = 160.2°C

Figure E.1– PV data measured for the n-butane/bitumen (Mixture B in Chapter 2).

Appendix F. PV data measured for the n-butane/bitumen/water (Mixture C in Chapter 2).

T, °C	P,	V_{total},	Phase	V_w,	V_{L2},	V_{L1},	V_g,
50.1	21.475	32.324	1		32.324		
50.1	19.234	32.451	1		32.451		
50.1	17.131	32.546	1		32.546		
50.1	15.104	32.665	1		32.665		
50.1	13.029	32.776	1		32.776		
50.1	11.030	32.903	1		32.903		
50.1	8.920	33.030	1		33.030		
50.1	6.686	33.189	1		33.189		
50.1	4.810	33.315	1		33.315		
50.1	3.445	33.450	1		33.450		
50.1	2.121	33.593	1		33.593		
50.1	1.363	33.640	1		33.640		
50.1	0.722	33.704	1		33.704		
50.1	0.536	36.043	1		36.043		
50.1	0.508	38.619	3	1.007	*	*	5.575
50.1	0.508	40.815	3	1.332	*	*	7.946
50.1	0.501	47.871	2	*	*	*	15.121
50.1	0.501	51.328	2	*	*	*	18.641
50.1	0.501	54.610	2	*	*	*	22.058
80.0	21.475	33.720	2	*	*		
80.0	19.076	33.910	2	*	*		
80.0	16.897	34.076	2	*	*		
80.0	15.091	34.211	2	*	*		
80.0	12.960	34.370	2	*	*		
80.0	10.857	34.576	2	*	*		
80.0	8.816	34.758	2	*	*		
80.0	6.700	35.020	2	*	*		
80.0	4.741	35.242	2	*	*	*	
80.0	4.086	35.313	2	*	*	*	
80.0	3.376	35.456	3	*	*	*	
80.0	2.583	35.567	3	*	*	*	
80.0	1.687	35.702	3	*	*	*	
80.0	1.101	35.797	3	*	*	*	
80.0	1.067	37.644	3	1.379	*	*	
80.0	1.053	40.728	4	1.736	*	*	6.059
80.0	1.053	42.908	4	2.553	*	*	8.271

Table F.1 – PV data measured for the n-butane/bitumen/water (Mixture C in Chapter 2).
*Note: * is the condition that the interface between phases could be visually observed but is not able to be measured clearly through cathetometer.*

T, °C	P,	V_{total},	Phase	V_w,	V_{L2},	V_{L1},	V_g,
80.0	1.039	45.588	4	3.512	*	*	11.141
80.0	1.032	47.633	4	2.347	*	*	12.821
80.0	1.025	51.518	3	*	*	*	17.444
80.0	1.018	55.046	3	*	*	*	20.631
110.0	27.494	35.131	2	0.159	34.972		
110.0	25.440	35.305	2	0.182	35.123		
110.0	23.337	35.488	2	0.262	35.226		
110.0	21.303	35.662	2	0.301	35.361		
110.0	19.158	35.868	2	1.245	34.623		
110.0	17.214	36.098	2	1.348	34.750		
110.0	15.001	36.352	2	1.403	34.949		
110.0	13.167	36.582	2	1.427	35.155		
110.0	11.023	36.859	2	1.538	35.321		
110.0	8.844	37.184	2	1.490	35.694		
110.0	7.017	37.509	2	1.506	*	*	
110.0	5.410	37.834	3	0.539	*	*	
110.0	4.928	37.914	3	0.626	*	*	
110.0	4.542	38.009	3	0.555	*	*	
110.0	3.928	38.151	3	0.563	*	*	
110.0	3.183	38.334	3	0.404	34.362	3.568	
110.0	2.549	38.572	3	0.357	34.790	3.425	
110.0	2.011	38.572	3	0.444	33.831	4.297	
110.0	1.949	42.139	4	2.616	30.927	3.472	5.123
110.0	1.942	44.851	4	3.409	30.531	3.496	7.415
110.0	1.942	47.443	4	2.045	31.403	3.742	10.253
110.0	1.935	49.758	4	3.496	30.126	3.290	12.845
140.0	25.515	37.914	2	3.266	34.647		
140.0	23.454	38.167	2	3.734	34.433		
140.0	21.420	38.429	2	3.639	34.790		
140.0	19.317	38.730	2	3.837	34.893		
140.0	17.407	38.976	2	3.576	35.400		
140.0	15.222	39.341	2	3.694	35.646		
140.0	13.098	39.785	2	3.512	36.273		
140.0	11.064	40.229	2	2.957	37.271		
140.0	9.147	40.815	3	2.783	*	*	
140.0	7.024	41.521	3	3.465	*	*	

Table F.1 (Continued) – PV data measured for the n-butane/bitumen/water (Mixture C in Chapter 2).

*Note: * is the condition that the interface between phases could be visually observed but is not able to be measured clearly through cathetometer.*

T, °C	P,	V_{total},	Phase	V_w,	V_{L2},	V_{L1},	V_g,
140.0	6.217	41.901	3	3.623	34.877	3.401	
140.0	5.569	42.250	3	3.861	35.282	3.108	
140.0	4.735	42.845	3	4.083	35.773	2.989	
140.0	4.121	43.217	3	4.456	36.082	2.680	
140.0	3.569	43.709	3	4.860	36.257	2.592	
140.0	3.445	46.515	4	4.876	34.431	3.211	3.998
140.0	3.425	48.283	4	6.358	32.782	2.925	6.217
140.0	3.418	49.909	4	4.004	33.860	3.639	8.406
140.0	3.418	51.423	4	5.375	32.822	2.902	10.324
140.0	3.418	53.595	4	3.274	33.321	3.742	13.258
140.0	3.418	56.219	4	3.488	31.617	4.392	16.722
140.0	3.411	59.169	4	3.449	30.903	4.337	20.480
159.9	27.687	40.506	2	5.922	34.584		
159.9	25.419	40.665	2	5.851	34.814		
159.9	23.647	40.950	2	5.883	35.067		
159.9	21.544	41.323	2	6.009	35.313		
159.9	19.393	41.775	2	5.994	35.781		
159.9	17.269	42.266	2	5.605	36.661		
159.9	15.270	42.686	2	5.700	36.986		
159.9	13.201	43.289	3	5.534	37.755		
159.9	11.188	44.090	3	5.629	*	*	
159.9	9.085	45.263	3	5.891	*	*	
159.9	8.258	45.778	3	5.399	37.906	2.474	
159.9	6.824	46.317	3	5.550	38.350	2.418	
159.9	6.203	47.118	3	5.526	39.095	2.497	
159.9	5.500	48.054	3	6.081	39.539	2.434	
159.9	4.790	50.464	4	4.765	41.259	4.440	*
159.9	4.783	52.898	4	4.511	39.315	4.685	4.386
159.9	4.597	54.761	4	3.409	36.675	6.136	8.540
159.9	4.583	56.433	4	3.488	34.883	5.954	12.108
159.9	4.576	58.558	4	3.568	32.537	5.875	16.579
159.9	4.576	59.200	4	3.377	32.021	5.946	17.856
159.9	4.576	61.269	4	3.663	29.944	5.843	21.820
159.9	4.548	63.315	4	3.679	28.049	5.716	25.871

Table F.1 (Continued) – PV data measured for the n-butane/bitumen/water (Mixture C in Chapter 2).

*Note: * is the condition that the interface between phases could be visually observed but is not able to be measured clearly through cathetometer.*

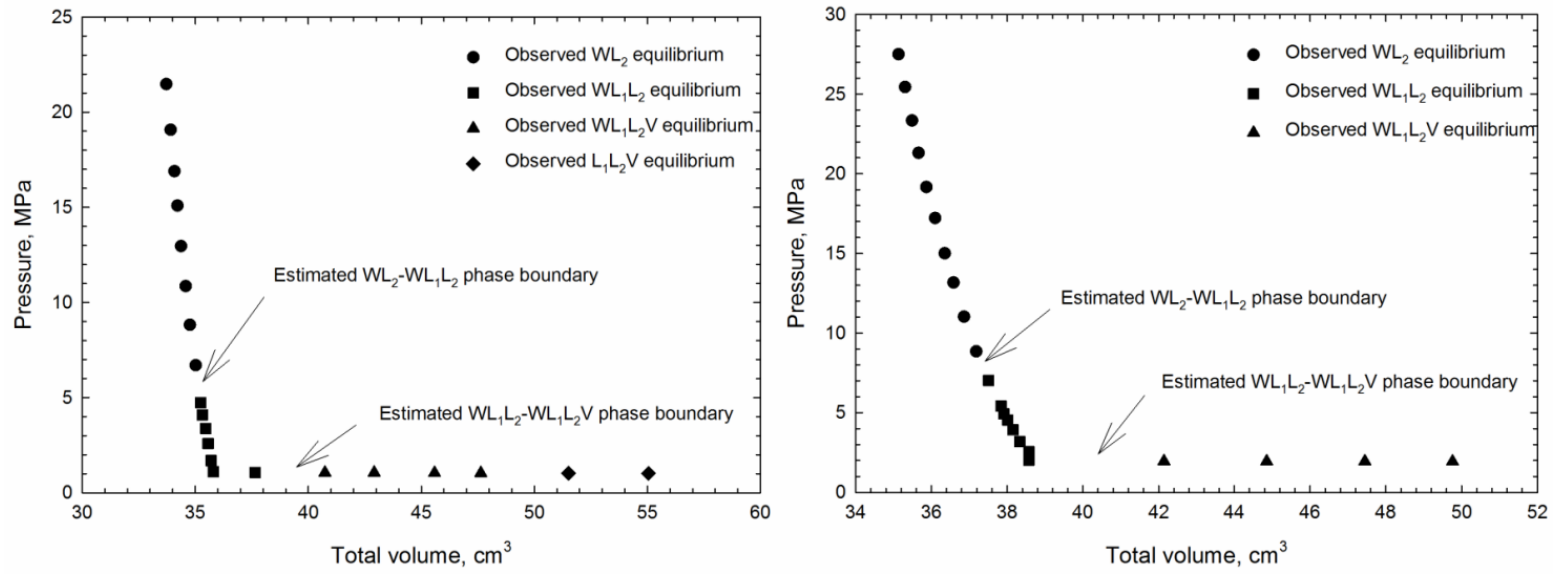

a. = 80.0°C

b. = 110.0°C

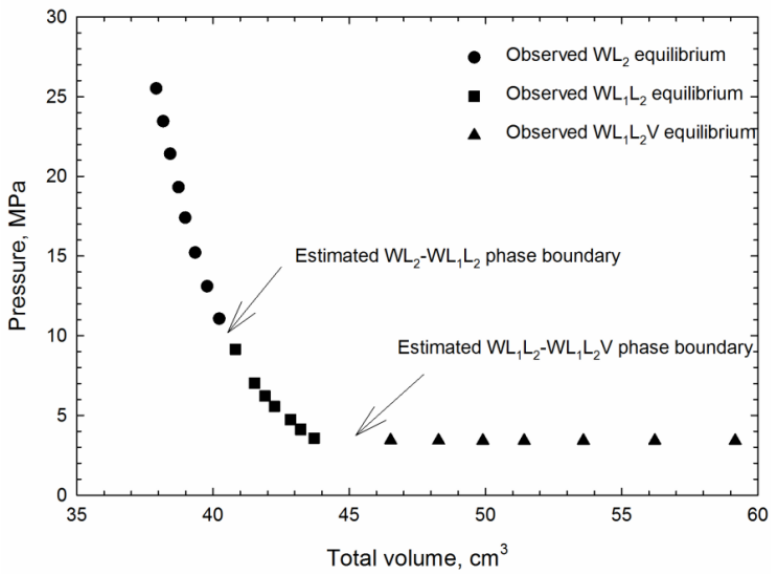

c. = 140.0°C

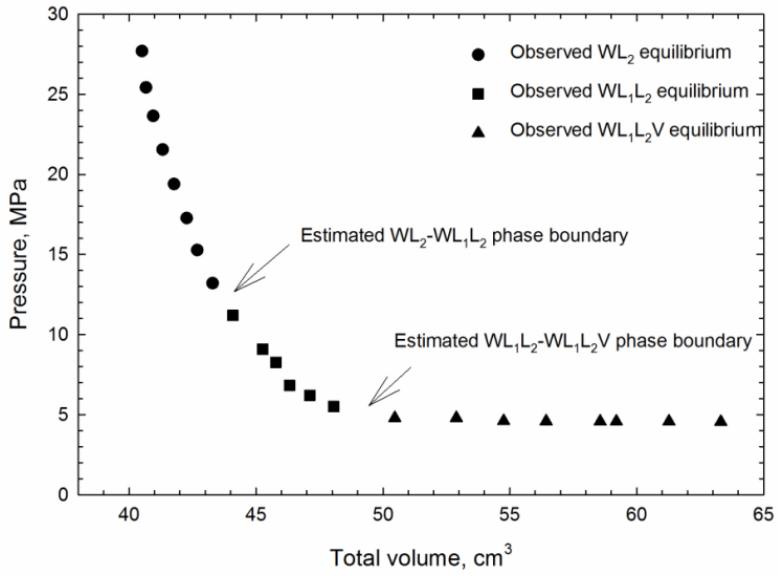

d. = 159.9°C

Figure F.1– PV data measured for the n-butane/bitumen/water (Mixture C in Chapter 2).

Appendix G. PV data measured for the n-hexane/bitumen mixture (Mixture HB1 in Chapter 3)

T, °C	P,	V_{total},	Phase	V_L,	V_g,	T, °C	P,	V_{total},	Phase	V_L,	V_g,
80.8	10.140	24.246	1	24.246		140.8	10.133	26.164	1	26.164	
80.8	8.375	24.309	1	24.309		140.8	8.596	26.228	1	26.228	
80.8	7.113	24.404	1	24.404		140.8	7.113	26.331	1	26.331	
80.8	5.776	24.484	1	24.484		140.8	5.748	26.394	1	26.394	
80.8	4.128	24.579	1	24.579		140.8	4.107	26.521	1	26.521	
80.8	2.425	24.698	1	24.698		140.8	2.763	26.624	1	26.624	
80.8	1.129	24.769	1	24.769		140.8	1.501	26.719	1	26.719	
80.8	0.232	24.999	1	24.999		140.8	1.101	26.759	1	26.759	
80.8	0.225	25.633	1	25.633		140.8	1.039	26.767	1	26.767	
80.8	0.219	26.592	1	26.592		140.8	0.901	27.060	1	27.060	
80.8	0.219	27.726	1	27.726		140.8	0.880	28.115	1	28.115	
80.8	0.191	28.844	2	*	*	140.8	0.867	29.470	1	29.470	
80.8	0.184	29.978	2	*	*	140.8	0.853	30.580	2	*	*
80.8	0.177	31.373	2	28.218	3.155	140.8	0.846	31.611	2	30.073	1.538
80.8	0.170	32.332	2	28.051	4.281	140.8	0.839	32.737	2	30.065	2.672
80.8	0.170	33.474	2	28.130	5.343	140.8	0.832	34.084	2	30.041	4.043
111.1	10.133	25.142	1	25.142		140.8	0.818	35.289	2	30.049	5.240
111.1	8.644	25.221	1	25.221		159.6	10.126	27.147	1	27.147	
111.1	7.093	25.316	1	25.316		159.6	8.685	27.250	1	27.250	
111.1	5.810	25.411	1	25.411		159.6	7.100	27.361	1	27.361	
111.1	4.128	25.554	1	25.554		159.6	5.638	27.457	1	27.457	
111.1	2.763	25.649	1	25.649		159.6	4.114	27.591	1	27.591	
111.1	1.136	25.744	1	25.744		159.6	2.839	27.694	1	27.694	
111.1	0.570	26.022	1	26.022		159.6	1.480	27.829	1	27.829	
111.1	0.446	26.363	1	26.363		159.6	1.253	28.154	1	28.154	
111.1	0.439	27.227	1	27.227		159.6	1.246	29.232	1	29.232	
111.1	0.425	28.202	1	28.202		159.6	1.246	30.057	1	30.057	
111.1	0.418	28.796	2	*	*	159.6	1.239	31.191	1	31.191	
111.1	0.412	30.374	2	29.058	1.316	159.6	1.232	32.245	2	30.794	1.451
111.1	0.405	31.532	2	29.010	2.521	159.6	1.218	33.109	2	30.763	2.347
111.1	0.405	32.467	2	29.090	3.377	159.6	1.191	34.481	2	30.691	3.790
111.1	0.398	33.403	2	29.018	4.384	159.6	1.177	35.710	2	30.596	5.114
111.1	0.398	34.568	2	28.907	5.661	159.6	1.163	37.327	2	30.572	6.755

*Note: * refers to the scenario that the LV equilibrium could be visually observed but the interface is to fuzzy to be identified.*

Appendix H. PV data measured for the n-octane/bitumen mixture (Mixture OB1 in Chapter 3)

T, °C	P,	V_{total},	Phase	V_L,	V_g,	T, °C	P,	V_{total},	Phase	V_L,	V_g,
140.7	10.099	48.276	1			159.0	8.616	49.687	1	49.687	
140.7	8.630	48.402	1			159.0	7.100	49.869	1	49.869	
140.7	7.100	48.640	1			159.0	5.755	49.996	1	49.996	
140.7	5.686	48.886	1			159.0	4.100	50.162	1	50.162	
140.7	4.100	49.045	1			159.0	3.135	50.265	1	50.265	
140.7	3.135	49.124	1			159.0	2.032	50.424	1	50.424	
140.7	2.032	49.227	1			159.0	1.101	50.479	1	50.479	
140.7	1.094	49.330	1			159.0	0.232	51.423	1	51.423	
140.7	0.543	49.488	1			159.0	0.232	52.327	1	52.327	
140.7	0.177	50.781	1			159.0	0.232	52.850	1	52.850	
140.7	0.170	51.732	1			159.0	0.225	53.659	1	53.659	
140.7	0.170	53.238	1			159.0	0.219	54.808	2	*	*
140.7	0.163	53.944	1			159.0	0.219	56.965	2	49.923	7.042
140.7	0.156	54.840	2	48.400	6.439	159.0	0.212	57.916	2	50.121	7.795
140.7	0.150	56.037	2	48.567	7.470	159.0	0.205	58.844	2	50.168	8.675
140.7	0.143	56.521	2	47.734	8.786	159.0	0.191	62.506	2	49.835	12.671
159.0	10.099	49.560	1	49.560							

*Note: * refers to the scenario that the LV equilibrium could be visually observed but the interface is to fuzzy to be identified.*

Appendix I. Capillary viscometer measurement

Section one: set up and cleaning

- Set up

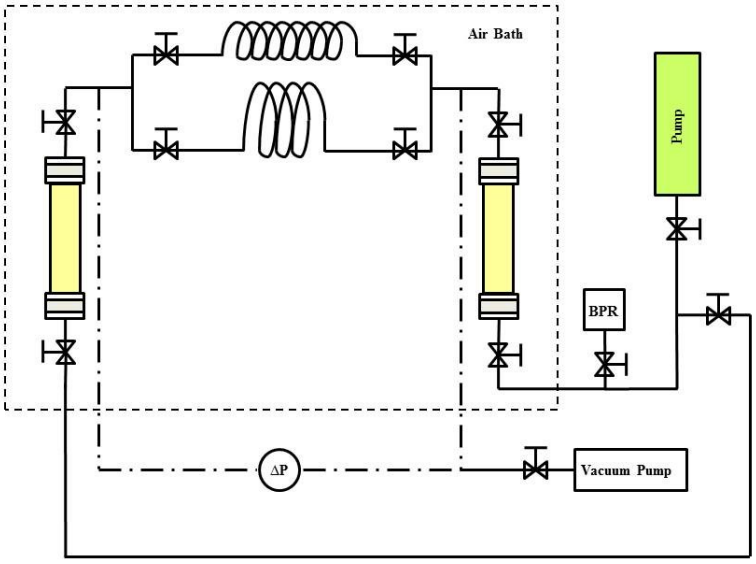

- Cleaning

1. Transfer cylinder:

Transfer cylinder should be taken apart first. Push the piston to the bottom. Then remove the bottom cup and use force or gas cylinder pressure to push the piston out of the body. Clean and change orings. And use toluene and paper tower to clean the body part. Then reassemble it carefully.

2. Tubing:

Each tubing should be cleaned by toluene, methanol, acetone and water. Then use strong air flow to blow the left liquid outside the tubing.

3. Differential pressure gauge:

Differential pressure gauge should be cleaned by toluene and water. Then totally vacuum it.

4. BPR:

BPR should be cleaned at atmospheric pressure by toluene and water. Then totally vacuum it.

Section two: preparation work

1. Check the viscosity by use of viscometer and compare with manufacture data:

Firstly, communicate with the technician to check the shear rate range of the Brookfield viscometer measurement. Then measure the known-viscosity sample several times. Compare with manufacture data and measured data by capillary viscometer to do the error analysis for capillary viscometer.

2. Calibrate pressure gauge:

The pressure gauge was calibrated by manufacture. But we could also double check the calibration for the pressure range in our measurement.

3. Calibrate pump flow rate:

Pump flow rate should be calibrated at different flow rates by measuring flowing volume at certain time. The ISCO pump has been calibrated at the flow rate range from 0.2 cc/min to 10 cc/min. And the results showed that the pump is not accurate if the flow rate is smaller than 1 cc/min. Therefore, we need a correlation equation to calibrate the pump flow rate below 1 cc/min and use this correlated flow rate in Hagen-Poiseuille equation.

4. Measure the effective volume:

Step 1: After reassemble transfer cylinder, vacuum from the bottom. At the same time, push the hydraulic oil to the bottom of cylinder. Then close the bottom valve and connect cylinder with pump. Then open valve.

Step 2: Refill the transfer cylinder with distillated water. Close top valve. Set 100 psi to push the fluid. Check if the cylinder is leaking.

Step 3: Keep pressure as 100 psi and open top valve. Push fluid to the valve before capillary viscometer (which is closed now). Lose tubing connection right ahead of valve. After see fluid flow outside from the tubing, tight the connection of valve again.

Step 4: Keep valve closed. Vacuum from the end of capillary viscometer until readings of pressure gauge reach stable. Close valve. And check if pressure readings increase (check if somewhere is leaking).

Step 5: Record volume reading of pump before open valve before capillary viscometer. Set constant pressure (eg, 100 psi) to fill viscometer. After reading of pressure gauge reach stable. Record the fluid volume (the volume of viscometer and tubings connected to differential pressure gauge).

5. Measure the effective radius by distillated water:

Step 1: After measure the effective volume, decrease pressure to 20 psi. After reading of pressure gauge is stable, close the pump.

Step 2: Open valve at the end of capillary viscometer. After readings of pressure gauge reach stable, reset zero for pressure gauge.

Step 3: Set constant flow rate for pump. Start from 1 cc/min to 10 cc/min and measure the differential pressure of water at atmospheric pressure.

Step 4: Decrease flow rate back to 1 cc/min. Keep pump running when connect BPR into the system and do not close any valves. Set BPR for 4 MPa. Measure the differential pressure of water from 1 cc/min to 10 cc/min.

Section three: experiment

1. Calibration:

After cleaning all items in the system, follow the same procedures of measuring the effective volume and radius. The differential pressure of standards which have similar viscosity with sample should be measured at the same shear rate range as Brookfield viscometer. Then

calculate the viscosity by Hagen-Poiseuille equation with effective flow rate and radius. Do error analysis for capillary viscometer.

2. Measurement:

The procedure of sample measurement is as same as calibration.